

Quantitative Assessment of Submodes of Stress Corrosion Cracking on the Secondary Side of Steam Generator Tubing in Pressurized Water Reactors: Part 3

R.W. Staehle[†]* and J.A. Gorman*

ABSTRACT

The work in this article is part of a project to develop a quantitative description of stress corrosion cracking (SCC) on the secondary side of pressurized water reactor (PWR) steam generator tubing based on existing information from operating plants and from laboratory experiments. This work is the second step in developing a predictive model for SCC on the secondary side. The first step involved developing a statistical framework into which dependencies of the various submodes of SCC can be inserted. The results of the present work will lead to quantitative descriptions of corrosion processes that, in turn, will be incorporated into the statistical framework. The chemistry of heat-transfer crevices will then be assessed to determine the proper inputs to the dependencies of the various submodes of SCC, and these will be connected to bulk environments. The modeling here is directed toward predicting the early occurrence of SCC that is too shallow to be detected by nondestructive examination (NDE).

The various submodes of SCC considered in this article include: alkaline stress corrosion cracking (AlkSCC), low-potential stress corrosion cracking (LPSCC), acidic stress corrosion cracking (AcSCC), high-potential stress corrosion cracking (HPSCC), lead stress corrosion cracking (PbSCC),

low-valence stress corrosion cracking (S^{2-} SCC), organic stress corrosion cracking (OgSCC), doped steam stress corrosion cracking (DSSCC), and low-temperature stress corrosion cracking (LTSCC). To develop a model for each of these submodes, their dependencies on the seven primary variables are evaluated in this article; these variables are pH, potential, species, alloy composition, alloy structure, temperature, and stress. For some of these submodes, there is broad agreement in the literature on dependencies. In other cases there is some disagreement, but these are mostly related to lack of information or to inconsistencies among experiments that have been conducted under different conditions. To develop a framework for this discussion of submodes, supporting sections are included on designs of steam generators as they affect corrosion, bulk water chemistry as it relates to chemistry in heat-transfer crevices, and the chemistry of heat-transfer crevices. At the end of each section, the state of present knowledge is summarized including the lessons learned from service and laboratory experience. In addition, possible problems for future reliable performance as affected by corrosion are identified.

KEY WORDS: Alloy 600, Alloy 690, Alloy 800, heat-transfer crevices, secondary side, steam generator, stress corrosion cracking, water chemistry

TABLE OF CONTENTS

Abstract

- 1.0 Introduction
- 2.0 Types of Steam Generators
- 3.0 Secondary Environments
- 4.0 The Heat-Transfer Crevice and Deposits
- 5.0 Modes and Submodes of Corrosion

Part 1 of this manuscript, with the complete set of references, appeared in *CORROSION* 59, 11 (2003), p. 931-994. Part 2 appeared in *CORROSION* 60, 1 (2004), p. 5-63.

[†] Corresponding author.

* 22 Red Fox Road, North Oaks, MN 55127.

** Dominion Engineering, Inc., 11730 Plaza America Drive, Suite 310, Reston, VA 20190.

Note References, figures, and tables are sometimes referred to out of order. This has been necessary first to maintain the integrity of sections and second to show connections among previous and succeeding sections.

- 5.1 Introduction
 - 5.1.1 Modes and Submodes
 - 5.1.2 Seven Primary Variables
 - 5.1.3 Initiation and Propagation
 - 5.1.4 Chronology
 - 5.1.5 Continuity between HPSCC and LPSCC
 - 5.1.6 SCC of SG Vessel
 - 5.1.7 Statistical Behavior of SCC
- 5.2 Submodes of SCC
 - 5.2.1 Alkaline SCC (AkSCC), Including Alumino-Silicates
 - 5.2.2 Low-Potential SCC (LPSCC)
 - 5.2.3 Acidic SCC (AsSCC), Including Cl^- , SO_4^{2-} , and Cu^{2+}
 - 5.2.4 High-Potential SCC (HPSCC)
 - 5.2.5 Lead SCC (PbSCC)
 - 5.2.6 Reduced Sulfur SCC (S^- -SCC)
 - 5.2.7 Doped Steam SCC (DSSCC)
 - 5.2.8 Organic SCC (OgSCC)
 - 5.2.9 Low-Temperature SCC (LTSCC)
- 5.3 Development of Alloy 690
- 5.4 Significance
 - 5.4.1 Experience
 - 5.4.2 Potential Problems with Alloy 690TT
- 6.0 Conclusions
- Acknowledgments
- References
- Abbreviations and Acronyms

5.2.2 Low-Potential SCC (LPSCC) — LPSCC, as shown in the mode diagrams of Figures 82(a) and 84, is usually considered to occur only on the primary side of tubing in steam generators (SGs) and in relatively pure deoxygenated water containing low concentrations of lithium and boron. Part of this predisposition is associated with the increased intensity of LPSCC with the lower potentials that are characteristic of the primary side that result from the addition of hydrogen. Higher temperatures on the primary side, relative to the secondary side, also exacerbate the LPSCC. LPSCC is also characterized by its relatively slow rates and high threshold stresses for initiation from smooth surfaces at primary temperatures. The relatively high value of the activation energy would reduce the intensity of LPSCC on the secondary side, but this trend might be countered by the possible accelerating effects of concentrated impurities in heat-transfer crevices on the secondary side.

The occurrence of LPSCC on the primary side has been characterized by statistical correlations, examples of which are shown in Figures 24, 94(a), and 94(c); the various failure locations due to LPSCC are characterized in Figure 21.

LPSCC is a potential submode of stress corrosion cracking (SCC) for the secondary side for four reasons:

- First, LPSCC occurs within the temperature range of the secondary side as shown in Figure 103, from Begley, et al.,²⁸¹ where data are shown from highly stressed Row 1 U-bends. These data from highly stressed locations are relevant to the secondary side where scratches have occurred and have produced substantial SCC as shown in Figure 17 for a cold leg and Figure 71 for an once-through steam generator (OTSG) scratch. Scratches at which SCC is focused are a main contributor to SCC in the upper bundle of OTSGs, as noted in Figure 71. The intensity of the SCC in the upper bundle of OTSGs is shown in Figure 25. LPSCC also has been observed at 280°C at Connecticut Yankee.²⁸²

- Second, adding hydrazine (N_2H_4) to the secondary side tends to lower the potential into the range of LPSCC, as shown in Figures 33, 43, and 45(a). However, this lowering is slight and much less than suggested by the half-cell equilibrium. While there is a conflict in directions of the potential due to the combined effects of low hydrogen and the N_2H_4 , the latter seems to dominate. In fact, if the N_2H_4 did not dominate, several of the submodes of SCC would be activated following the dependence of AkSCC on potential, as shown in Figures 97 and 123. The practice of using high N_2H_4 on the secondary side should be evaluated carefully because it can intensify LPSCC, especially at locations of high stress and where the N_2H_4 can partition to the vapor.

- Third, LPSCC has never been investigated adequately with respect to effects of impurities that occur on the secondary side in heat-transfer crevices; and it is likely that its intensity would increase with some additions such as contaminants accelerate high-potential stress corrosion cracking (HPSCC) for sensitized Type 304 (UNS S30400)⁽¹⁾ and Alloy 600 (UNS N06600) in boiling water reactor (BWR) technology, as shown in Figure 88(e). Further, the doped steam data shown in Figure 75 indicate that certain species accelerate what might otherwise be LPSCC in steam. The interaction of impurities with LPSCC might also produce SCC in Alloy 690 (UNS N06690) where none has yet been observed. Such a pattern occurred in acidic stress corrosion cracking (AcSCC) where Alloy 690 was originally thought to be immune, as shown in Figure 121(a). Now, Alloy 690 has been shown to sustain AcSCC in certain environments, as discussed in Section 5.2.3.

- Fourth, a small but important amount of what appears to be LPSCC has occurred on outside diameter (OD) surfaces of the free-span of OTSGs (Figure 17). Whether this can be specifically attributed to LPSCC is not clear. However, this SCC has occurred in the absence of heat-transfer crevices where only an elevated stress due to a scratch occurred. This SCC is noteworthy for its extent once it moves be-

⁽¹⁾ UNS numbers are listed in *Metals and Alloys in the Unified Numbering System*, published by the Society of Automotive Engineers (SAE International) and cosponsored by ASTM International.

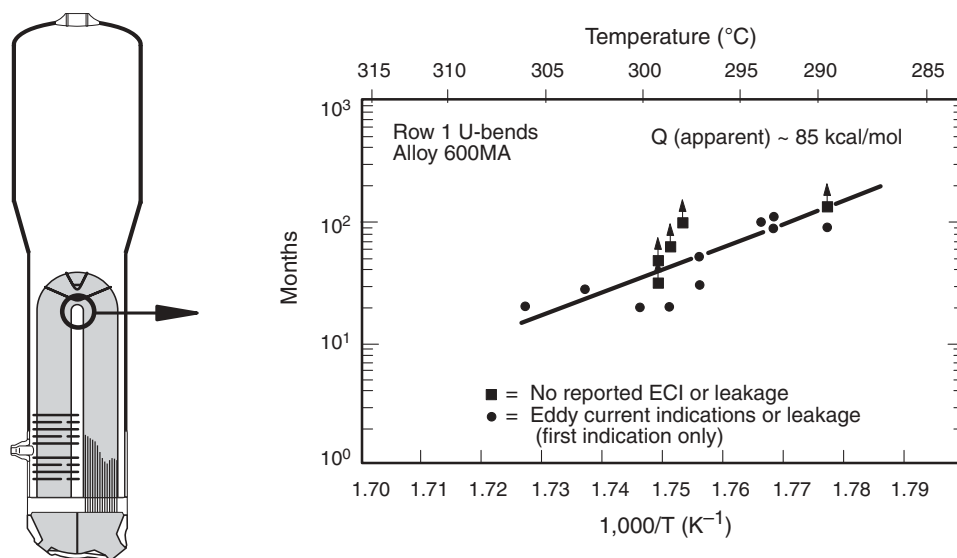


FIGURE 103. Time to failure for Row 1 U-bends of PWR steam generators on the primary side. From Begley, et al.²⁸¹

yond the relatively shallow depth, affected by the scratch, and perforates the thickness of the tube wall.

In general, Alloy 690 has shown negligible susceptibility to LPSCC, and this has been one of the reasons for using this alloy in replacement steam generators. Whether this immunity to LPSCC persists in the presence of contamination, which is characteristic of the secondary side, has not been investigated, except that doped steam tests in Figure 75 show Alloy 690 to be resistant to SCC in that environment,¹⁸⁷ which implies that it might be immune to LPSCC in contaminated secondary environments. However, such a generality needs to be investigated.

Developing a mechanistic interpretation of LPSCC has invoked considerations of hydrogen with respect to its influence on dislocation motion, internal oxidation, film rupture, gas bubbles at grain boundaries, and a special weakness in protective films at the Ni-NiO half-cell equilibrium. This work has been undertaken to rationalize why this submode can occur in pure water and how it can be predicted in the future and especially for Alloy 690, which has been shown to be immune to LPSCC.

As background for a summary of mechanisms of LPSCC, the location of LPSCC in Figure 82(a) shows that it occurs at lower potentials than the other major submodes such as alkaline stress corrosion cracking (AkSCC) and AcSCC, as well as the HPSCC, which occurs in the range of even higher potentials. This location of LPSCC is supported by the data shown in Figures 106(b) through (e), where the maximum in LPSCC intensity occurs about at the NiO/Ni half-cell equilibrium. This location places it below the range of potentials for AkSCC as shown in Figure 97 and for AcSCC as shown in Figure 123 as well as the expected E_{corr} on the secondary side at normal secondary-side hydrogen pressure (p_{H_2}). Also, the

present evidence for lead stress corrosion cracking (PbSCC) places it in the same range with respect to the H₂O/H₂ half-cell equilibrium as AkSCC and AcSCC. Prior to the availability of the data shown in Figures 106(b) through (e), the best available information for the dependence of LPSCC on potential was given by Figure 106(a), which had been determined using applied potentials rather than a range of dissolved hydrogen. Incidentally, a similar approach is used for obtaining data for HPSCC as applicable to BWR technology as shown in Figure 88(e), but this extends to higher potentials. While alkaline species accumulate on specimen surfaces that are made more cathodic, acidic species accumulate when the surface is made more anodic by higher applied potentials. The validity of more noble and more active applied potentials should be reviewed. Also, the range of potentials achieved by changing the hydrogen pressure, as shown in Figures 106(b) through (f), is small with respect to the range of Figure 106(a). Possibly, the large difference in scale obscures the validity of lower potentials in Figure 106(a).

For LPSCC, where the outside surface is deaerated and the crack tip is similarly deaerated, this condition is illustrated in Figure 41. Figure 41 shows that, for LPSCC on the primary side, the electrochemical conditions at the outside surface and at the crack tip surfaces are virtually the same. This means that the crack tip is operating at a potential where the equilibrium hydrogen pressure is about 0.3 atmosphere on the primary side. The situation on the secondary side may be somewhat different with respect to the schematic view shown in Figure 41. On the secondary side, the hydrogen pressure is lower by about 3 orders of magnitude than on the primary side. As a boundary, the potential on the outside surface of the tube on the secondary side, and inside

a liquid phase heat-transfer crevice, could be about 200 mV above that of the NiO/Ni half cell. It is possible that the potential inside an advancing SCC would be lowered by hydrogen from localized corrosion at the crack tip, and the potential gradient from the outside surface to the crack tip would cause anions to migrate toward the crack tip. However, the presence of N_2H_4 , possibly decomposing to H_2 , inside the heat-transfer crevice would lower the surface potential relative to the crack tip, which would cause anions to move outward. Details of these hypotheses need to be evaluated.

The essences of the important mechanistic proposals for LPSCC are as follows:

1. Hydrogen—Hall and coworkers have developed a quantitative interpretation based on hydrogen produced by local corrosion at the crack tip being the principal contribution to advancing LPSCC through a hydrogen-enhanced creep process.²⁸³⁻²⁸⁴ This model accounts for local strain hardening at the tip of the advancing SCC. It is not clear how this model accounts for the shape of the SCC intensity, as a function of potential, shown in Figures 106(b) through (e). Magnin, et al.,²⁸⁵ have proposed a deformation-hydrogen model that accounts for both intergranular and transgranular SCC involving slip, anodic dissolution, hydrogen-facilitated slip, and sharpening of the crack tip. This model is somewhat similar to that of Hall and coworkers. One support for the Magnin model is the increased strain rate observed in hydrogen atmospheres. Another is the appearance of cleavage facets on the intergranular faces of LPSCC. This model also requires some dissolution to produce hydrogen.
2. Internal oxidation—Scott and coworkers have proposed that LPSCC could be explained by the preferential entry of oxygen into grain boundaries, thereby weakening them and permitting cracks to proceed in these weakened regions.²⁸⁶⁻²⁸⁹ This model avoids the necessity of relying on a hydrogen model, especially if the region of LPSCC is restricted as suggested by Figures 106(b) through (e). Staehle and Fang²⁹⁰ have raised questions about the internal oxidation model based on two concerns: (a) The kinetics of diffusion of oxygen at grain boundaries are not adequate to account for the growth of LPSCC, although this is a well-known process for higher-temperature internal oxidation. (b) The oxygen pressure is maximum and constant above the NiO/Ni half-cell equilibrium and decreases rapidly below this line. The occurrence of LPSCC does not follow such a pattern. Also, this model does not account for the peak in crack growth

rates being coincidental with the NiO/Ni equilibrium half cell. Finally, the internal oxidation model does not account for the effect of sensitization in reducing the intensity of LPSCC.

3. Film rupture—Andresen and coworkers^{242,291-292} have suggested that the propagation of LPSCC follows the same film rupture process as for the HPSCC of interest to BWR environments for sensitized materials. However, it is not clear how such a mechanism would provide for the shape of the LPSCC dependence on potential as shown in Figures 106(b) through (e). Also, Figure 93 suggests that there is no connection between the domains of LPSCC of mill-annealed materials and HPSCC of sensitized material. Finally, Table 16 shows that sensitized Alloy 600 mitigates LPSCC.
4. Gas bubbles at grain boundaries—Shewmon and coworkers²⁹³⁻²⁹⁶ have proposed that LPSCC proceeds by the diffusion of hydrogen into the metal forming CH_4 bubbles as a result of the reaction between carbon and hydrogen. These bubbles then produce a weakness that promotes failure under stress. The possibility of this model working seems to depend on there being a much higher fugacity of hydrogen than the electrochemical potentials can support. Further, there does not seem to be metallographic support for the CH_4 bubbles.
5. Weakness of film—The generally symmetric shape of the intensity of LPSCC around the NiO/Ni half-cell equilibrium suggests that the initiation and propagation of LPSCC has something to do with the stability of the NiO passive film as possibly modified by Cr and Fe. How such a condition of weakness would produce LPSCC is not clear.

The models for SCC have been reviewed in detail by Smialowska and Rebak²⁴ where they examined a broader range of possible mechanisms but concluded that none could account for the existing data, although many of the mechanisms provided some good practical correlations.

None of the existing mechanisms accounts for the role of the seven primary variables, although the Hall model for hydrogen-affected creep provides the most quantitative fit with existing data.

The important dependencies of LPSCC on the primary variables relevant to the secondary side are as follows:

1. pH

In general, changes in pH seem to produce minor effects on the LPSCC of Alloy 600 for practically achievable values of pH for specimens with both initially smooth surfaces and pre-cracked specimens, as shown in Figures 104 and 105(a), and Table 22. Effects of pH on LPSCC have been studied by

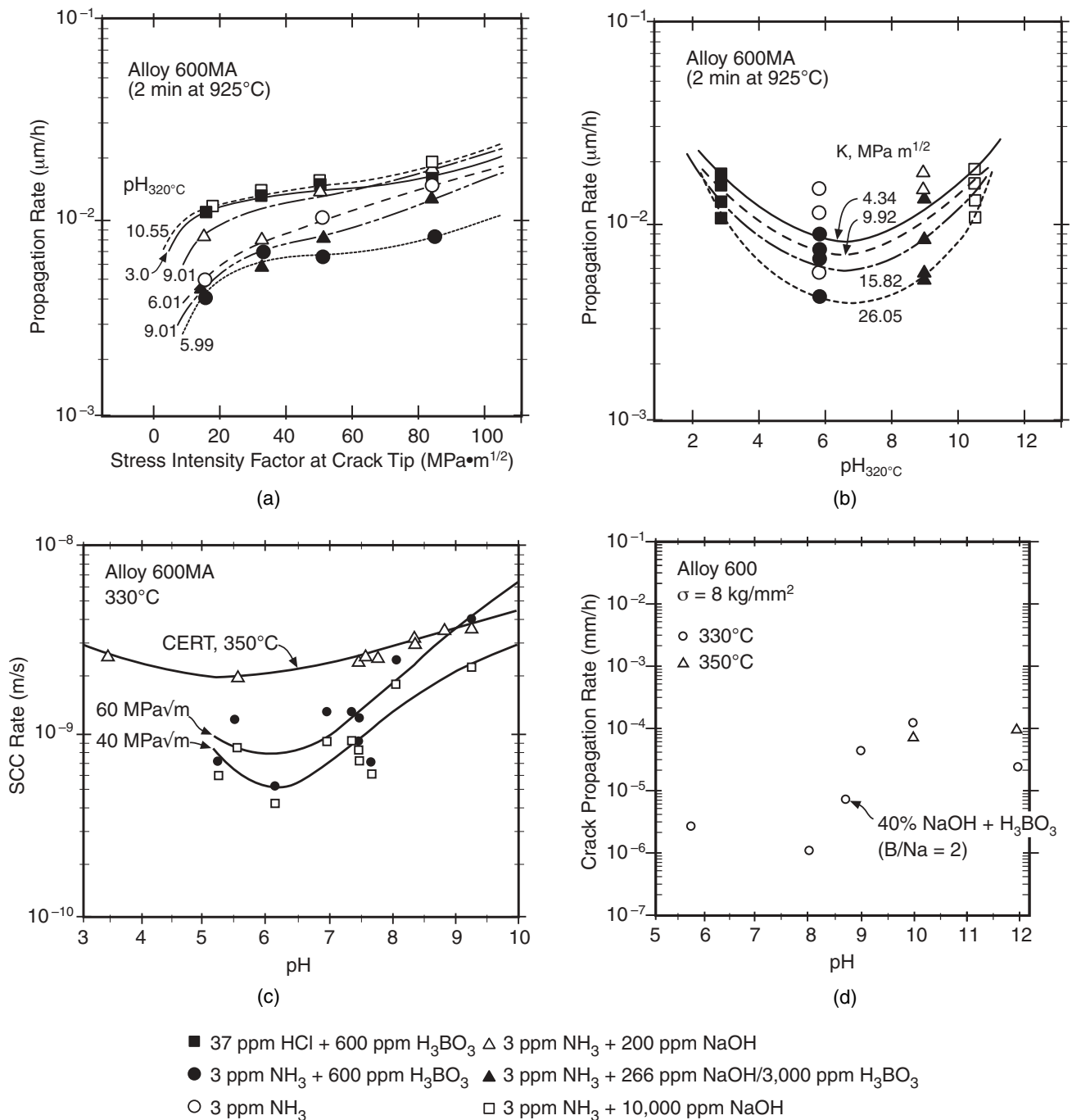


FIGURE 104. (a) Crack propagation rate vs stress intensity for LPSCC at 320°C for four values of pH. From Kawamura, et al.¹⁴⁵ ©1995 NACE International. (b) Propagation rate vs pH for constant values of stress intensity. From Kawamura, et al.¹⁴⁵ ©1995 NACE International. (c) SCC rate vs pH for Alloy 600MA at 350°C for CERT specimens and at 330°C for constant load pre-cracked specimens. From Smialowska, et al.²⁴⁹ ©1994 NACE International. (d) Crack propagation rate vs pH for Alloy 600 at 330°C and 350°C. From Takamatsu and Matsueda.²⁹⁷ ©1990 NACE International.

Kawamura, et al.,¹⁴⁵ Smialowska, et al.,²⁴⁹ Takamatsu and Matsueda,²⁹⁷ and Jacko²⁹⁸ using specimens with both pre-cracked and initially smooth surfaces.

While most of LPSCC follows intergranular paths, Table 22 shows a transgranular morphology at approximately pH 3.4.

2. Potential

In general, LPSCC seems to be most intense in the region of the NiO/Ni half-cell equilibrium potential, identified in Figure 33, based on tests with both smooth and pre-cracked specimens and shown in Figures 106(b) through (e). The region of potential

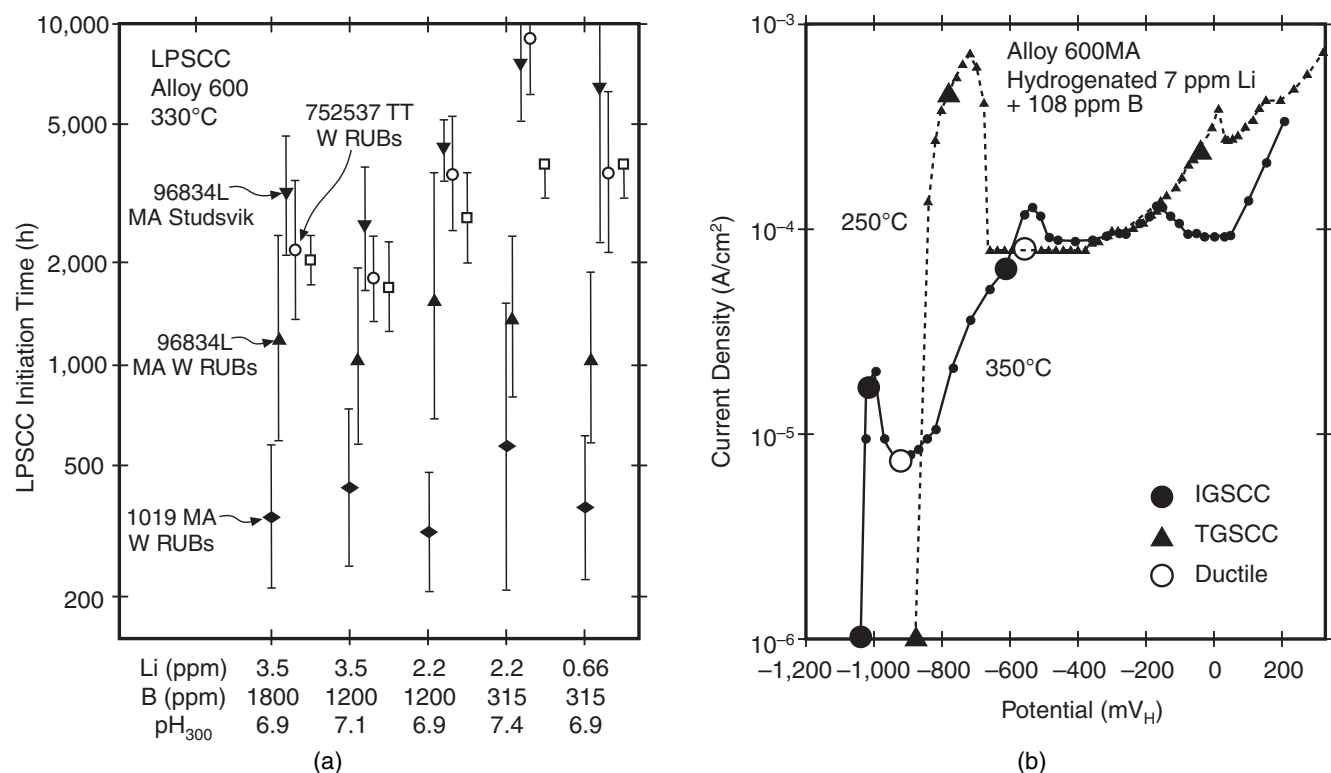


FIGURE 105. (a) LPSCC initiation time vs primary water chemistry for four heats of Alloy 600 exposed at 330°C. From Jacko.²⁹⁸ Used by permission of EPRI. (b) Current density vs potential for Alloy 600MA at 250°C and 350°C in hydrogenated 7 ppm Li + 108 ppm B. Locations of morphologies for SCC and ductile fracture noted. From Smialowska, et al.²⁴⁹ ©1994 NACE International.

between the outside surface and the crack tip in LPSCC is identified in Figure 41; this region is small being in the range of <200 mV depending on the hydrogen pressure. Further, LPSCC seems to occur in a different range of potential than does HPSCC, as demonstrated in Figures 93 and 82(a), and Table 22.

Figure 105(b) shows polarization curves corresponding to Table 22 for 250°C and 350°C in primary water. The most important feature of these results is the observation of transgranular SCC in the 250°C tests. This transgranular morphology persists over the range of potentials at 250°C, and the intergranular morphology persists over the range of potentials at 350°C. In both cases there is a clear change in character in the passive range where only ductile failure occurs. It appears from these curves that the passivity is quite different at the two temperatures. It appears that the 250°C case exhibits a submerged anodic peak.

The sensitivity of LPSCC to small changes in potential was first demonstrated by Blanchet, et al., as shown in Table 23,⁸⁰ using galvanic couples of Alloy 600 connected with relatively active or noble alloys. With the latter, LPSCC was suppressed according to the increase in potential that results from coupling with a more noble material. The LPSCC was intensified when the potential was lowered by coupling to

more active metals. It should be noted that the range of potentials that are accessible to such galvanic couples is small, owing to the deaeration of the solutions and the domination of potential by the hydrogen electrode.

The effect of potential was also investigated early using double U-bend specimens exposed to various intensities of oxidizing conditions as shown in Table 15 in experiments by Copson and Economy.²³⁰ The double U-bend specimen provided both a crevice geometry as well as an open surface. In the crevice, the local solution was presumably acidified and the potential would be lowered relative to the outside depending on the inside pH. The general trend of potentials here can be estimated from the trends shown in Figure 43. In general, in Table 15, LPSCC did not occur after 3,024 h at 316°C water with the pH initially adjusted to 10 with ammonium hydroxide (NH₄OH). As the oxidizing conditions were increased, more SCC occurred on the inside crevice. While the experiments in hydrogen and argon can be assumed to be relevant to LPSCC, the experiments with oxidizing conditions are relevant to HPSCC. This set of experiments effectively distinguishes between LPSCC and HPSCC, as shown also in Figure 93.

For the secondary side, the dependence on potential is similarly important owing to the competing

TABLE 22
CERT of Alloy 600 Specimens with a Cold-Pressed Hump:
Influence of Temperature, pH, and Potential on Cracking Susceptibility^(A)

Test	Temperature (°C)	B (ppm)	Li (ppm)	pH (RT)	pH (HT) ^(B)	E (mV _{SHE})	SCC Mode	% SCC	Crack Growth Rate (m/s)
1	350	108	7	8.0	9.0	-1,025 (OCP)	IG	70	3.55 × 10 ⁻⁹
2	350	108	7	8.0	9.0	-1,025 (OCP)	IG	50	2.61 × 10 ⁻⁹
3	350	108	7	8.0	9.0	-1,070 (OCP - 45)	IG	48	2.9 × 10 ⁻⁹
4	350	108	7	8.0	9.0	-1,270 (OCP - 245)	IG	70	3.8 × 10 ⁻⁹
5	350	108	7	8.0	9.0	-1,970 (OCP - 945)	IG	68	4.3 × 10 ⁻⁹
6	350	108	7	8.0	9.0	-1,000 (OCP + 25)	IG	30	2.71 × 10 ⁻⁹
7	350	108	7	8.0	9.0	-960 (OCP + 65)	IG	10	4.86 × 10 ⁻⁹
8	350	108	7	8.0	9.0	-910 (OCP + 115)	Ductile	0	—
9	350	108	7	8.0	9.0	-860 (OCP + 165)	Ductile	0	—
10	350	108	7	8.0	9.0	-650 (OCP + 375)	Ductile	0	—
11	350	108	7	8.0	9.0	-615 (OCP + 410)	IG	25	2.4 × 10 ⁻⁹
12	350	108	7	8.0	9.0	-1,010 (1 h at -1,325)	IG	75	4.2 × 10 ⁻⁹
13 ^(C)	350	—	—	7.0	5.5	-596 (OCP)	IG	40	2.0 × 10 ⁻⁹
14 ^(D)	350	—	—	3.5	≈3.4	-337 (OCP)	TG	45	2.6 × 10 ⁻⁹
15	350	200	0.3	6.5	7.7	-866 (OCP)	IG	30	2.5 × 10 ⁻⁹
16	350	200	1.0	6.8	8.3	-940 (OCP)	IG	60	3.1 × 10 ⁻⁹
17	350	200	6.0	7.6	8.8	-1,000 (OCP)	IG	65	3.4 × 10 ⁻⁹
18	350	1,200	0.3	5.8	7.4	-830 (OCP)	IG	30	2.41 × 10 ⁻⁹
19	350	1,200	1.0	6.0	7.5	-842 (OCP)	IG	40	2.54 × 10 ⁻⁹
20	350	1,200	6.0	6.5	8.3	-940 (OCP)	IG	50	2.93 × 10 ⁻⁹
21	250	108	7	8.0	≈7.6	-762 (OCP)	Ductile	0	—
22	250	108	≈15	9.0	≈8.6	-866 (OCP)	TG	25	9.8 × 10 ⁻¹⁰
23	250	108	≈15	9.0	≈8.6	-790 (OCP + 75)	TG	15	6.2 × 10 ⁻¹⁰
24	250	108	≈15	9.0	≈8.6	-860 (OCP + 810)	TG	10	4.5 × 10 ⁻¹⁰

^(A) From Smialowska, et al.²⁴⁹ ©1994 NACE International.

^(B) HT = high temperature.

^(C) Pure water.

^(D) 5 × 10⁻⁴ M H₂SO₄.

effects of very low hydrogen concentrations due to boiling and additions of N₂H₄, as shown in Figures 33 and 45(a). It is unfortunate that the possible occurrence of LPSCC on the secondary side in the presence of N₂H₄ additions has not been studied.

The first explicit definition of the potential dependence of Alloy 600 in the LPSCC submode was published by Totsuka and Smialowska.²⁴³ Their results in Figure 106(a) show a sharp change in intensity of LPSCC around the deaerated open-circuit potential, which was generally coincident with the NiO/Ni equilibrium as identified in Figure 33.

However, the characteristic of extensive LPSCC to be independent of potential, as shown in Figure 106(a), has apparently been superseded by work using hydrogen pressure as the means for controlling potential. The first such work was published by Economy, et al.,²⁹⁹ and is shown in Figure 106(b) with the pressures converted to equivalent potentials relative to the NiO/Ni equilibrium.³⁰⁰ Lee, et al.,³⁰¹ also have conducted experiments similar to those in

Figure 106(b) and have obtained the results shown in Figure 106(d). Totsuka, et al.,³⁰² also have studied the effect of hydrogen using slow strain rate test (SSRT) at 360°C to 320°C. The dependence on hydrogen determined by Totsuka, et al., and shown in Figure 106(e), is similar to that in other data of Figure 106. Also, Tsuruta, et al.,³⁰³ have obtained similar results. Another study, by Morton, et al.,³⁰⁴ shown in Figure 106(c), using pre-cracked specimens at two stress intensities, showed a dependency upon potential and hydrogen pressure similar to that for smooth surfaces, as shown in Figures 106(b) and (d). Work by Andresen and Angeliiu,²⁹¹ using pre-cracked specimens at 288°C, showed results partly similar to Morton, et al.,³⁰⁴ but not revealing any peak in velocity except at zero hydrogen. The work from Figures 106(b) through (f) occupies a narrow range of potential relative to that in Figure 106(a). It is not clear whether there is a conflict between these approaches or not. This question has yet to be quantitatively resolved. It is possibly noteworthy that the data of

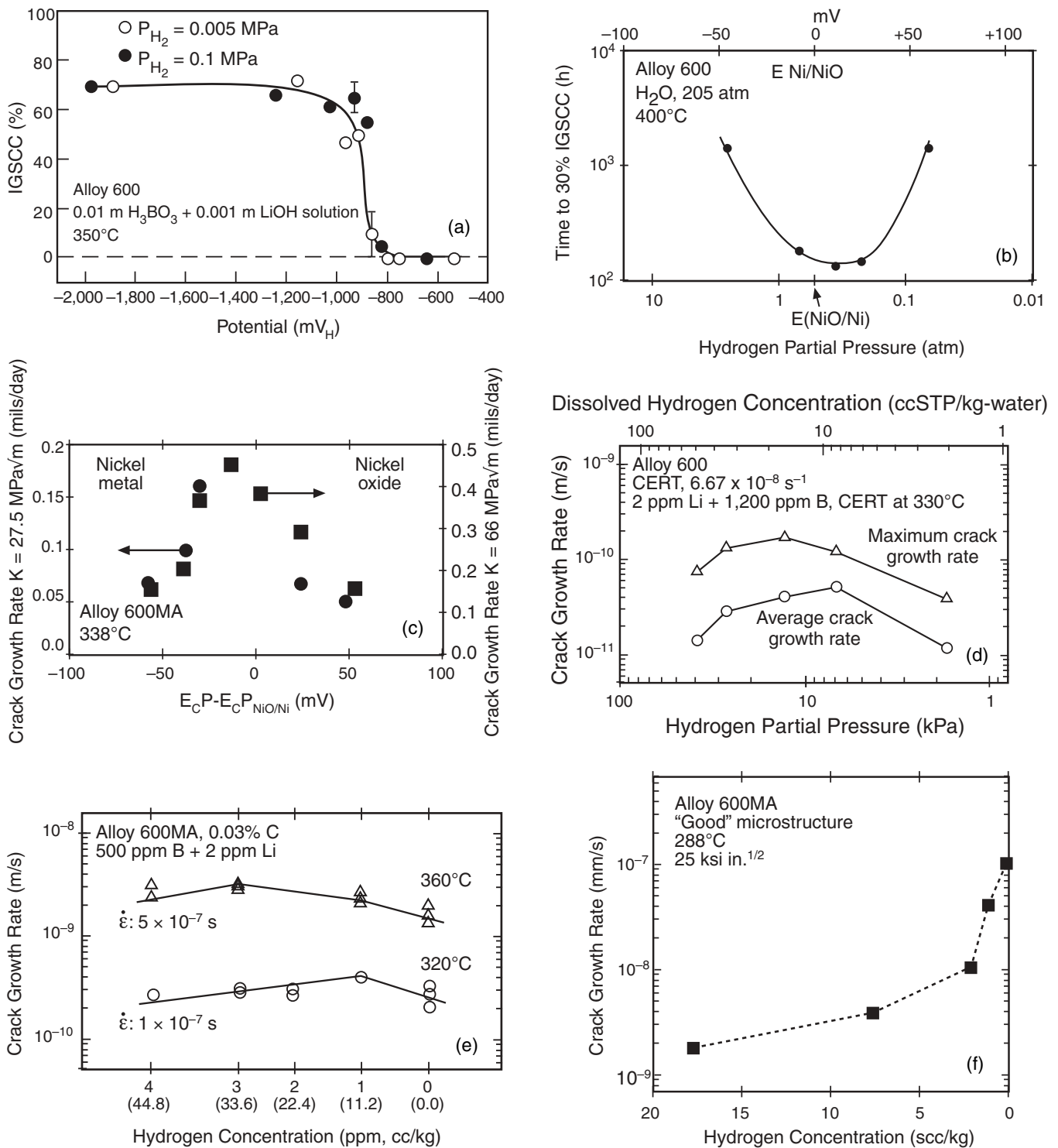


FIGURE 106. (a) Percent of fracture surface with IGSCC as a function of applied potential for Alloy 600 tested at 350°C using CERT for two pressures of hydrogen. From Totsuka and Smialowska.²⁴³ Courtesy of TMS, Warrendale, Pennsylvania, USA. (b) Time to 30% IGSCC vs hydrogen pressure and potential reference to NiO/Ni equilibrium. Experiments at 400°C and 205 atm pressure of steam. Original data from Economy, et al.²⁹⁹ Data recalculated by Scott and Combrade.²¹⁷ ©1997 by the American Nuclear Society, La Grange Park, Illinois. (c) Crack growth rate at two stress intensities vs potential ($E_C P = \text{electrochemical potential}$) relative to the NiO/Ni equilibrium potential for Alloy 600MA at 338°C. From Morton, et al.³⁰⁴ ©2003 NACE International. (d) Crack growth rate vs hydrogen pressure for Alloy 600 at 330°C using CERT at $6.67 \times 10^{-8} \text{ s}^{-1}$. From Lee, et al.³⁰¹ ©2003 NACE International. (e) Crack growth rate vs hydrogen concentrations for Alloy 600MA at two temperatures in simulated primary water obtained using SSRT. From Totsuka, et al.³⁰² ©2003 NACE International. (f) Crack growth rate vs hydrogen concentration for Alloy 600MA at 288°C and with a stress intensity of 25 ksi in^{1/2}. From Andresen and Angelii.²⁹¹ ©1997 NACE International. Note that some of the plots have been reversed; low potentials (high hydrogen) are shown at the left for all figures (a) through (f).

Figure 106(a) were obtained by a constant extension rate test (CERT) experiment while the other data were taken with direct measurements of crack growth.

The effect of potential on LPSCC has been considered extensively because the onset of LPSCC is sensitively related to conditions of potential at the open circuit of both primary and secondary sides. In fact, early studies that could not reproduce the work of Coriou were most likely conducted with sufficient oxygen that LPSCC was prevented.

The generally parabolic dependence of LPSCC on hydrogen pressure, over the relatively narrow range of potential, with the center more or less at the NiO/Ni half-cell equilibrium, as shown in Figures 106(b) through (e), raises some questions concerning the validity of a hydrogen model compared with the rather more supportive pattern from the work of Totsuka and Smialowska,²⁴³ in Figure 106(a) with potentiostatically controlled specimens. Such mechanistic questions have yet to be resolved.

3. Species

Consideration of effects of additional species for LPSCC is important because secondary surfaces are expected to sustain a wide range of chemistries in the heat-transfer crevices and because the relative immunity of Alloy 690 to LPSCC has been studied only in relatively pure primary environments and in “doped” steam, in equilibrium with somewhat dilute solutions, as shown in Figure 75. LPSCC has been investigated mainly in either pure water or primary water containing boric acid (H₃BO₃) and lithium hydroxide (LiOH) in concentrations relevant to commercial operation. Little work has been conducted outside these environments. From a practical point of view, relative to the primary side, there has been no incentive for such investigations; however, from the point of view of the secondary side, such investigations are important. The work of Jacko²⁹⁸ in Figure 105(a) showed negligible effects of varying concentrations of boron and lithium when results from the same heats were compared. Some effects of species are associated with studies of effects of pH, as described in Section 5.2.2.1, and this work showed relatively small differences among tests at various values of pH. If the work of Dehmlow in Figure 75¹⁸⁷ can be used as an indication here, various chemical species may intensify LPSCC. However, it also should be noted that Dehmlow’s work showed that Alloy 690 did not sustain SCC.

4. Alloy Composition

The dependence of LPSCC on alloy composition is relevant to the extensive LPSCC that occurs in Alloy 600 compared with what appears to be the immunity of Alloy 690. The effect of chromium concentration has been investigated by Yonezawa and Onimura³⁰⁵ and is shown in Figure 107. While this was not the original basis for choosing Alloy 690, as

TABLE 23
Frequency of SCC for Alloy 600
in Galvanic Couples of Various Compositions
Exposed to Neutral and Alkaline pH Environments

Galvanic Couple	Number of Samples Cracked after 12,000 h (Examined by Optical Microscopy)	
	Water	LiOH at pH = 10.5
Uncoupled	0/9	0/9
Coupled to gold	0/9	0/9
Coupled to platinum	0/9	0/9
Coupled to 18/10 stainless steel	1/10	0/9
Coupled to mild steel	4/10	2/10

(A) From Blanchet, et al.⁸⁰ ©1977 NACE International.

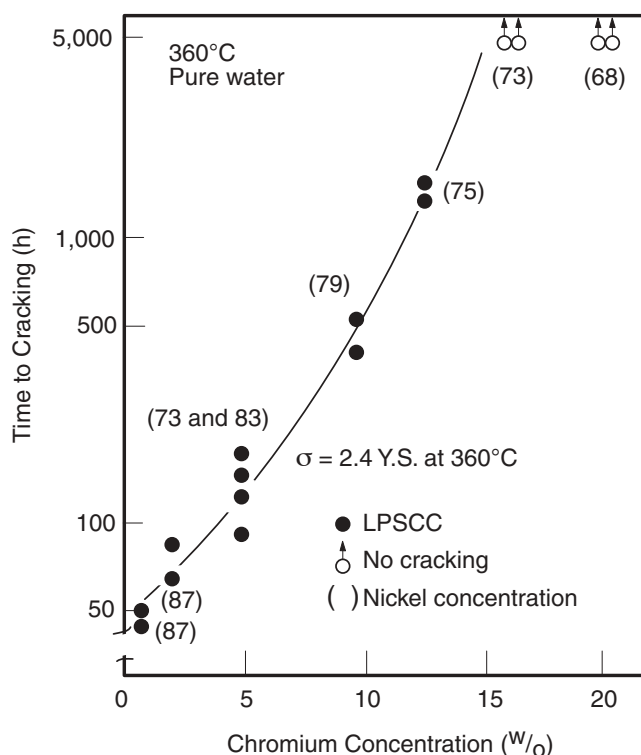


FIGURE 107. Time-to-cracking vs concentration of chromium for Ni-Cr-Fe alloys exposed in pure water at 2.4 Y.S. at 360°C. From Yonezawa and Onimura.³⁰⁵ Courtesy Iron and Steel Institute of Japan.

discussed in Sections 5.1 and 5.3, this dependence vindicates the early decisions relative to the composition of the alloy. The fact that LPSCC occurs readily with low Cr, at about 1%, as noted in Figure 107, suggests that the presence of Cr is not critical to the mechanism of LPSCC. Also, such alloys would lack the beneficial presence of chromium carbides at grain boundaries. Coriou, et al.,³⁰⁶ have investigated the dependence upon Ni at 20% Cr and have shown that LPSCC occurs as low as 45% Ni. Extensive practical experience with Alloy 800 shows it does not

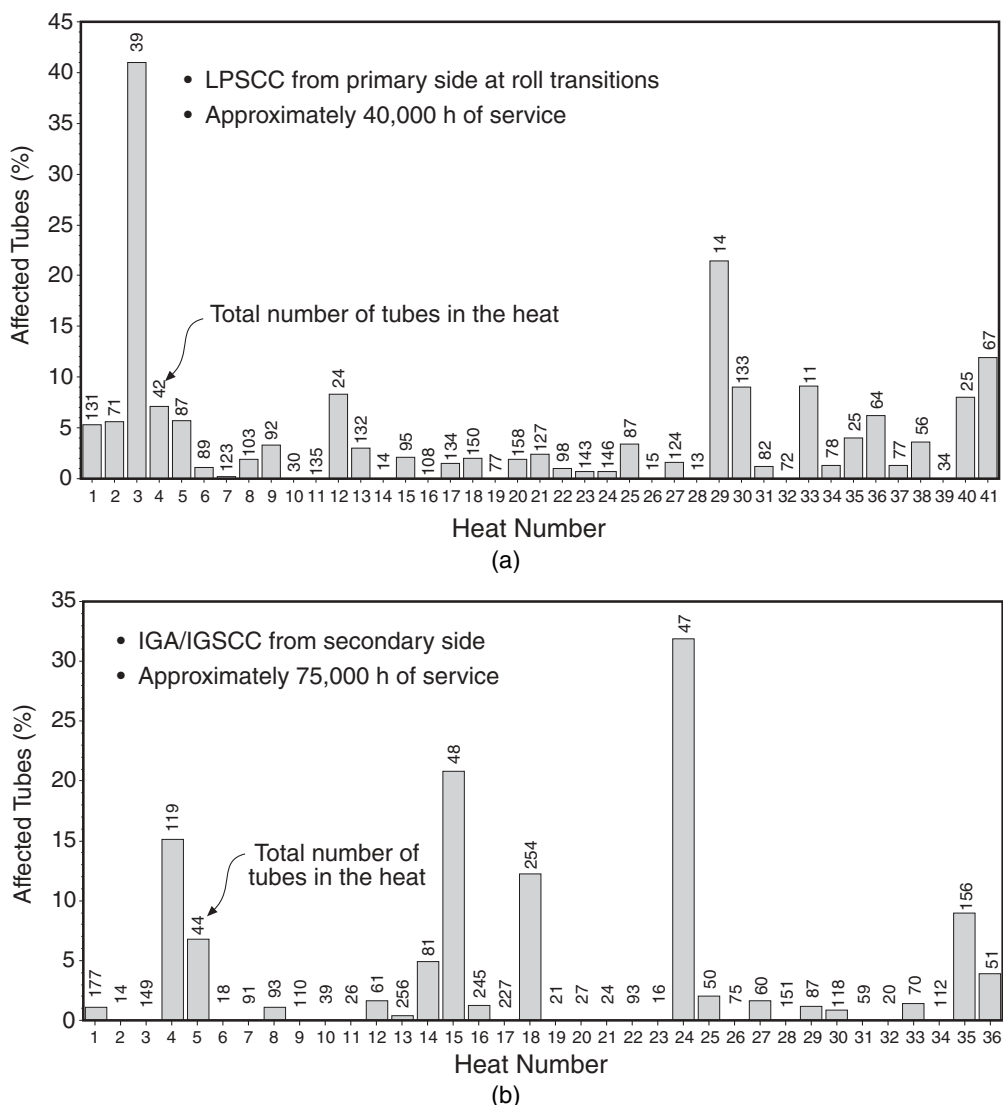


FIGURE 108. Percent of Alloy 600MA tubes affected by LPSCC from the primary side of a PWR steam generator vs heat number determined at roll transitions after approximately 40,000 h of service. Primary surface temperature at this location about 310°C. All heats from the same manufacturer and produced in sequence shown. Environment primary water. (b) Percent of tubes affected by IGA and IGSCC vs heat number from secondary side of a PWR steam generator in heat-transfer crevices after approximately 75,000 h of service. From Scott.³⁰⁹ ©2000 NACE International.

sustain LPSCC. Sung and Was³⁰⁷ have shown that LPSCC occurs in specially prepared alloys with 0.002 w/o carbon, thus indicating that the presence of carbides is not critical for LPSCC.

While Alloy 690 exhibits general resistance to LPSCC, Sui, et al.,³⁰⁸ have shown that LPSCC can occur in a hydrogen/steam environment at 380°C, if the mill annealing temperature is low, in testing carried out for 13,824 h. Specimens with higher mill annealing temperatures in the range of commercial treatments did not sustain LPSCC in these experiments.

5. Alloy Structure

The properties of alloys, including the corrosion properties of Alloys 600 and 690, are greatly affected

by their metallurgical history. Small changes in the processing produce large effects on the performance. Of specific interest in this section are heat-to-heat variability, sensitization and thermal treatments, effects of carbide distribution, effects of cold work, effects of strength, effects of surface condition on initiation of SCC, and effects of shot peening.

The subtle influences of metallurgical structure on LPSCC and outside diameter stress corrosion cracking (ODSCC) are particularly well illustrated by the data in Figure 108 from the work of Scott.³⁰⁹ In this figure, the percentage of Alloy 600MA tubes affected by corrosion from each heat used in a specific steam generator is plotted vs the chronology of the heats from a single manufacturer. At the top of each

bar, the number of tubes in the respective heats is given. Figure 108(a) shows data from the primary side, LPSCC, at the roll transitions, as shown in Figure 4, after 40,000 h of service from a single steam generator. Figure 108(b) gives comparable data for ODSCC from the secondary side for a steam generator with 75,000 h of service.

These data in Figure 108 show that there is no prevailing pattern for the fraction of tubes failed with heat or indeed among the heats (e.g., heat number 11 has 135 tubes and no affected tubes; whereas, heat number 3 has 39 tubes with 41% of tubes affected). Similar patterns occur for corrosion on both primary and secondary sides except that the fraction of heats with no affected tubes on the secondary side, 50%, greatly exceeds the same fraction for the primary side, 24%, in these particular cases, although the peak percentages affected are about the same. These data illustrate the consequence of heat-to-heat variability that arise from the variability of metallurgical processing as well as the variability of local chemistries in heat-transfer crevices. A similar heat-to-heat variability is shown in Figure 105(a) for four heats exposed to a variety of primary water chemistries.

Sensitizing retards LPSCC in Alloy 600 as first demonstrated by Blanchet, et al.,⁸⁰ and shown in Table 16. Here, mill-annealed (MA) treatments are compared with sensitized treatments for three concentrations of carbon. Sensitizing is clearly beneficial, although it does not prevent LPSCC. The response to sensitizing is one of the features that distinguishes LPSCC from HPSCC. In the latter case, as shown in Figure 127 in Section 5.2.4, sensitized Alloy 600 behaves similarly to sensitized Type 304 and the intensity increases with increased potential as shown in Figures 88(e) and 93. This dependence is contrary to the pattern shown for the MA treatment at lower potentials in Figure 93.

The results from Coriou's work in Table 16 were the basis for developing the thermally treated (TT) heat treatment. This treatment has been optimized and retards at least both AkSCC and LPSCC; it also retards AcSCC as shown in Figures 121 and 122. The effect of the TT treatment on LPSCC is shown in Figure 109(a) from the work of Jacko.²⁶⁸ This work shows that the TT treatment improves the performance, as it does with AkSCC, especially for the earlier failure times, which is desirable; however, the TT treatment does not prevent LPSCC. Figure 109(b) from Cattant, et al.,³¹⁰ shows data comparing the performance of MA and TT tubes from EDF (Electricité de France) SGs at the sludge pile level. Here, the TT tubes performed substantially better. Figure 109(c), from Cattant, et al.,³¹⁰ shows data from tubes where early failure of the TT condition was sustained; however, this figure shows that these early failures are associated with carbon concentration exceeding a

0.032 w/o limit. In general, the improvement factor for Alloy 600TT is a factor of 2 to 5 in life dependency depending on the magnitude of stress and cold work. In French plants the factor has been about 2. In U.S. plants with lower cold work and stress the improvement factor may approach 5, which reflects changes in both material and design, e.g., use of hydraulic expansion vs hard roll. It is not clear that the improvements from the TT treatment would provide great improvements to all of the tubes considering the high heat-to-heat variability of the MA tubes illustrated by the data in Figure 108. The recent observation of intergranular attack/stress corrosion cracking (IGA/SCC) in nominally TT tubes at Seabrook confirms this concern.⁸⁵

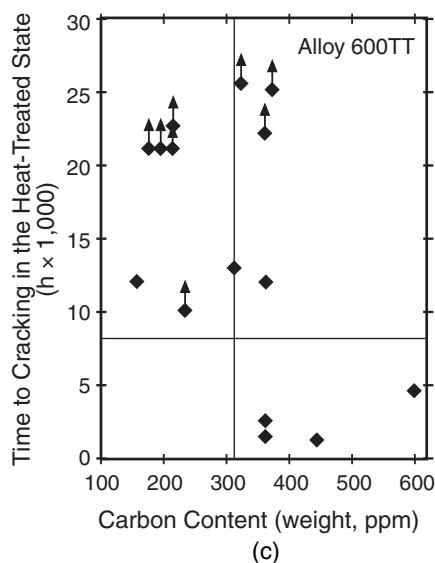
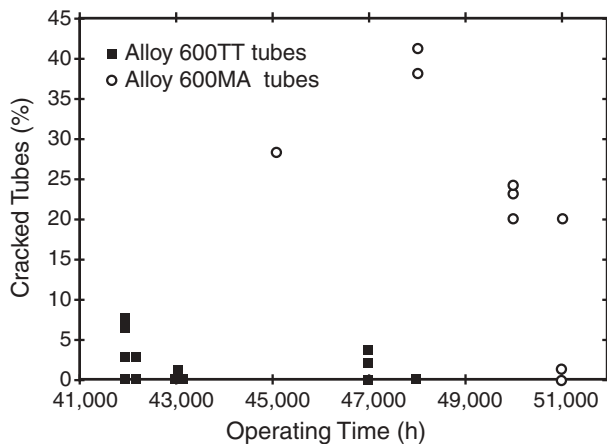
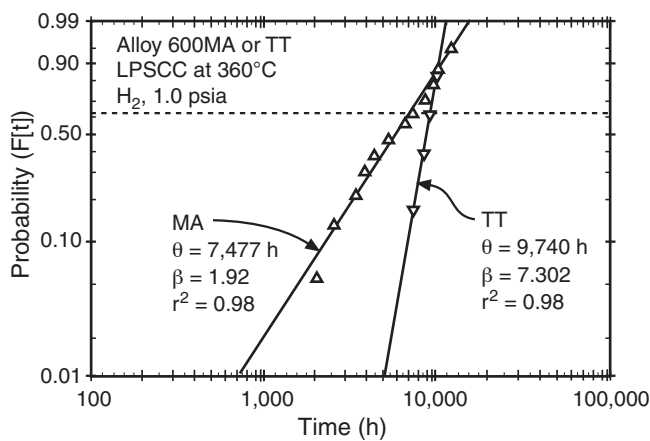
Some distinction, especially for LPSCC, has been made between high-temperature mill annealing (HTMA) and low-temperature mill annealing (LTMA) with the latter being more prone to LPSCC. Data illustrating the magnitude of this difference, from Airey,³¹¹ are shown in Figure 109(d). These data show that annealing in the range of 955°C substantially accelerates LPSCC relative to annealing in the 1,010°C range. In general, this effect does not apply to other submodes and does not make the difference in LPSCC between cracking and not. A slight difference between the HTMA and LTMA conditions was observed by Cullen³¹² in acidic solutions, as shown in Figure 126. However, the data in Figure 109(d) show clearly that the mill annealing temperature is important for LPSCC.

Angeliu and Was³¹³ showed that thermal treatment of Alloy 690 reduced the concentration of chromium at the grain boundary to concentrations as low as 18.8%. They also showed that the chromium profile became more shallow with time at heat treating temperatures.

A dominating correlation for the occurrence of LPSCC is the distribution of carbides relative to grain boundaries and the grain matrices. In general, metallurgical structures where the carbides are predominantly in the grain boundary mitigate LPSCC; where the carbides are predominantly in the grain matrix, LPSCC is accelerated. This trend is shown in Figure 110. As the concentration of carbides at the grain boundaries is increased, the time to initiate LPSCC is increased based on the work of Norring, et al.,²⁵¹ Gras,²² Cattant, et al.,³¹⁰ Saint-Paul and Zacharie,³¹⁴ and Garriga-Majo, et al.³¹⁵

Cold work accelerates LPSCC for both surface-initiated and pre-cracked specimens as shown in Figure 111 from the work by Airey³¹⁶ and Speidel and Magdowski.³¹⁷ This accelerating effect of cold work on crack growth is consistent with the general effect of strength on crack growth as correlated by Speidel and Atrens.³¹⁸

An important feature of the principal variable of structure is the condition of the surface. Figure 112



Processing Parameters, Hardness, Grain Size, and SCC Performance of MA Tubing, Heats E and F†

Processing Schedule	Furnace Mill Anneal Parameters °C:in./min	Tube Temperatures, °C	Hardness, R _B	Grain Size, μm	SCC Initiation Time, h
		T _{Peak} /t > 871, min.	Heat E/Heat F	Heat E/Heat F	Heat E/Heat F
1	1,066:6	1,043/22	57/57	75/90	*/*
2	1,010:24	977/4	65/65	32/35	*/*
3	982:24	949/3.5	72/68	19/27	4,000/*
4	954:24	910/3	76/70	13/18	1,700/2,900
5	927:24	893/2	74/72	15/16	2,900/1,700
6	899:24	866/-	76/75	13/13	2,900/*

† Tubing was not straightened or polished.

* No evidence of SCC when the test was terminated after 4,500 h.

(d)

FIGURE 109. (a) Probability vs time comparing the LPSCC of MA and TT specimens in 360°C pure water with a partial pressure of hydrogen at 1.0 psia. Four heats of material used. From Jacko.²⁹⁸ (b) Percent of tubes cracked in primary water vs operating time for TT and MA tubes. LPSCC located at sludge pile level. Results from eddy-current testing. From Cattant, et al.³¹⁰ ©1991 by the American Nuclear Society, La Grange Park, Illinois. (c) Time-to-cracking in primary water vs concentration of carbon for Alloy 600TT tubes. From Cattant, et al.³¹⁰ ©1991 by the American Nuclear Society, La Grange Park, Illinois. (d) Effect of mill annealing conditions for two heats of Alloy 600 on LPSCC. Tubing specimens as reverse U-bends (RUBs) exposed to pure recirculating water at 360°C with 20 psi hydrogen in make-up water. From Airey.³¹¹ ©1984 NACE International.

from the work of Rao³¹⁹ and Berge, et al.,³²⁰ shows examples where the surface and near-surface regions exhibit relatively high hardness or cold work as influenced by techniques of machining. Such hardness and the accompanying distortions strongly affect the initiation of LPSCC.

Berge, et al.,³²⁰ have shown that the depth and stresses of the machined layer are critical to the evolution of overall cracking. They have shown that the surface layer and its stresses are critical to the transition from the initiation stage to the propagation stage as defined by the depth at which K_{ISCC} is reached, as shown in Figure 87. If the stress in the surface layer is higher than that in the substrate, the

depth of cracks for transitions to the first stage of the crack growth curve is decreased and time-to-failure is earlier. Berge, et al.,³²⁰ in an example, start with the expression for the critical crack depth of $a_c = (1/4)(K_{ISCC}/\sigma)^2$. From this expression, if the stress in the surface layer is 1,000 MPa, due to superposition of the mean stress and that in the cold work layer, and the stress in the adjacent, nondisturbed substrate is 500 MPa, the critical values of a_c are, respectively, 25 μm and 105 μm for a K_{ISCC} of 9 MPa m^{1/2}. These values indicate three cases for the evolution of cracks:

1. If the depth of the disturbed layer is less than 25 μm, rapid propagation will not be reached until the initiation depth is 105 μm.

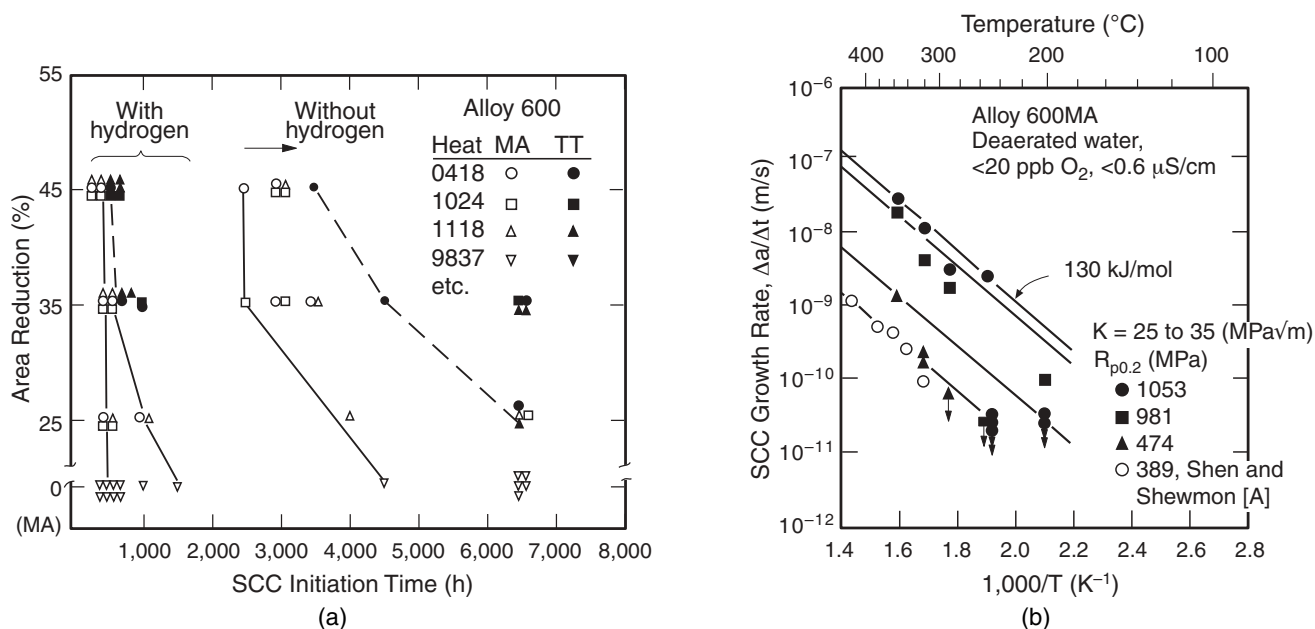


FIGURE 111. (a) Reduction of area as it affects LPSCC initiation time for Alloy 600MA and TT exposed to 360°C pure water with and without hydrogen additions for four heats of material. From Airey.³¹⁶ (b) Crack growth rate vs $1,000/T$ for Alloy 600MA with various yield strengths. From Speidel and Magdowski,³¹⁷ with data from [A] Shen and Shewmon.²⁹⁶ Courtesy of Electricité de France.

and 51.6 kcal/mol, respectively, have been determined. Figure 74 shows that the activation energy is continuous over water and steam environments.

Cassagne, et al.,³²² have reviewed various experiments for crack growth and have summarized their results in Figure 114(c), where both constant extension rate testing (CERT) and wedge opening loading (WOL) specimens have been used for testing LPSCC. Results in Figure 114(c) exhibit apparent activation energies of 19 kcal/mol to 54 kcal/mol, which are similar to the ranges described by Smialowska and Rebak.²⁴ However, the results of Speidel and Magdowski in Figure 111³¹⁷ exhibit activation energies for crack growth of 15.6 kcal/mol for the MA and cold-worked data.

While there is high variability in the experimentally determined activation energies for LPSCC initiation and growth rates, there appears to be a reasonable consensus that the most reliable and widely applicable activation energies for initiation and growth rate are in the ranges of 40 kcal/mol to 55 kcal/mol for initiation, and 30 kcal/mol to 35 kcal/mol for growth rate. For example, EDF has concluded that the best values are 43 kcal/mol and 31 kcal/mol for initiation and growth rate, respectively.⁽³⁾

7. Stress

Stress is important to LPSCC both for initiation from smooth surfaces and for propagation from pre-existing cracks. For tubing in SGs, which has ini-

tially smooth surfaces, Figure 115 applies. Pre-cracked specimens are most relevant to thicker cross sections such as those described in Table 17. The dependence of LPSCC on stress is shown in Figures 115 and 116 for specimens with smooth and pre-cracked surfaces, respectively. For specimens with smooth surfaces shown in Figure 115, the stress exponents are -4.0 and -5.7 , which are in the range expected for such tests. LPSCC of Alloy 600 in high-purity water and primary water exhibits a relatively high threshold stress, as shown in Figure 102(a) for initially smooth surfaces where LPSCC is compared with AkSCC, which exhibits a lower threshold stress.

Dependence of propagation of LPSCC on stress intensity is shown in Figure 116. Figure 116(a) shows the widely used correlation for LPSCC proposed by Scott,³²³ with some of the data used to develop the correlation. Figure 116(b) from Krasodonski, et al.,³²⁴ shows an extensive and uncensored database for Alloy 600MA. Figure 116(c), from Krasodonski, et al.,³²⁴ shows a censored database. Figures 116(d) and (e), from Jansson and Morin,³²⁵ compare uncensored and censored data for crack growth rate vs stress intensity for Type 304 stainless steel and are comparable to corresponding approaches for Alloy 600 in Figures 116(b) and (c), respectively.

The crack velocities in Figures 116(a) and (c) are compared with those from others obtained for LPSCC, HPSCC, and AkSCC in Figure 117. Here, the data are normalized to 320°C using $Q = 33$ kcal/mol, and stress intensities are taken as close to 30 MPa m^{1/2} as possible. The crack velocities include 4 orders of

⁽³⁾ Courtesy of F. Vaillant of EDF, 2002. Private communication.

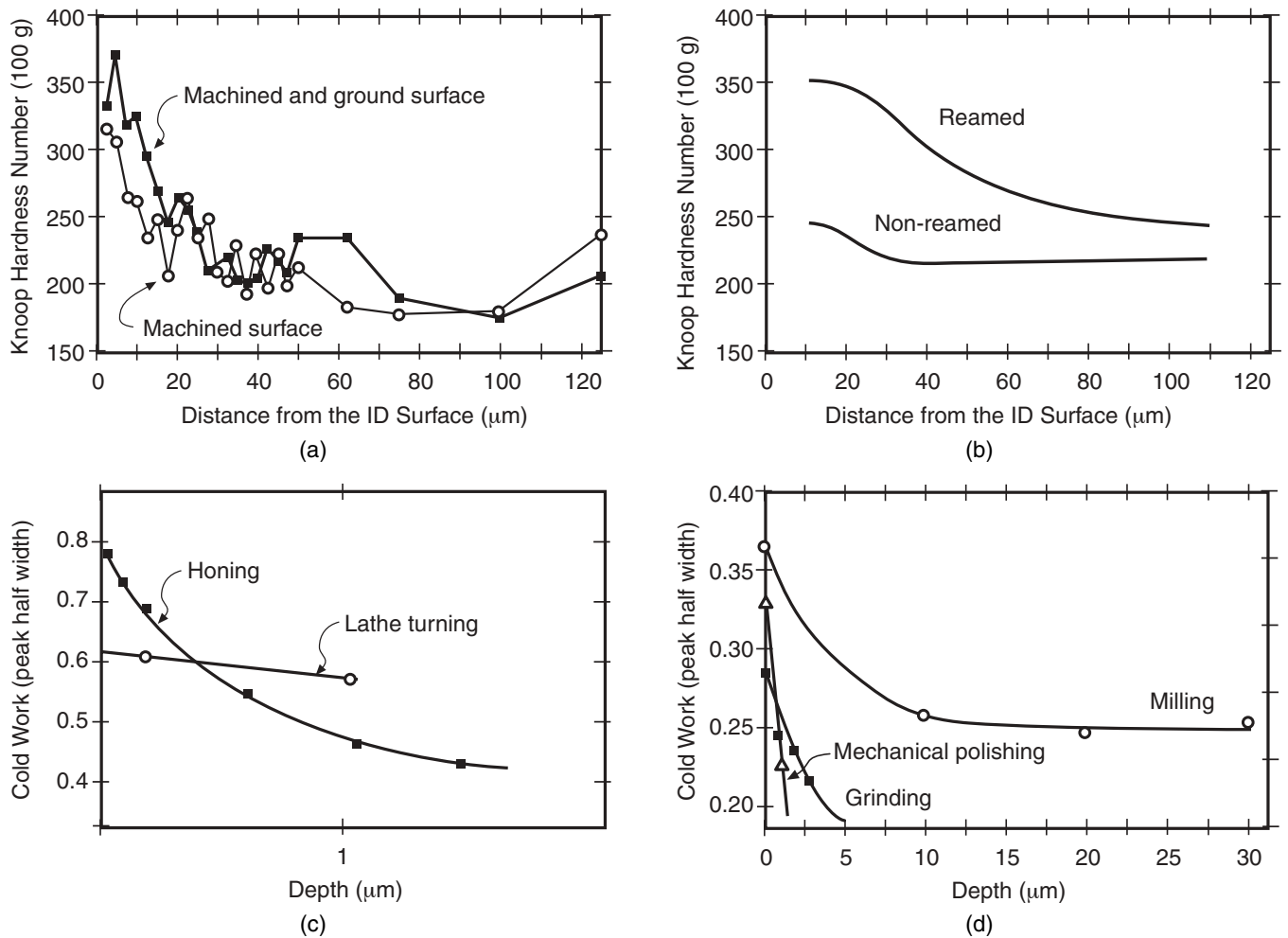


FIGURE 112. (a) Microhardness vs distance for surfaces machined and ground and only machined determined at the ID surface of a PWR reactor vessel closure penetration. From Rao.³¹⁹ Courtesy of TMS, Warrendale, Pennsylvania. (b) Microhardness vs distance from surface as affected by reaming at the ID surface of a pressurizer heater sleeve penetration used in pressurizer of a PWR primary system. From Rao.³¹⁹ Courtesy of TMS, Warrendale, Pennsylvania. (c) Cold work vs depth from measurements with grazing x-ray diffraction on Alloy 600 reactor vessel penetration. From Berge, et al.³²⁰ Reproduced Courtesy of Australasian Corrosion Association Inc. (d) Cold work vs depth for grazing x-ray diffraction on austenitic stainless steel. From Berge, et al.³²⁰ Reproduced Courtesy of Australasian Corrosion Association Inc.

magnitude. Within this range, the crack velocities for the three submodes from which data are taken are comparable. This comparability suggests that the propagation phases for these three submodes are similar. However, such a proposition has never been explored in detail.

A comparison of the threshold stresses for initiation and the K_{ISCC} and plateau velocities for propagation is relevant to the conditions for the transition from initiation to propagation shown in Figure 87. Since the threshold stress for initiation of LPSCC, as shown in Figures 102(a) and 115, is in the range of the yield stress, the transition from initiation to propagation will occur at more shallow depths for LPSCC than for AkSCC, as shown in Figure 87(b), since the latter tend to have lower threshold stresses, about 1/4 to 1/2 of the yield stress.

Figure 103 shows that LPSCC will occur as low as 288°C. Such an occurrence was related to Row 1 U-bends that are highly stressed. In addition, LPSCC has been reported²⁸² at the cold leg roll transitions of Conn. Yankee with a metal temperature of about 280°C. By the 18th cycle outage in 1995, 132 tubes in four steam generators had been plugged in the cold leg roll region compared with 217 tubes in the hot leg roll region. These data suggest an interaction between stress and temperature, which is actually well known based on the study of such interactions by Jiang and Staehle.²²²⁻²²³ The fact that what appears to be LPSCC occurred on the cold leg of the secondary surface in McGuire, shown in Figure 17, suggests that scratches provide high local stresses and further that such stresses may be in the range required for LPSCC at lower temperatures. Similar

TABLE 24
 Summary of LPSCC Failures for Alloy 600MA Exposed in Deaerated Pure Water at 349°C for 242 Days^(A)

Heat	Form	Total Failures	
		Pickled	Unpickled
A ^(B)	Bolted U-bend (4.0 in. x 0.688 in. x 0.125 in.)	4/4	1/4
B	Bolted U-bend (3.75 in. x 0.375 in. x 0.125 in.)	0/7 ^(C)	0/4
C	Biaxial disc (1.5 in. x 0.9 in.); spring-loaded at center	4/8 ^(C)	0/4

(A) From Rentler and Welinsky.²³⁴

(B) This heat was only slightly attacked by the pickling solution, whereas the other heats were extensively penetrated at the grain boundaries.

(C) Higher total number includes additional specimens pickled as a check on the pickling effect.

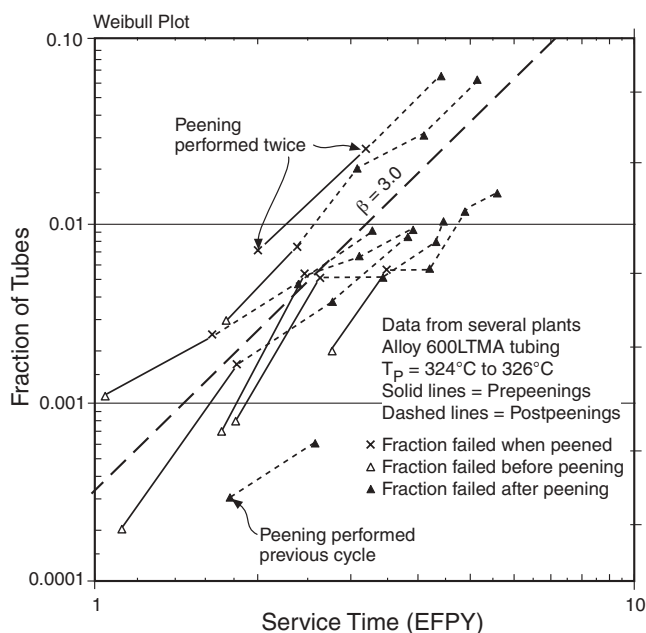


FIGURE 113. Probability vs service time using Weibull coordinates for the fraction of tubes failed at the P*/F* LPSCC in Model D SGs with full depth rolls. $T_p = 324^\circ\text{C}$ to 326°C . LTMA tubing. From Gorman, et al.³²¹ Used by permission of EPRI.

scratches are associated with the occurrence of SCC, possibly LPSCC, on the secondary side of the upper bundle of OTSGs, as shown in Figure 72. Cold leg LPSCC has been observed in plants other than McGuire and Catawba.

Welding stresses also have produced LPSCC at instrument nozzles as shown in Figure 118 from Alter, et al.,³³⁴ Boudot, et al.,³³⁵ and as noted in Table 17. Here, welding of the nozzle on the inside of the pressurizer caused it to deform, thereby producing high residual stresses and subsequent SCC. This SCC would have been accelerated since pressurizers operate at 10°C to 20°C above hot leg temperature (T_H). The high residual stresses, plus the higher temperatures, produce LPSCC similar to that produced by scratches shown in Figure 17.

Only a limited amount of work has been conducted to determine the corrosion fatigue behavior of Alloy 600MA. Data from Jacko and Willertz,³³⁶ for the

corrosion fatigue behavior of Alloy 600MA, are shown in Figure 119(a). These data have been obtained using smooth specimens exposed to water with various chemistries in the temperature range from 300°C to 316°C . The higher amplitude of the pH 12.6 data relative to the pH 2.0 data is consistent with the improved state of passivity at the higher pH. The higher oxygen produced no significant change at pH 2.0; this is expected since there is a broad range of film-free conditions at this pH. These data would be applicable to high cyclic frequencies since they were conducted at 20 kHz. However, such data would not be typical of low cyclic frequencies, especially with the environments used.

Figure 119(b) shows data from Ogundele and Lepik³³⁷ for crack propagation taken at 0.5 Hz and at $R = 0.1$ and 0.8 for Alloy 600MA in air, water, and a simulated crevice environment calculated for CANDU steam generators. Here, the crack growth rates for water and air are not significantly different. The data for the base crevice environment seem out of place relative to an expectation of acceleration from the chemistry used. However, it appears that the testing encountered a crack closure problem as corrosion products accumulated in the advancing cracks. Such a problem is common at low stress intensities in corrosive environments.

5.2.3 Acidic SCC (AcSCC), Including Cl^- , SO_4^{2-} , and Cu^{2+} — AcSCC, as defined in the mode diagrams of Figures 82, 84, and 85, has analogs in steel as shown in Figure 83 and in stainless steels, including the boiling magnesium chloride (MgCl_2) solutions studies, for example, by Copson²²⁷⁻²²⁸ in Figure 89 and by Warren⁵⁹ in Figure 9. This submode includes both mildly acidic and neutral regions.

AcSCC is important because heat-transfer crevices are generally in the neutral region of pH as shown by Figure 53; and AcSCC extends from strongly acidic to about $\text{pH}_T 9$ (pH at temperature and calculated or measured at temperature). Further, molar ratio control using additions of Cl^- can shift the crevice pH in the acidic direction. Finally, anodic corrosion processes tend to acidify local regions. For the present, this is a nominal confusion between what is classified here as AcSCC or AkSCC. In view

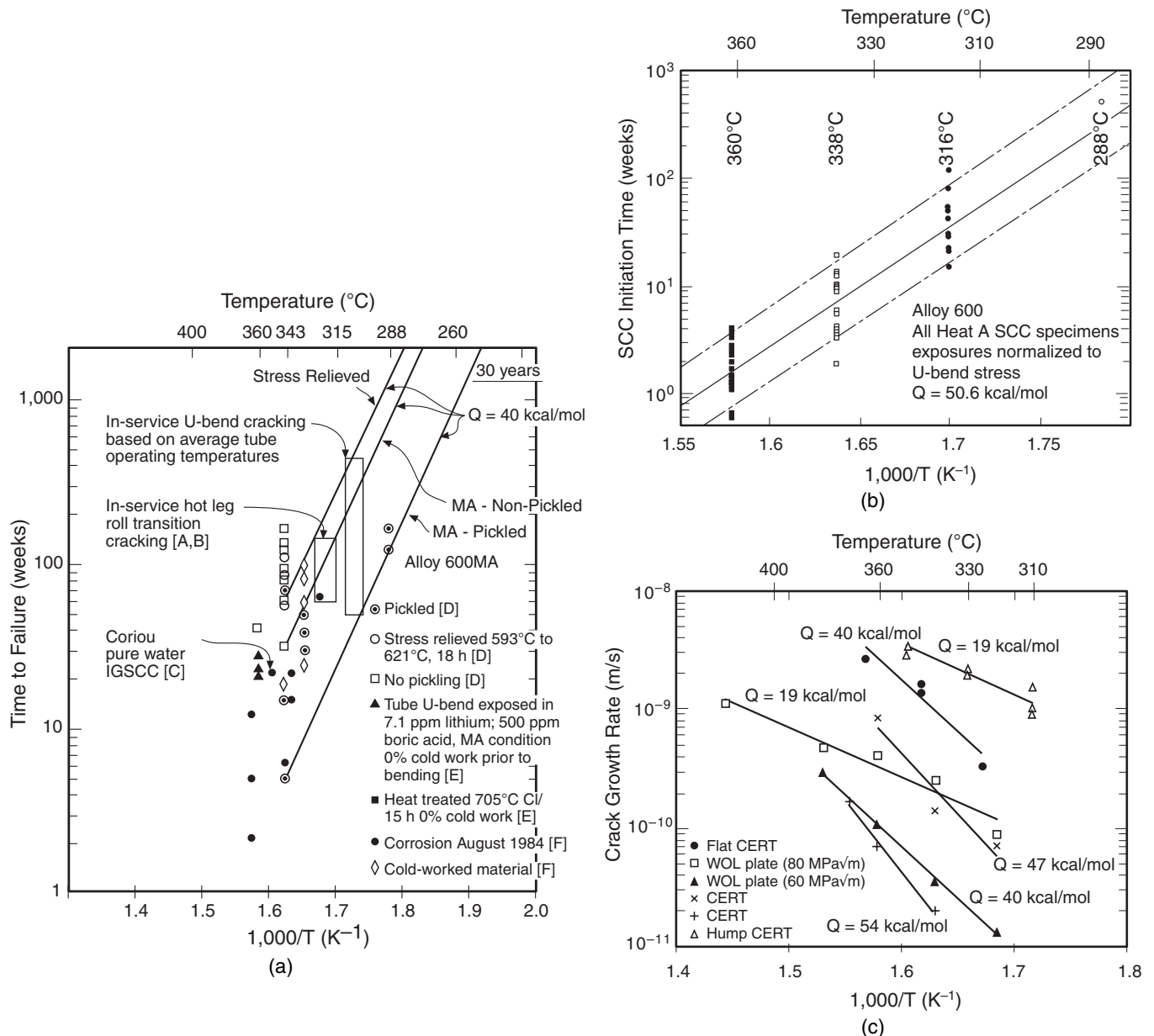


FIGURE 114. (a) Time-to-failure vs $1,000/T$ for laboratory and service results of LPSCC in Alloy 600MA. From McIlree, et al.,³²⁶ with data from [A] Schenk,³²⁷ [B] Shoemaker,³²⁸ [C] Coriou, et al.,¹ [D] EPRI,³²⁹ [E] Domain, et al.,³³⁰ and [F] Pathania and Lim.³³¹ Used by permission of EPRI. (b) SCC initiation time vs $1,000/T$ for Alloy 600 using U-bend specimens in water. From Webb.³³² Courtesy of TMS, Warrendale, Pennsylvania. (c) Crack growth rate vs $1,000/T$ for Alloy 600MA from six authors using CERT- and WOL-type specimens. From Cassagne, et al.^{23,322} Courtesy of TMS, Warrendale, Pennsylvania.

of the data in Figures 121 and 122, the domain of AkSCC extends into nominally alkaline pH but at a progressively lower rate. However, owing to the chemical similarities, data from complex environments in Table 20, where pH is in the neutral range, seem more related to AkSCC. These classifications may need to be reviewed as more data become available.

AcSCC is distinct from reduced sulfur low-valence stress corrosion cracking (S^vSCC) and is discussed in Section 5.2.6. In the case of reduced

sulfur, SCC probably can be accelerated at any pH (although experiments at pH less than that of all volatile treatment [AVT] have not been conducted), and Alloy 600 in MA and sensitized heat treatment (SN) conditions are particularly prone to SCC in this submode. Further, this effect is mainly related to anions with sulfur valences of -2, +2, and +2.5; AcSCC is limited mainly to +6 valences and from strongly acidic, about pH 2, to mildly alkaline, pH 9. Possibly, +4 valences are part of this set, but no SCC has been investigated for this valence, although some

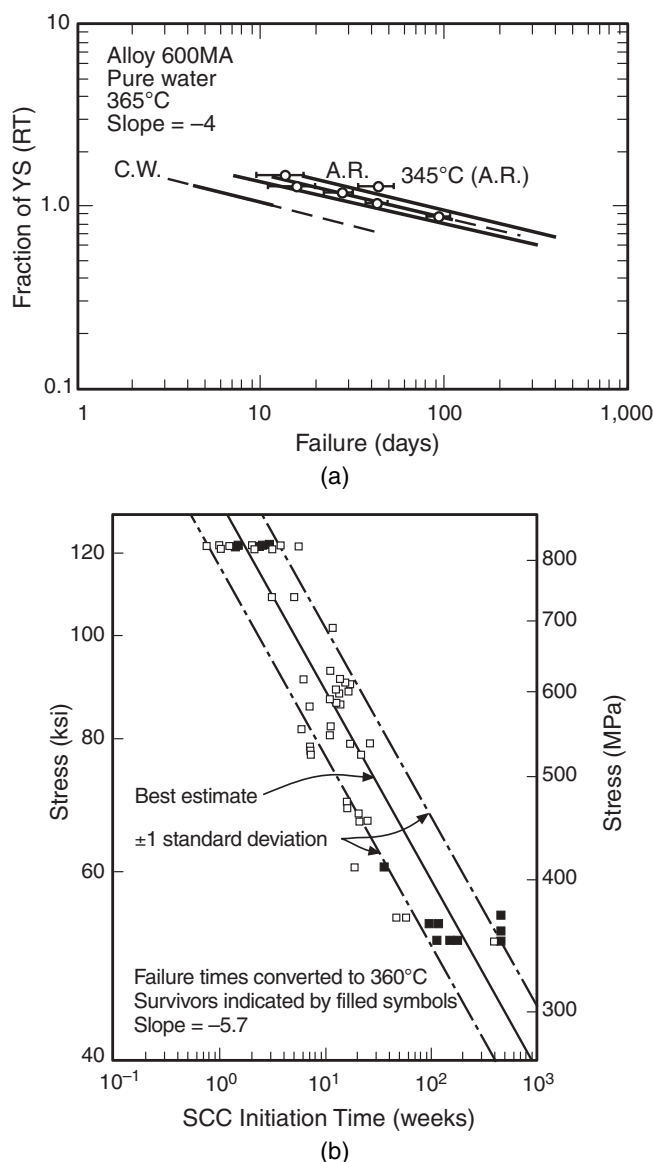


FIGURE 115. (a) Fraction of RT yield stress vs time to failure for Alloy 600MA at 365°C in pure water. Stress exponent about -4 . Yield point stresses in the range of 323 MPa to 386 MPa. From Bandy and van Rooyen.³³³ (b) Applied stress vs SCC initiation time for Alloy 600MA tested at 360°C. Stress exponent about -5.7 . (Data on yield stress not available in the publication. However, if 350 MPa is assumed and the data were plotted as a function of a fraction of the yield stress, as in Figure 115[a], the general shapes of the data in both figures are similar.) From Webb.³³² Courtesy of TMS, Warrendale, Pennsylvania.

electrochemical correlations with SCC have been carried out by Fang and Staehle.³³⁸

As discussed in this section, AcSCC includes the submodes described in Figure 82(b) of copper stress corrosion cracking (CuSCC) and chloride stress corrosion cracking (ClSCC), as well as those associated with sulfate solutions. There is not much information on effects of chloride solutions except those containing lead, as discussed in Section 5.2.5.

However, the lack of such information should not imply that chloride-based acidic solutions do not produce SCC; in fact, the reverse is true, as shown Figure 89 and in two publications by Berge and coworkers,²¹²⁻²¹³ where ClSCC was observed in the range of 100°C.

There is some question of whether AcSCC intersects with LPSCC as suggested in Figure 82(a). For example, the results of Berge and Donati²¹² in Figure 89 at pH 2.0 to 2.3 and those of Smialowska, et al.,²⁴⁹ at pH 3.4 both exhibit transgranular SCC.

As background, Figure 120 shows work from Cullen³¹² in Figure 120(a) and work from Choi and Was³³⁹ in Figure 120(b), both of which relate to the combined effects of Cl^- and SO_4^{2-} environments. These figures show that the general corrosion associated with SO_4^{2-} proceeds more rapidly than that associated with Cl^- environments, there being an approximately 2-orders-of-magnitude difference at the same pH; the Cl^- environment is less corrosive and the correlation slopes for the two cases exhibit the same slope with pH. Further, the general corrosion for Alloys 600 and 690 is about the same. Figure 120(b) shows that the acuity of pits increases as the ratio of $\text{Cl}^-/\text{SO}_4^{2-}$ increases. The results of Figures 120(a) and (b) imply the same trends.

The result that Cl^- environments should inhibit dissolution, as shown in Figure 120(a), is not surprising since Cl^- inhibits the corrosion of steel, and this role has been studied extensively, although mostly in the range of room temperatures. With respect to corrosion in steam generators, the results in Figure 120(a) indicate that, at the same pH, the Cl^- and SO_4^{2-} anions may produce quite different effects on AcSCC. For example, in Figure 120(b), the pit acuity depends on the ratio of $\text{Cl}^-/\text{SO}_4^{2-}$ with increasing Cl^- increasing the acuity. The schematic illustration in Figure 120(c), of progressive increase of acuity associated with the data of Figure 120(b), suggests that such effects on acuity could lead toward a condition for SCC with increased chloride.

In this section, several nominally different submodes are combined, as identified in Figure 82(b); ClSCC, CuSCC, and AcSCC are combined and considered as a single submode. It appears from the present patterns that this is a reasonable approach. The three submodes, for the purpose of this discussion, are considered as a single one that depends in various functional ways on potential, pH, chloride, sulfate, and other conditions.

AcSCC has not been studied to the same extent as LPSCC and AkSCC. There is less information on effects of potential, concentration of the anions, alloy composition, alloy structure, temperature, and stress. Information is more complete regarding the effects of pH than it is for the other variables.

The dependence of AcSCC upon primary variables is as follows:

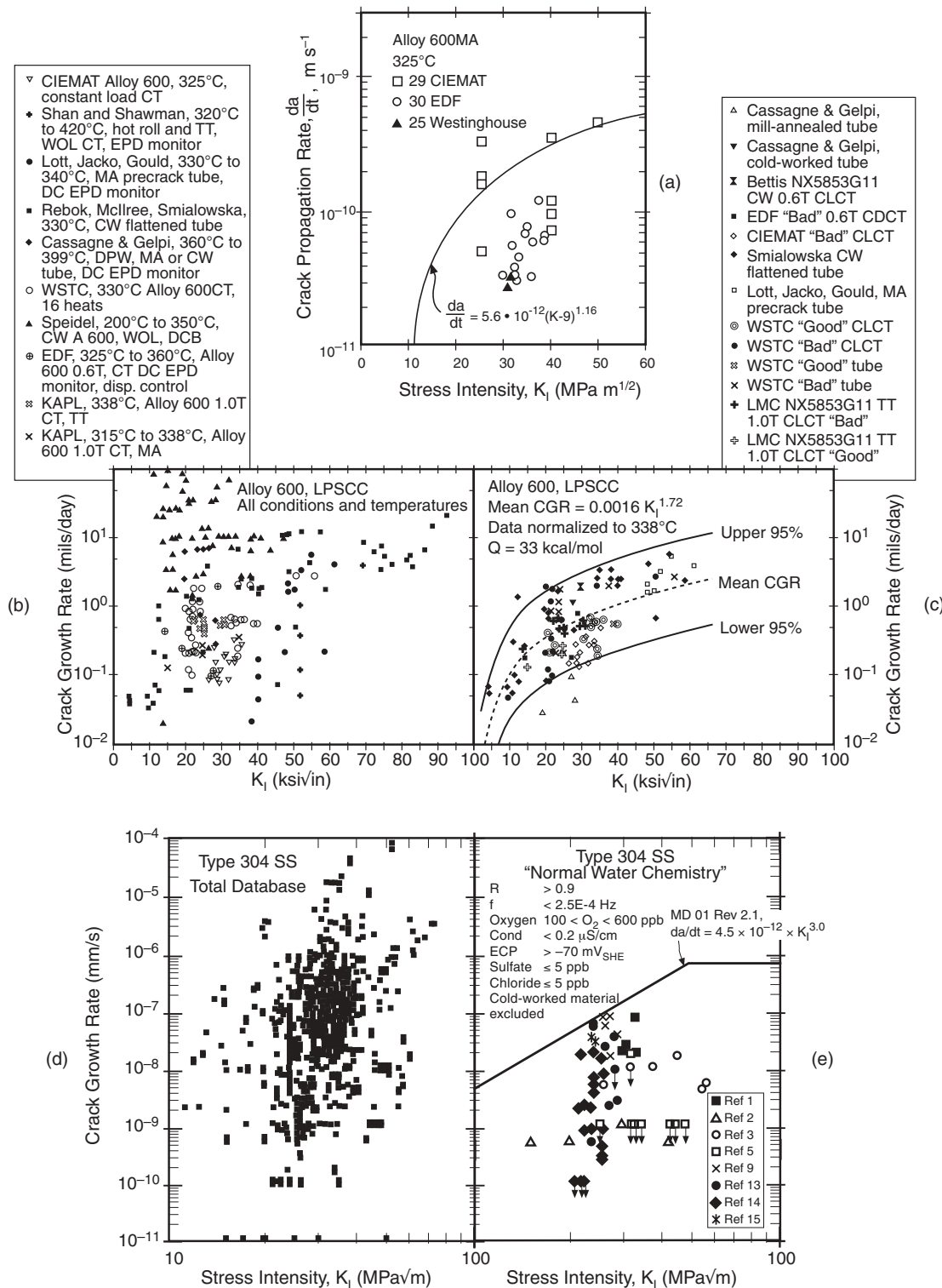


FIGURE 116. (a) Crack propagation rate vs stress intensity for Alloy 600MA at 325°C. From Scott.³²³ ©1996 NACE International. (b) Noncensored database for crack growth rate vs stress intensity for Alloy 600MA. Various fabrication conditions and temperatures included. From Krasodonski, et al.³²⁴ Used by permission of EPRI. (c) Censored database for crack growth rate vs stress intensity with all data normalized to 338°C using $Q = 33$ kcal/mol. Basis for censoring included: instrumented and/or constant or active load tests; pre-cracked fracture mechanics test specimens tested in high-purity water in a flowing autoclave with constant hydrogen over pressure; and good microstructure with high % of IG carbide coverage. From Krasodonski, et al.³²⁴ Used by permission of EPRI. (d) Available data for crack growth rates in a database for sensitized Type 304 stainless steel exposed to boiling water nuclear reactor (BWR) environments. From Jansson and Morin.³²⁵ ©1997 by the American Nuclear Society, La Grange Park, Illinois. (e) Censored data applicable to the conditions noted on the figure. Bounding line shown. From Jansson and Morin.³²⁵ ©1997 by the American Nuclear Society, La Grange Park, Illinois.

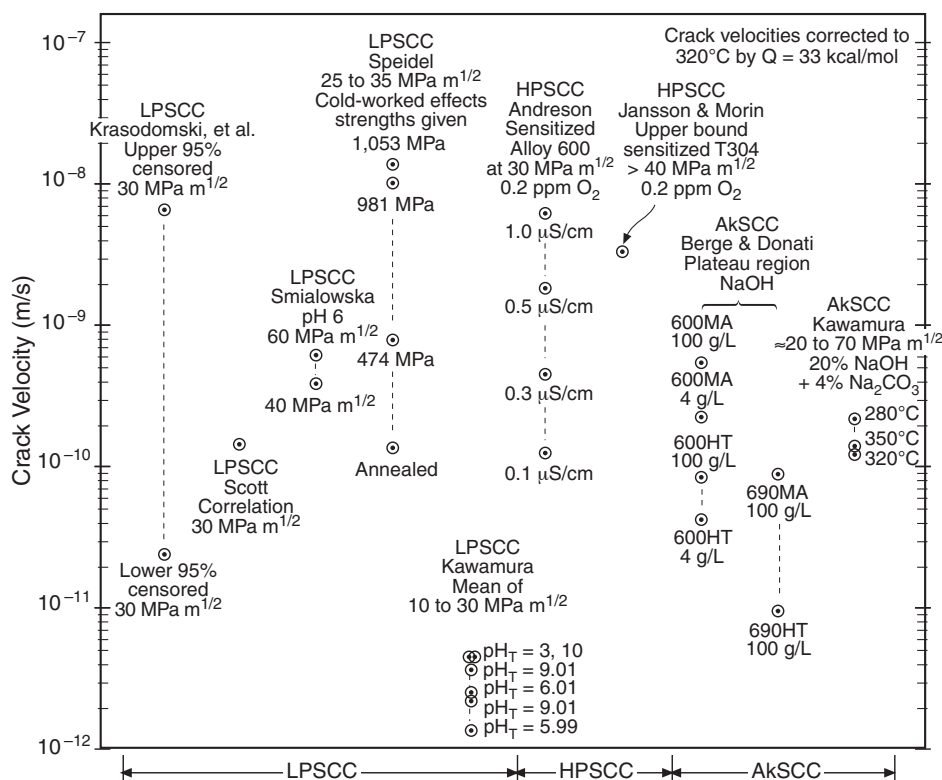


FIGURE 117. Crack velocity from various studies of LPSCC, HPSCC, and AkSCC. All data normalized to 320°C with $Q = 33$ kcal/mol. Where possible, crack velocities were taken at 30 MPa $m^{1/2}$. From left to right data taken from: Krasodomski, et al.,³²⁴ Scott,³²³ Smialowska, et al.,²⁴⁹ Speidel and Magdowski,³¹⁷ Kawamura, et al.,¹⁴⁵ Ford and Andresen,²²⁶ Jansson and Morin,³²⁵ Berge and Donati,²¹² and Kawamura and Hirano.²⁶⁰

1. pH

AcSCC is relatively intense at values of pH as low as 2 and decreases monotonically with increasing pH to about pH 10, as shown in Figures 121 and 122. As shown in Figure 121, studies by Smith, et al.,²⁸⁰ Newman,³⁴⁰ and deBouvier, et al.,¹⁵³ agree on this pattern. It appears that AcSCC is negligible at about the pH where AkSCC becomes significant, as defined in Figure 96 and Table 19. This pattern of AcSCC decreasing with increasing pH to some point, and AkSCC increasing starting at about the same point is similar to that for carbon steels as shown in Figure 83, as well as in Figure 46, and is a consequence of the location of minimum solubility as a function of pH as shown in Figures 38, 46, and 83. However, the experiments summarized in Figure 85 for Alloy 600MA do not show AcSCC occurring at higher values of pH, although the general trend is the same.

Also, at pH 2.0 to 2.3, AcSCC occurs relatively rapidly and transgranularly in a H_3BO_3 -chloride electrolyte at 100°C. For reference, the pH of a boiling 42% $MgCl_2$ solution at 154°C is 4.1. This transgranular result is similar to that observed by Smialowska, et al.,²⁴⁹ for pH 3.4 in Table 21. Why such transgranular SCC should occur while the other SCC is IG is not clear, although it should be noted that

PbSCC exhibits both morphologies as shown in Figure 136.

2. Potential

Figure 123(a) shows that AcSCC depends on potential in much the same way, although not quite in a symmetrical bell curve, as does AkSCC shown in Figure 97; whereas, the work of deBouvier, et al.,³⁴¹ in Figure 123(b) shows that the maximum AcSCC occurs at about the corrosion potential and decreases at both higher and lower potentials. Results from Figure 85 also show that increasing the potential increases the intensity of AcSCC for Alloys 600MA and 600TT while Alloy 690TT does not sustain AcSCC. This work agrees generally with that of Cullen,³¹² where the AcSCC is not intense at the deaerated corrosion potential. From these data an upper limit is not so clear as it is in Figures 123(a) and (b).

Figure 124 from Pierson and Laird²¹⁰ shows data where the potential has been varied using hydrogen and cupric oxide (CuO) at two values of pH and for Alloys 600MA (LTMA) and 690TT, although the potentials were not measured. Here, increasing the potential to a maximum value by adding copper and omitting hydrogen increases the cracking rate for both Alloys 600MA and 690TT. The potential, as increased by adding CuO and omitting hydrogen,

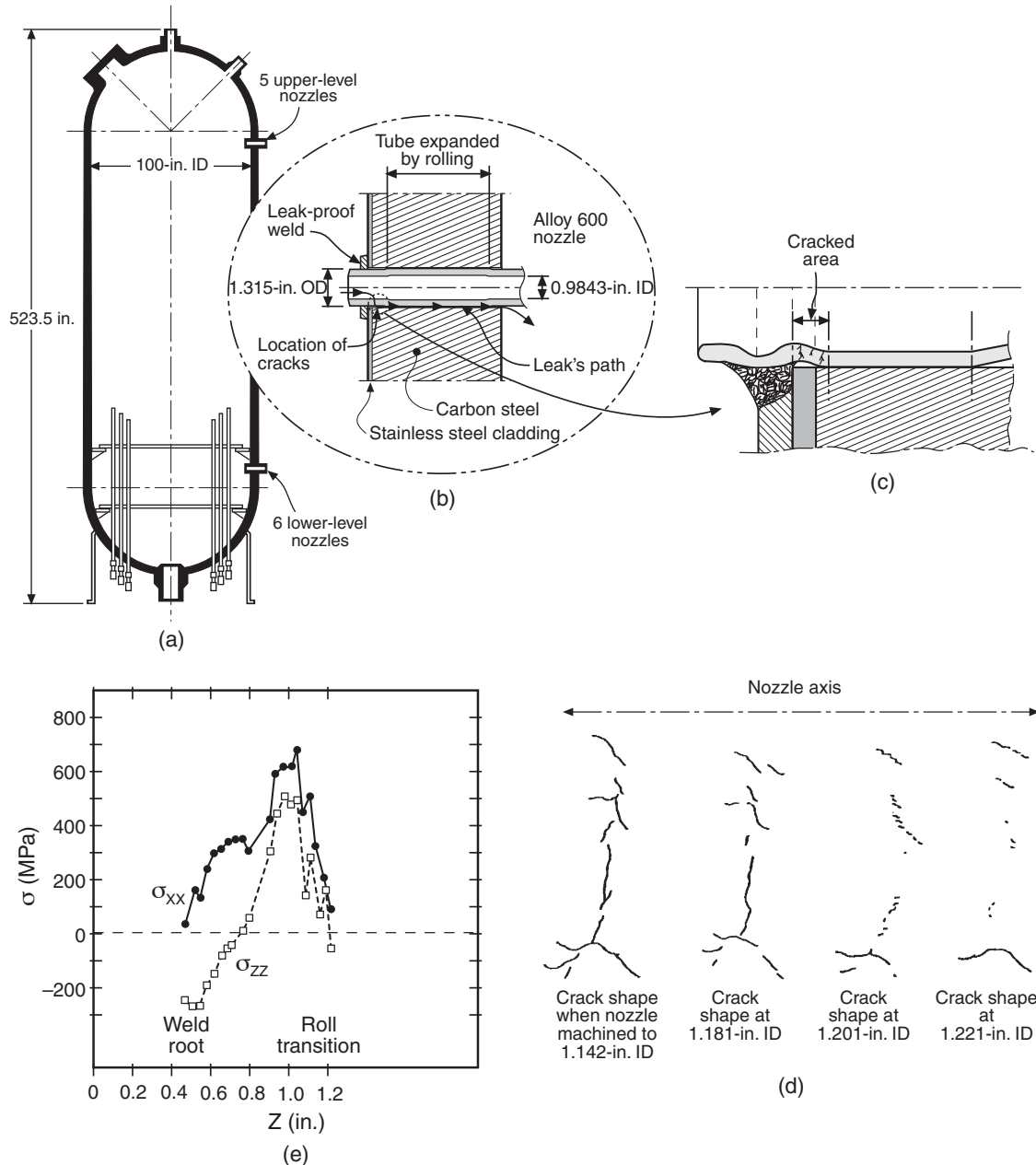


FIGURE 118. (a) Overall view of pressurizer from 1300 MW plant showing locations of instrument nozzles. (b) Overview of nozzle showing locations of weld and leaks. (c) Detailed view of nozzle showing effect of welding on the roll transition zone and location of cracks. (d) Detailed view of SCC with dimensions given in terms of ID and successive machining to reveal shape of SCC. Destructive examination of one nozzle from Flamanville-2. (e) X-ray diffraction measurements of the inner surface residual stresses. From Alter, et al.³³⁴ ©1992 by the American Nuclear Society, La Grange Park, Illinois.

seems to affect the SCC of Alloy 600MA in the same way as shown in the work of Cullen³¹² in Figure 123(a). Raising the potential increases the rate of SCC for Alloy 690TT contrary to the work in Figures 85 and 123(b). The effect of potential on the SCC of Alloy 690TT seems controversial since the work of deBouvier, et al.,³⁴¹ intentionally investigated the effect shown by Pierson and Laire²¹⁰ and emphasized the absence of any SCC in the Alloy 690TT. However, it appears that the conditions of the two investiga-

tions were not quite the same, and more work is needed to understand this difference.

3. Species

Contrary to the prediction of Copson²²⁷⁻²²⁸ shown in Figure 89(a), Alloy 600MA sustains AcSCC in acidified chloride solutions at temperatures as low as 100°C, as shown by Berge and Donati²¹² in Figure 89(b) and by Berge, et al.,²¹³ although most of the work shown in Figures 121 through 124 was conducted in sulfate solutions. The data of Cullen³¹² and

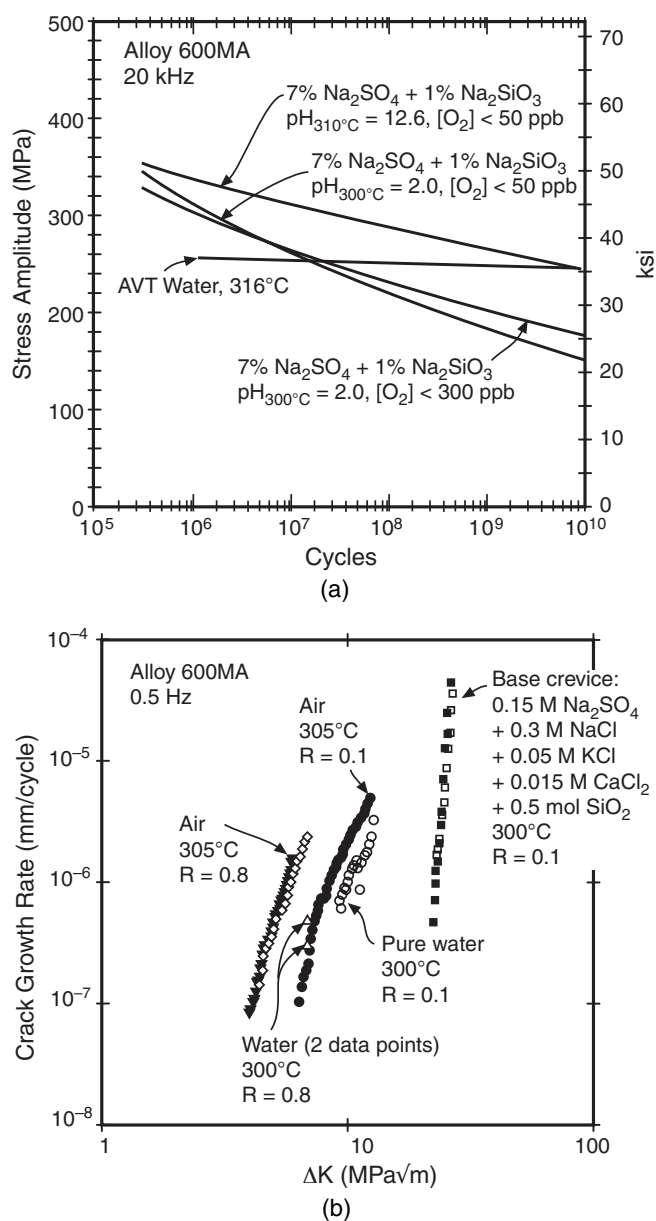


FIGURE 119. (a) Stress amplitude vs number of cycles at 20 kHz for Alloy 600MA exposed to various deaerated solutions and pH in temperature range of 300°C to 316°C. From Jacko and Willertz.³³⁶ ©1984 NACE International. (b) Crack growth rate vs ΔK for Alloy 600MA exposed at 0.5 Hz to air, water, and a base crevice environment for two values of R . From Ogundele and Lepik.³³⁷ Reproduced with permission of Canadian Nuclear Society.

Choi and Was³⁴² in Figure 120 suggest that chloride environments should be more aggressive than sulfate, owing to the increased acuity of localized corrosion and the suppression of steady-state dissolution. While this speculation has not been tested, the ready occurrence of AcSCC in chlorides shown by Berge and Donati²¹² supports this proposition.

The addition of CuO to solutions most likely functions by raising the potential in accordance with the equilibrium half-cell potential shown in Figures 7

and 40(b). Such additions of CuO to alkaline solutions, as discussed in Section 5.2.1.2, were used extensively to achieve higher potentials. Figure 124(c) shows that copper exerts its effect through the higher half-cell potential of CuO as compared to Cu⁰; this is a reasonable result. Variations in hydrogen as used by Pierson and Laire²¹⁰ in Figure 124 also affect potential, according to its effect on the equilibrium half cell as illustrated in Figure 42 and demonstrated in Figure 40(c).

Figure 122 shows that increasing the concentration of sulfate at the same pH increases the rate of SCC; this is contrary to the speculation based on Figure 120(a) that sulfate should not intensify SCC but rather should promote general corrosion (GC). Figure 124 from Pierson and Laire²¹⁰ shows that cationic resins with sodium silicate (Na₂SiO₃) and magnetite (Fe₃O₄) do not exert much effect.

Cullen³¹² has shown that adding zinc oxide (ZnO) significantly decreases the corrosion rate of Alloys 600MA and 690TT in both acidified sulfate and chloride solutions, as shown in Figure 125. The activation energy is about 15 kcal/mol and is consistent with a dissolution or chemical process; this activation energy for generalized corrosion is the same for the presence and absence of the ZnO.

Some complex environments at mid to slightly acidic pH are discussed in Table 20 in Section 5.2.1.3 in connection with AcSCC. This table also shows results from acidic environments. However, the pattern of these environments does not agree with the regular ones such as shown in Figures 121 and 122. More needs to be known about these complex environments.

4. Alloy Composition

In general, as shown in Figures 85, 121, and 122, Alloy 600MA is more prone to AcSCC; Alloy 600TT also sustains AcSCC but at lower rates. Alloy 800 (UNS N08800) sustains AcSCC as shown in Figure 121(b), but the AcSCC does not persist above about pH 6. At the open-circuit potential, Alloy 690TT does not seem to sustain AcSCC in the environments studied; however, this alloy seems to increase its proneness to AcSCC with increased potentials based on the work of Pierson and Laire,²¹⁰ although the work of deBouvier, et al.,³⁴¹ possibly contradicts the Pierson and Laire work. These general patterns are similar to those for AcSCC, although there is more agreement on the proneness of Alloy 690 to AcSCC. Possibly, the difference between the deBouvier work and the Pierson and Laire work is due to very high stresses and cold work in the capsules used by Pierson and Laire.

5. Alloy Structure

There are no significant data for effects of alloy structure on AcSCC except for effects due to the TT treatment relative to MA as discussed in the Alloy Composition section above and the difference be-

tween LTMA and HTMA treatments shown in Figure 126. There are no data concerning cold work or the distributions of carbides.

6. Temperature

Cullen³¹² has shown that general corrosion follows a 1/T pattern with an activation energy of 15 kcal/mol, as shown in Figure 125. There do not appear to be other significant data regarding the effects of temperature on AcSCC.

7. Stress

Effects of stress on AcSCC have been investigated only by deBouvier, et al.,¹⁵³ and Cullen.³¹² Cullen has studied the number of cracks and their depth as a function of the angle around C-ring specimens taken from tubes. His data are given in Figure 126 and show that the number of cracks nucleated is generally independent of the angular distribution around his C-ring specimens despite a regular variation in strain. The increase in potential increases the number of cracks, and the depth of the cracks decreases with decreasing strain. The results suggest that the nucleation of SCC does not depend much on the amount of plastic strain but that the propagation does. The increase in number of cracks follows the dependence of AcSCC on potential.

The extensive AcSCC shown in Figure 126 suggests that the threshold stress is probably low and much like that for AkSCC.

In Figure 126, the HTMA and LTMA heat treatments are also studied. While there are some differences in detail, more generally, it seems that these heat treatment conditions are not significantly different as they are in LPSCC as discussed in Section 5.2.2.5 in connection with Figure 109(d).

5.2.4 High-Potential SCC (HPSCC) — HPSCC, as shown in Figure 82(a), is generally not relevant to SGs since the additions of N₂H₄ eliminate oxidizing species and lower the potential; while the low concentration of hydrogen on the secondary side of SGs tends to raise the potential, relative to the primary side, this influence may be offset by the effect of N₂H₄. The bases for these two conflicting trends are shown in Figure 33 where the 1-ppb line for the H₂O/H₂ half cell is shown to be about 250 mV above the standard H₂O/H₂ line, and the equilibrium half cell for the N₂/N₂H₄ is about 500 mV below the standard H₂O/H₂ line. According to direct measurements as shown in Figure 45(a), adding N₂H₄ is effective in lowering the potential, although the problem of competing low hydrogen and high N₂H₄ effects on the electrochemical potential has not been investigated directly. One evidence for lowered potentials in crevices has been the decreased extent of SCC with increased N₂H₄ additions.

HPSCC is possibly relevant to SGs if N₂H₄ were not added or if there were an infusion of oxygen or oxygen surrogates such as Cu⁺⁺ at startup. However, N₂H₄ is added to AVT water during normal power op-

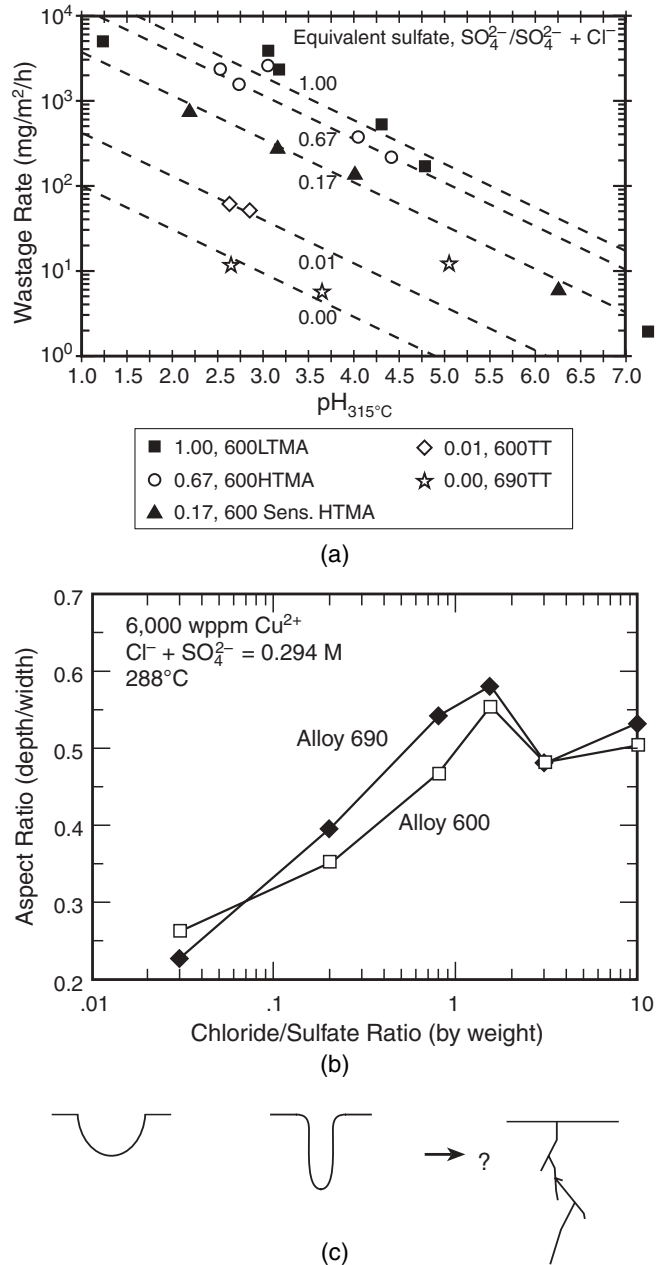


FIGURE 120. (a) Wastage rate vs pH for retort tests using Alloys 600 and 690 in various heat treatments in concentrated acidified sulfate and chloride solutions at a test temperature of 315°C. From Cullen.³¹² ©1996 NACE International. (b) Aspect ratio for pits vs Cl⁻/SO₄²⁻ ratio for Alloys 600 and 690 exposed in 6,000 wppm Cu²⁺ at 288°C for Cl⁻ + SO₄²⁻ = 0.294M. From Choi and Was.³³⁹ ©1990 NACE International. (c) Schematic view of implications of increasing acuity. From Staehle.¹⁹ ©1996 NACE International.

eration to both recirculating steam generators (RSGs) and OTSGs. Also, in the case of AkSCC, chromic oxide (Cr₂O₃) becomes soluble at relatively lower potentials according to the steeper slopes of the Cr⁶⁺/Cr₂O₃ lines, as shown in Figure 73, relative to the H₂O/H₂ equilibrium half cells. This trend may increase susceptibility to AkSCC. This lowering of the Cr⁶⁺/Cr³⁺

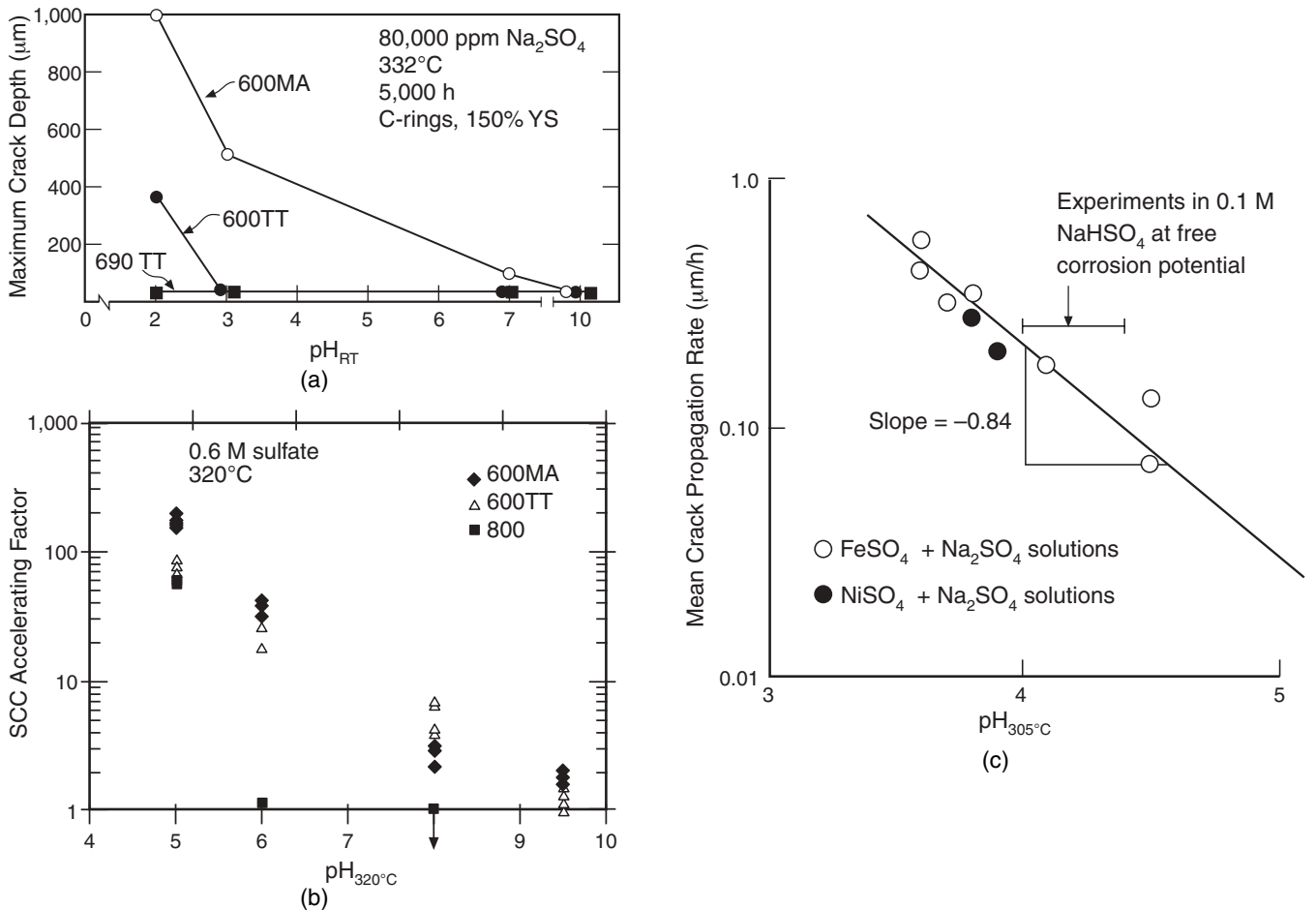


FIGURE 121. (a) Maximum crack depth vs room temperature pH for Alloy 600MA, Alloy 600TT, and Alloy 690TT exposed in acidic sulfate solutions at 332°C for 5,000 h as C-rings stressed to 150% of the yield strength. From Smith, et al.²⁸⁰ ©1985 by the American Nuclear Society, La Grange Park, Illinois. (b) SCC accelerating factor vs pH for three alloys in 0.6 M sulfate environments at 320°C. Accelerating factor taken from the rate of crack initiation at 0.001 M ($\text{pH}_{320^\circ\text{C}} = 5$) being the reference. 150% YS refers to the “two legs touching” (TLT) condition of the branches of the C-ring; below this stress, specimens were stressed at 0.8 YS and 1.0 YS. From deBouvier, et al.¹⁵³ Courtesy of TMS, Warrendale, Pennsylvania. (c) Mean crack propagation rate vs pH for nonsensitized Alloy 600MA in sulfate at 305°C. From Newman.³⁴⁰

equilibrium half cell relative to the $\text{H}_2\text{O}/\text{H}_2$ half cell makes the HPSCC submode coincident with the AkSCC submode above about pH 9.

HPSCC differs from LPSCC with respect to the influence of sensitization. Sensitization accelerates HPSCC in Alloy 600 and Type 304 similarly, as shown in Figures 88(e) and 117. Sensitization mitigates, but does not prevent, LPSCC of Alloy 600; and sensitized Type 304 does not sustain significant SCC in the LPSCC region.

The HPSCC submode is mainly of interest to BWR technology where normal water chemistry has been characterized by relatively high potentials according to the dependence of potential on oxygen as shown in Figures 40(a), 88(d), and 88(e). The normal water chemistry in BWRs contains about 0.2 ppm of oxygen. The newer technology of BWR water chemistry includes using hydrogen water chemistry with noble metal additions; the resulting potentials on

structural materials now approach those of pressurized water reactors (PWRs) relative to the standard $\text{H}_2\text{O}/\text{H}_2$ half-cell equilibrium, as shown in Figure 93. However, the BWR technology operates at lower pH since no alkalizers are added to the water chemistry. Also, most of the work in support of BWRs has been conducted with sensitized alloys induced by welding. Little of this is applicable for the lower potential PWR SG case.

Essential dependencies of HPSCC on primary variables that may be relevant to SGs during incursions of O_2 or CuO , particularly at startup, are as follows:

1. pH

The pH relevant to BWRs is in the general range of 5.5 at temperature, whereas that on the secondary side of steam generators is in the range of 7 to 8 at temperature. Virtually no work has been conducted in support of BWR technology that is relevant to the

range of pH on the secondary side of SGs, although it does not follow that the results themselves are irrelevant. Some work by Totsuka and Smialowska³⁴³ has been conducted at values of pH that are relevant to BWRs, as shown in Table 22, but the temperatures are higher according to typical PWR temperatures.

2. Potential

The most extensively explored variable in work to support BWR technology has been potential since the occurrence of SCC of sensitized stainless steels depends acutely upon the oxygen concentration. Below about -240 mV at pH_T 5.6, sensitized Type 304 SS does not sustain significant HPSCC, as shown in Figures 88(d) and (e). Partly relevant to SGs is the fact that sensitized Alloy 600, which is present in OTSGs, exhibits the same dependency upon potential as the Type 304 in the HPSCC regime; and the potential below which SCC is negligible is the same.²⁴² Figure 127 shows the dependence of HPSCC on K_I for sensitized materials, and this is one of the bases for the similarity of Alloy 600 and Type 304.³⁴⁴

The work of Shoji²⁴⁸ is shown in Figure 128, where he has determined the dependence of HPSCC using sensitized, mill-annealed, and special surface treatments for Alloy 600. These results show that the Alloy 600MA sustains SCC only at such high potentials that HPSCC is irrelevant to the MA condition of SGs. Similar results are shown in Table 22 and Figure 85, indicating that HPSCC for both Alloys 600 and 690 are not relevant to SGs. Also, Figure 130 confirms the high threshold stress for Alloy 600MA.

Experiments under less precise conditions of high potential have been conducted by Copson and Economy,²³⁰ as shown in Table 15. In these experiments, specimens were exposed as double U-bends with a free surface and a crevice. All the SCC occurred on the crevice surface that was stressed in tension. The intensity of SCC increased with increasing oxygen. The fact that no SCC occurred on the outside and noncreviced surface suggests that some acidification was required for SCC to occur as would be expected inside a crevice in an oxygenated system. While neither the potentials nor the pH were measured inside the double crevice or for the bulk environment for the experiments in Table 15, it can be assumed that the potentials outside the crevice were in the HPSCC range but that the pH inside the crevices would be relatively low, perhaps in the range of pH 4 or possibly lower.

4. Alloy Composition

Most work relevant to BWR technology has been conducted on Type 304, Alloy 600, Alloy 182, and other weld metals. Results of such investigations have shown that Type 304, Alloy 600, and Alloy 182 behave similarly, as shown in Figure 127.

Table 25 shows results from studying the effects of chromium and carbon concentrations for a Ni-based material in aerated pH_{RT} 10 (pH at room tem-

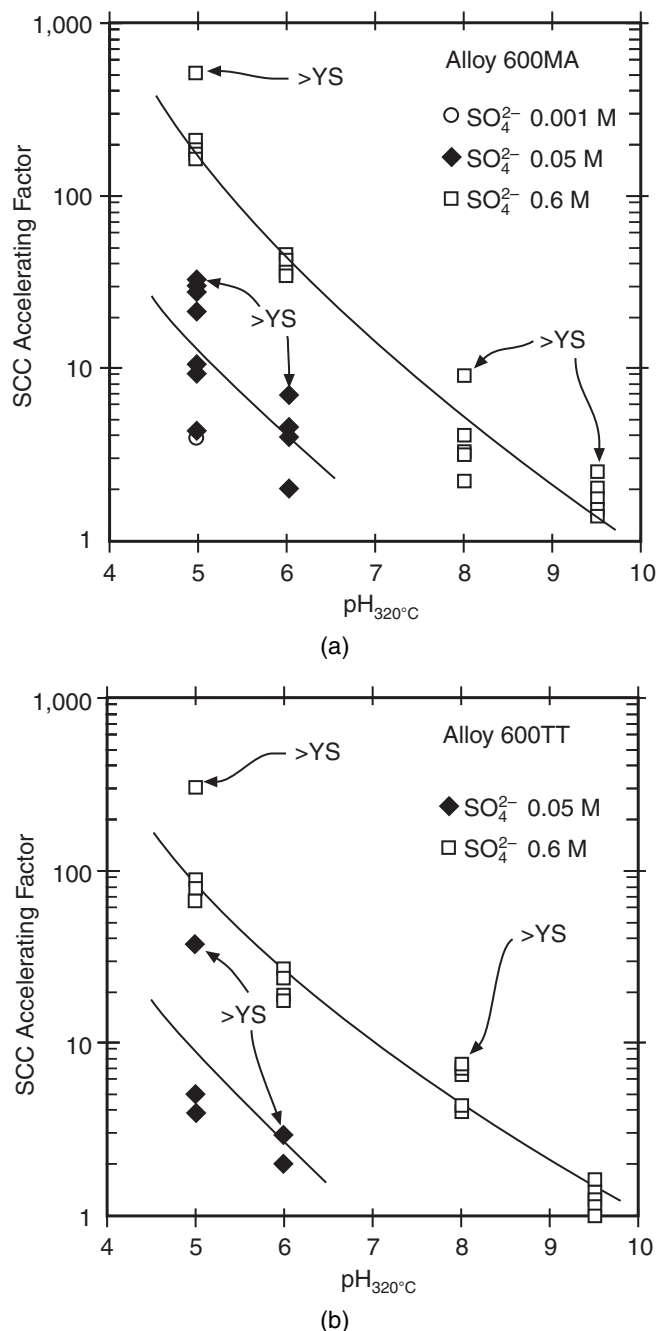


FIGURE 122. SCC accelerating factor vs pH with different concentrations of SO_4^{2-} and with different stresses for: (a) Alloy 600MA and (b) Alloy 600TT. Accelerating factor taken from rate of crack initiation at 0.001 M ($pH_{320^{\circ}C} = 5$) being the reference. >YS refers to TLT condition of the branches of the C-ring; below this stress, specimens were stressed at 0.8 YS and 1.0 YS. From deBouvier, et al.¹⁵³ Courtesy of TMS, Warrendale, Pennsylvania.

perature) solutions at $316^{\circ}C$ using double U-bends as were used also in Table 15. These results show that SCC does not occur at 28% and 30% Cr. They also show that the carbon concentrations seem to exert little regular influence. These data, as for Table 15, are not relevant to SGs, owing to the high poten-

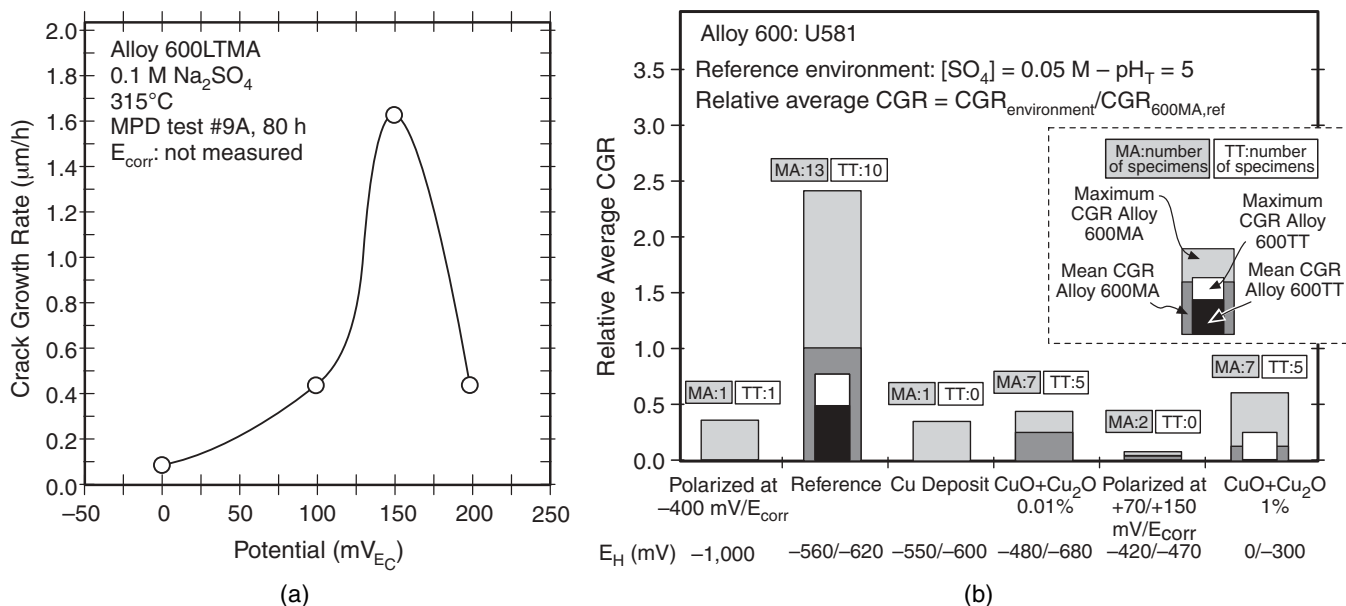


FIGURE 123. (a) Crack growth rate vs applied potential for Alloy 600LTMA exposed in 0.1 M Na₂SO₄ at 315°C. From Cullen.³¹² ©1996 NACE International. (b) Relative average crack growth rate vs potential for Alloys 600MA and 600TT exposed in 0.05 M SO₄²⁻ at pH_{320°C} = 5. From deBouvier, et al.³⁴¹ ©2003 NACE International.

tials that are produced by aeration, although the magnitude of the potential inside the crevices is not known. These data, as discussed in Section 5.3, are tangentially relevant to the overall bases for choosing Alloy 690 as a material for tubes in SGs.

5. Alloy Structure

Extensive work has been conducted on Type 304 stainless steel relevant to BWR applications and has been concerned mainly with effects and the extent of sensitization as related to Type 304 and to weld metals. Since most of this work has been conducted in the higher BWR range of potentials, it is not directly relevant to PWR SGs.

6. Temperature

No significant work on Alloys 600MA nor 690TT has been conducted in the HPSCC range. Work on temperature dependence of the crack growth rate for sensitized Type 304 and Alloy 600 is shown in Figure 129 from Andresen.³⁴⁵ These results are unusual with respect to the change in sign of the slope, in general, but not for the HPSCC. Such changes in slope have not been observed for MA or TT conditions of Alloys 600 or 690 in the deaerated solutions as shown in Figure 114. However, tests to below 250°C have not been conducted for mill-annealed nor TT 600 or 690.

7. Stress

There are few data for the stress dependence of HPSCC of Alloy 600 with smooth specimens. Figure 127 shows the general features of the crack growth rate dependence on stress intensity; these data are compared with other rates of crack growth in Figure 117.

Figure 130 shows the effects of potential, heat treatment, and pH on the propagation rate of HPSCC at 305°C in slightly acidic solutions. The lightly sensitized specimens exhibit a lower potential for acceleration of crack growth exhibited by the non-sensitized and the thermally treated specimens. These data are consistent with those in Figure 128 and with the lines in Figure 82(a) relating to sensitization and annealed conditions with environments of varying contamination. The lower boundary of the annealed and thermally treated data is consistent with the available and relevant data in Figure 85 and with the data in Table 22. The data in Figure 130 are also consistent with the implication of the comparison in Figure 93, which shows that the connection between sensitized Alloy 600 and mill-annealed is not monotonic. Figure 130 confirms that nonsensitized Alloy 600 is not prone to HPSCC in ranges of potential of interest to SGs.

5.2.5 Lead SCC (PbSCC) — PbSCC is relevant to the performance of SGs because small amounts in solutions, in the range of 1 ppm, can produce rapid SCC in both Alloy 600 over a broad range of pH and in Alloy 690 at low and high pH. Further, relative to the small concentrations that can produce SCC, there are relatively large amounts of Pb in deposits throughout steam generators as shown in Figures 59 through 68, and Tables 11, 12, and 14. Further, as shown in Figure 67, lead monoxide (PbO) concentrates inside the crevice relative to the adjacent free-span. Therefore, there are two essential questions to be asked relative to predicting performance: (1) How does lead exert its substantially deleterious effects?

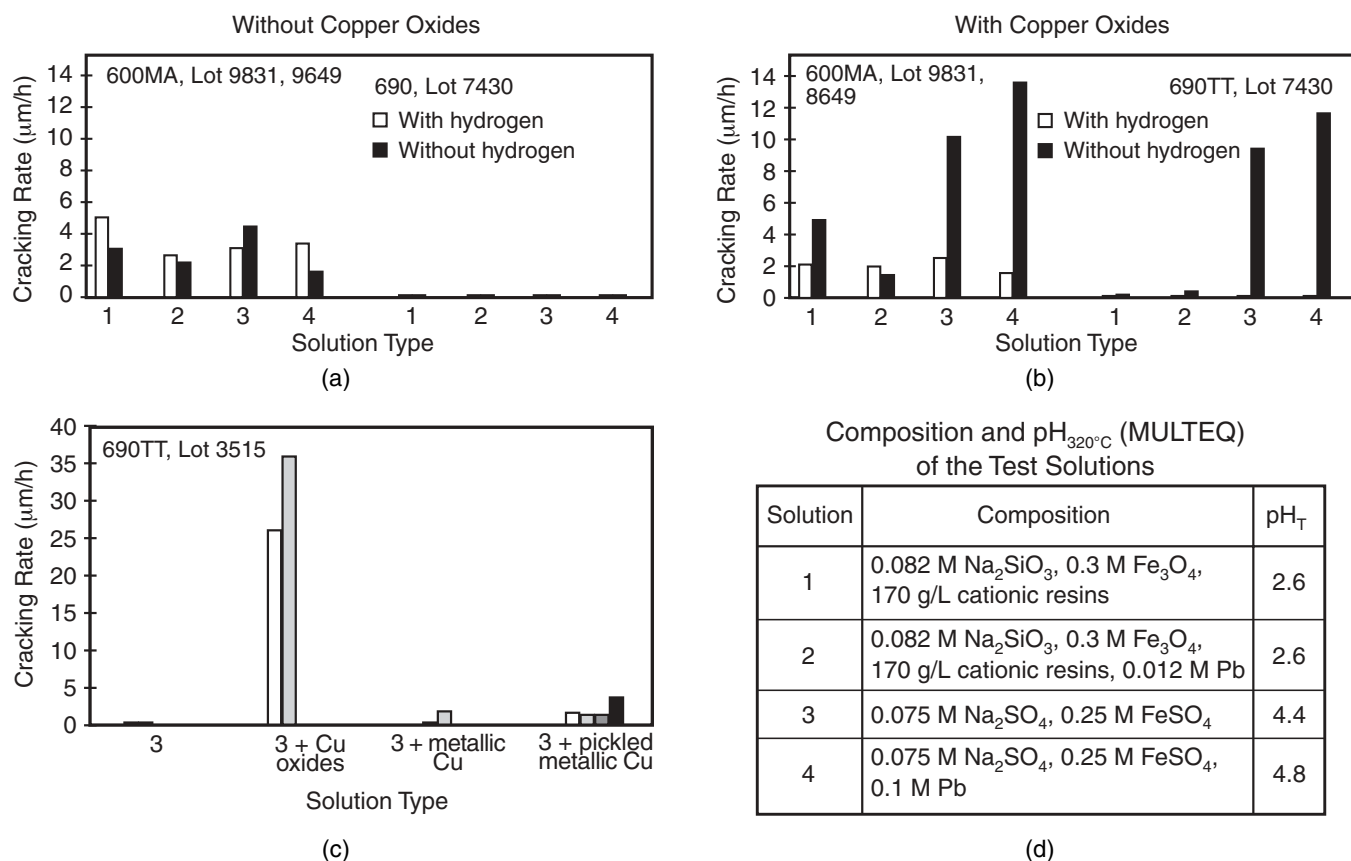


FIGURE 124. (a) Maximum cracking rates for Alloys 600MA and 690TT in acidic solutions without copper oxides with and without 5% H₂ added to argon cover gas in capsules at 320°C. (b) Maximum cracking rates for Alloys 600MA and 690TT in acidic solutions with copper oxides with and without 5% H₂ added to argon cover gas in capsules at 320°C. (c) Maximum cracking rates obtained for Alloy 690TT with solution #3 with no copper, with copper oxide, and with metallic copper at 320°C. (d) Compositions of environments. From Pierson and Laire.²¹⁰ Courtesy Laborelec.

(2) Why do the relatively high concentrations and general ubiquity of lead in deposits not produce extensive PbSCC?

Since there are so many submodes for producing SCC in SGs as described herein, proving that Pb is a unique cause of observed SCC, even when it is observed inside advancing cracks, is not readily accomplished. While one of the nominally unique indications for PbSCC has been the occurrence of transgranular SCC, this is not in fact unique since PbSCC occurs also in the intergranular morphology and since transgranular SCC occurs in Alloy 600MA as well as Alloy 690TT for other reasons, as has been noted in Figure 89 and Table 22 for acidic solutions.

While distinguishing PbSCC from other submodes is generally problematic, Table 26 summarizes the cases where SCC is attributed to Pb and the bases for these attributions. There seems to be little question that PbSCC occurs in some well-defined and unique cases. There is a larger question as to whether other failures are also related to PbSCC, but there is no way of determining these more extensive possibilities.

PbSCC as a submode of SCC was first investigated by Copson and Dean²¹⁴ and reported in 1965; their results are shown in Table 27 for experiments in pH_{RT} 10 water. These experiments were initially undertaken as a means for explaining the earlier results of Coriou, et al., who had identified the fact that Alloy 600 would sustain SCC.¹ The experiments reported by Copson and Dean in Table 27 show that PbSCC was produced regardless of the form in which lead was used. The test environment was aerated and ammoniated. It seems that the PbO produced SCC most rapidly. Copson and Dean found that both intergranular stress corrosion cracking (IGSCC) and transgranular stress corrosion cracking (TGSCC) were associated with PbSCC.

After the Copson and Dean work, little additional work was reported until Flint and Weldon reported in 1972⁸² their lead-containing environments used to evaluate alloys with higher chromium. Their work is part of Figure 142 discussed in connection with Section 5.2.5.4 concerning alloying effects. The next work on effects of Pb to be reported was that of Pement, et al.,¹⁷⁴ where they investigated several al-

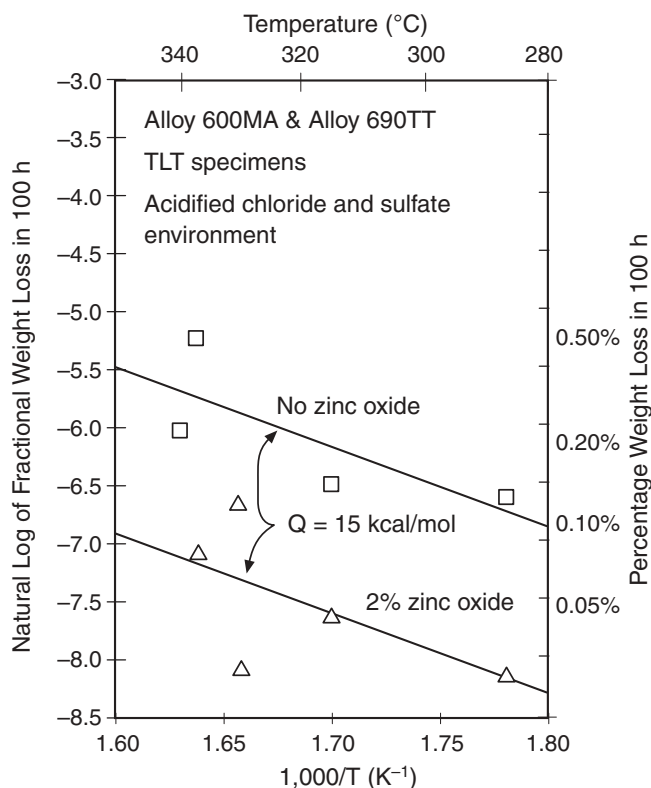


FIGURE 125. Fractional weight loss vs $1,000/T$ for Alloys 600MA and 690TT with and without additions of ZnO to the solutions of acidified chloride and sulfates. Chemistry of all tests was $0.082\text{ M Na}_2\text{SO}_4 + 0.10\text{ M (NH}_4)_2\text{SO}_4 + 1.64\text{ M NaCl} + 0.24\text{ M ZnO}$. TLT specimens used. From Cullen.³¹² ©1996 NACE International.

loys in the mill-annealed and sensitized heat treatments and mainly in a 50% KOH + NaOH (potassium hydroxide + sodium hydroxide) environment in the 327°C to 332°C temperature range with various additives. They showed that Alloy 690, but not Alloy 600, would sustain SCC with PbO additives and that an arsenic additive would also produce SCC for Alloy 600 but not 690. Their experiments in pure water with PbO + H₂O produced SCC in both mill-annealed and sensitized Alloy 600. This, then, was the state of PbSCC by the end of the 1970s.

It was not until the middle 1980s that more work on lead was undertaken; since then, investigations into PbSCC have increased. Agrawal and Paine³⁵³ summarized the state of PbSCC by 1989 and identified sources of Pb in plants as well as research to date. In this review they identified the following sources of Pb on the secondary sides of SGs:

- Plant makeup water
- Condenser cooling water leaks
- Copper alloys in condensers and feedwater heaters
- Seals and gaskets in pumps and pipe fittings
- Babbitt alloys—Pb-containing bearing alloys in pumps and turbines

- Paints and preservatives
- Marking pencils
- Lead chromate tinting in polyethylene wrappings

Rocher, et al.,³⁴⁸ reported on measurements of Pb in French units for the period 1986 through 1991. From 43 and 24 analyses they found 0.11 and 0.01 w/o Pb in deposits and sludge, respectively (specifically excluding Bugey-3, which had been contaminated). This survey also determined that most Pb contamination comes from various sources in turbines, including: turbine gap measurement operations with lead gap wires, certain rupture discs, lead masses used for assembly, certain coatings, certain greases especially for extreme pressure, some paints especially containing lead chromate, and lead cylinders used as handholes and eyeholes to assure biological protection during work. They concluded that materials in the feedwater train were not significant contributors of lead.

Agrawal and Paine³⁵³ also identified the following plants known to have lead in their steam generators (in alphabetical order):

Arkansas-1	Palisades
Beznau-1	Point Beach-1
Calvert Cliffs-1	Prairie Island-1
Farley-2	Prairie Island-2
Genkai-1	Ringhals-2
Genkai-2	Robinson
Ginna	San Onofre
Indian Point-2	St. Lucie-1
Indian Point-3	Surry-2
Kori-2	Tihange-1
Millstone-2	Trojan
North Anna-1	Turkey Point-4
Obrigheim	Zion
Ohi-1	Zorita

Mechanistically, Pb as a species that produces electrochemical reactions leading to SCC, pitting, or GC was not familiar to the corrosion community as were the common corrodents from various mineral sources including Na, Mg, Li, Ca, Cl, S, F, and P. An early explanation for PbSCC suggested that the Pb functioned more in the mode of liquid metal embrittlement since an aqueous mode seemed without precedent. There was precedent for this interpretation.^{214,354} However, the melting temperature for lead is 327.46°C, and lead is unlikely to be available as a liquid metal on the secondary side. The phenomenon of solid metal embrittlement (SME) might be considered, but this is quite unlikely in view of the reactions between lead and water. Further, Figure 131 shows that the crack growth rate in liquid lead is significantly below that of water + PbO over a range of temperature. Also, Figure 131 shows that water + PbO produces SCC more rapidly than water alone over a range of temperatures. Taken together, and considering the melting point of lead, it seems more likely that neither liquid metal embrittlement nor

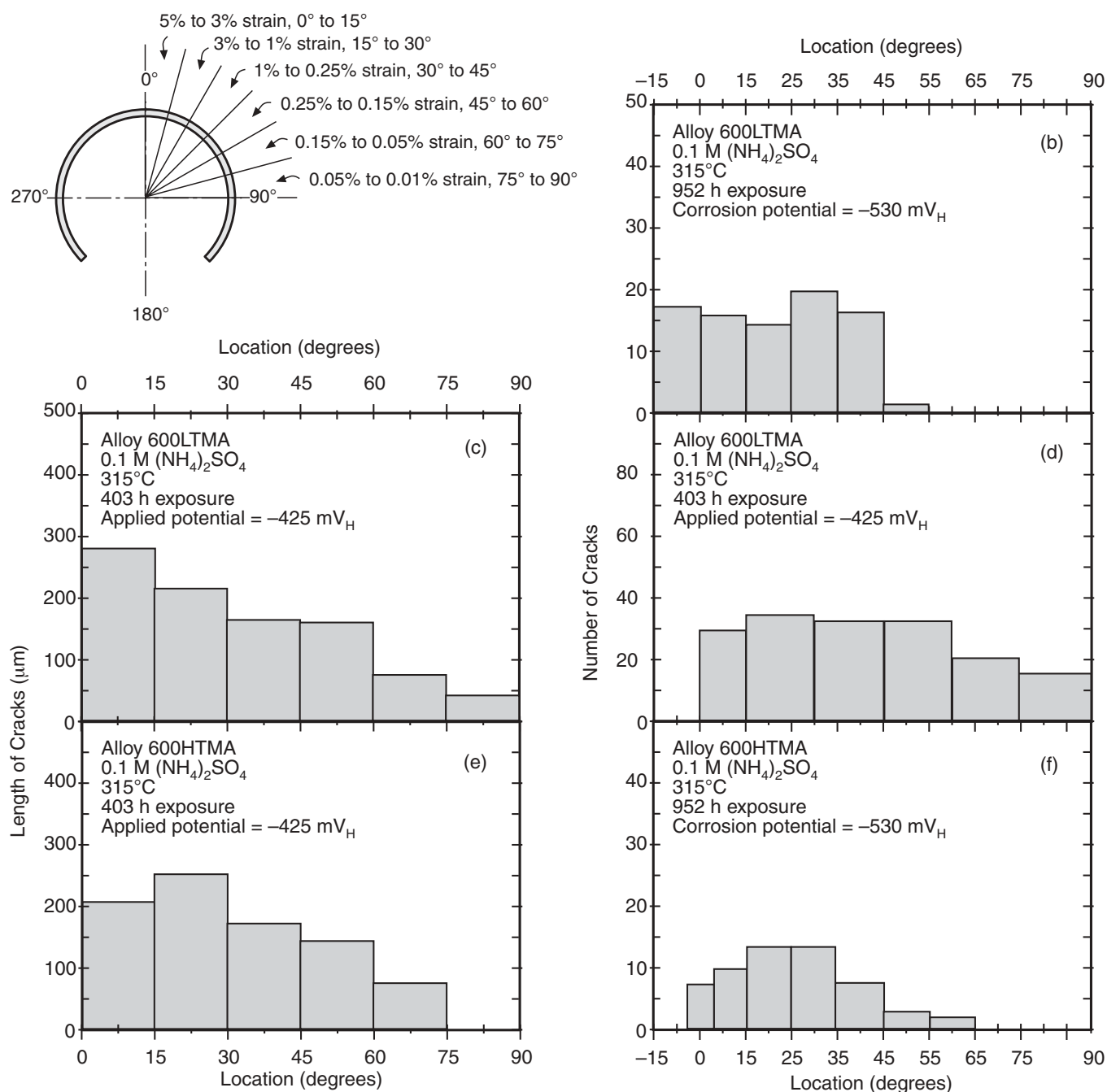


FIGURE 126. (a) Strain in angular sectors of a C-ring SCC test. (b) Number of cracks vs sector for Alloy 600LTMA exposed to 0.1 M (NH₄)₂SO₄ at 315°C and about -530 mV_H (E_c) for 952 h and $pH_{315^\circ C} = 4.33$ (MULTEQ). (c) Length of cracks vs sector for Alloy 600LTMA exposed to 0.1 M (NH₄)₂SO₄ at 315°C and about -425 mV_H for 403 h and $pH_{315^\circ C} = 4.33$. (d) Number of cracks vs sector for Alloy 600HTMA exposed to 0.1 M (NH₄)₂SO₄ at 315°C and about -425 mV_H for 403 h and $pH_{315^\circ C} = 4.33$. (e) Length of cracks vs sector for Alloy 600HTMA exposed to 0.1 M (NH₄)₂SO₄ at 315°C and about -425 mV_H for 403 h and $pH_{315^\circ C} = 4.33$. (f) Number of cracks vs sector for Alloy 600HTMA exposed to 0.1 M (NH₄)₂SO₄ at 315°C and about -530 mV_H for 952 h and $pH_{315^\circ C} = 4.33$. From Cullen.³¹²

solid metal embrittlement are feasible as a mechanistic explanation for PbSCC and that lead participates as an oxidized ion in PbSCC by some other process.

The potential-pH diagram for lead in water in Figure 7(f) shows that Pb is soluble over the full range of pH and oxidizes from Pb to various soluble

species along half-cell equilibrium lines that are close to the standard hydrogen half cell, as well as to the NiO/Ni half-cell equation line, with a decrease below the standard H₂O/H₂ line at about pH 5.5. This suggests that Pb is most likely in a soluble aqueous form as it produces PbSCC.

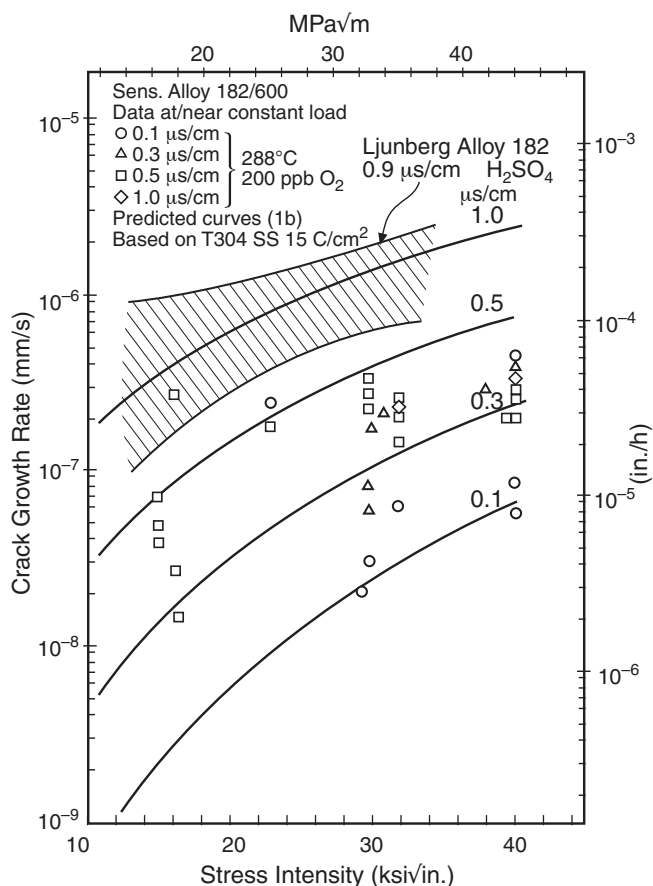


FIGURE 127. Crack growth rate vs stress intensity for sensitized Alloys 182 and 600 at various conductivities at 288°C and 200 ppb O_2 based on predicted lines for sensitized Type 304 stainless steel. From Ford and Andresen.²²⁶ Courtesy Marcel Dekker Inc.

Polarization studies by Kilian³⁵⁶ of Alloy 690 in a 1-M NaOH solution at 300°C, shown in Figures 132(a) and (b), indicate that increasing the concentration of PbO generally increases the height and breadth of the anodic peak. At 10% PbO the trend is reversed, and no anodic peak is observed; most likely there is a deposit on the surface that impedes breakdown. From Figure 132, together with Figure 7(f), it appears most likely that lead acts to decrease the integrity of the passive film especially at lower potentials near the anodic peak. The possibility of this region of instability being the region of PbSCC is based on the prediction by Staehle.¹⁸ It is likely that the range of potential over which PbSCC occurs is defined at the upper limit by the onset of stable passivity after the active peak and at the lower potential by the half-cell equilibria involving the oxidation of lead. This pattern of the polarization curves suggests that the potential dependence of PbSCC would be similar to those of AkSCC and AcSCC shown in Figures 97 and 123(a), respectively.

Lead produces large changes in the properties of protective films. Figure 133(a)³⁵⁷ shows that the pres-

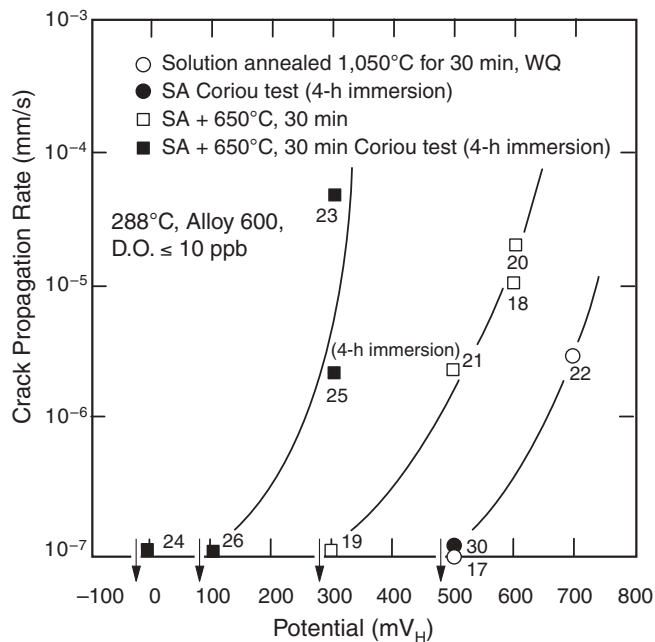


FIGURE 128. Crack propagation rate vs potential for Alloy 600 subjected to various heat treatments and exposed to water at 288°C with oxygen equal or less than 10 ppb. From Shoji.²⁴⁸

ence of lead in the environment significantly reduces the thickness of protective films in tests at pH 3, 4.5, and 7. Further, Figure 133(b) shows that the presence of lead changes the residual composition of protective films: nickel is significantly depleted and chromium is correspondingly enriched in the outer layers. Such behavior suggests either a special complexation with Ni or the formation of an acidic presence on the outer surface.

Some work³⁵⁸ demonstrates that PbSCC will propagate short distances if specimens, which have been exposed previously to Pb environments, are later exposed without Pb in the environment. The dimensions of this effect are not clear but are important.

Three investigations have measured the penetration of lead into advancing SCC.^{185,359-360} Table 14¹⁸⁵ shows results taken directly from an OD surface of Oconee-2 from the superheat region of the upper bundle of sensitized Alloy 600 and examined with an advanced transmission electron microscope (ATEM). The surfaces examined were from SCC that had proceeded into the metal and not from the outside surface. In another assessment by Hwang, et al.,³⁶¹ inside what is probably PbSCC, laboratory tests using Alloy 690TT in a 1-M NaOH solution containing 5,000 ppm Pb at 95 mV_{Ni} gave the results shown in Figure 134. Also, Byers, et al.,³⁵⁹ exposed Alloy 600MA specimens to a 0.2% NaOH + 0.2% PbO solution at 350°C for 163 h to 456 h. Their results are shown in Figure 135. Lead is observed to occur throughout cracks and at crack tips.

TABLE 25
Results from Double U-Bend Crevice Tests with Various Chromium and Carbon Concentrations Exposed in Aerated Water, pH_{RT} = 10 at 316°C^(A)

Alloy		Number Heats	Number Specs.	% Cracked	Test Time (weeks)			Penetration in Crevice Area (mils)		
%Cr	%C				Max.	Min.	Avg.	Max.	Min.	Avg.
20	0.01 to 0.03	5	10	100	8	2	5.6	100	5	64
20	0.05	1	2	100	2	2	2.0	90	83	87
20	0.09 to 0.10	2	4	100	2	2	2.0	110	80	100
22	0.02 to 0.03	3	7	100	8	8	8.0	62	37	50
22	0.09 to 0.10	2	4	100	8	2	5.5	110	60	73
24	0.01 to 0.02	3	8	100	8	8	8.0	36	8	23
24	0.05 to 0.07	5	16	50	8	6	7.9	110	0	21
24	0.09 to 0.11	2	4	100	8	8	8.0	49	5	37
26	0.01	1	2	100	8	8	8.0	5	2	4
26	0.04 to 0.07	3	9	44	8	8	8.0	20	0	5
28	0.03	1	2	0	8	8	8.0	0	0	0
28	0.05 to 0.07	3	15	0	8	8	8.0	0	0	0
30	0.03	1	4	0	8	8	8.0	0	0	0
30	0.06 to 0.07	3	14	0	8	8	8.0	0	0	0
30	0.07	1	2	0	48	48	48.0	0	0	0

^(A) From Copson, et al.²³⁹ ©1972 NACE International.

Figure 135 from Byers, et al., for specimens exposed to NaOH shows that Pb migrates significantly to the crack tip.³⁵⁹ Table 28 from Sakai, et al.,³⁶⁰ from specimens exposed to acidic environments also show that Pb has migrated to the crack tip of Alloys 600 and 690, although not in as much concentration as observed for Figure 135. This result may be due to the anionic and cationic nature of the Pb in the two cases. They also correlated the crack growth rate with the concentration of Pb on the surface, as shown in Figure 135(b).

The results from Table 14 and Figures 134 and 135 show that lead penetrates to crack tips in both possibly neutral and NaOH environments and that the concentration of the Pb is more or less uniform along the length of the SCC. From Figure 134, the number of cracks on the outside diminishes from Alloy 600MA to 600TT to 690TT; whereas, the average crack propagation rate changes little with the alloys and the maximum crack propagation rate is minimum for Alloy 600TT. The fact that Pb is so broadly distributed in the SCC suggests that it is migrating as a negative ion. It is also doubtful that the observations here are consistent with liquid metal embrittlement (LME), where the amount of liquid metal to produce LME is typically a single atom layer.

The interpretation of the mechanism of PbSCC relying on Pb-induced instability of the passive film is not an uncommon interpretation and is amply supported by the work of Kilian as shown in Figure 132.³⁵⁶

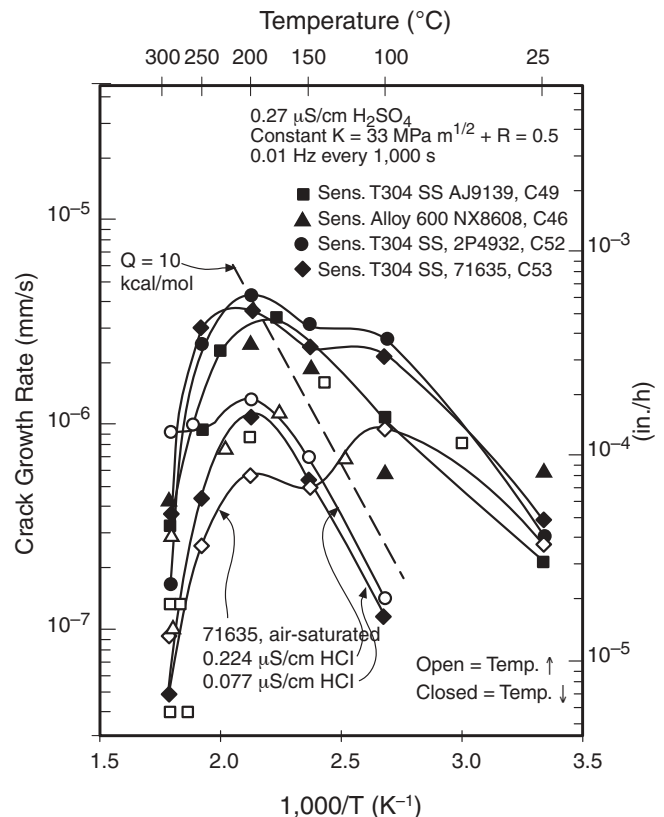


FIGURE 129. Crack growth rate vs 1,000/T for sensitized Type 304 SS and Alloy 600 at constant K = 33 MPa m^{1/2} plus R = 0.5, 0.01 Hz every 1,000 s. 200 ppb O₂, 0.27 μS/cm H₂SO₄. From Andresen.³⁴⁵ ©1998 NACE International.

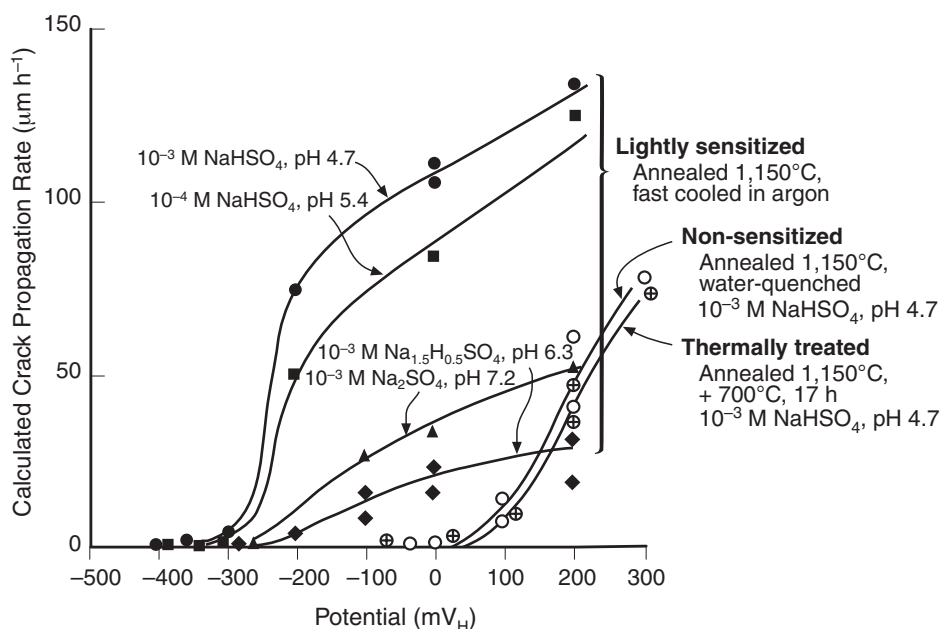


FIGURE 130. Calculated crack propagation rate vs applied potential for Alloy 600 in the lightly sensitized, quench annealed, and thermally treated conditions exposed to neutral and slightly acidic pH at 305°C. From Newman.³⁴⁰

Having a reasonable interpretation of PbSCC, a question still remains concerning why there is not extensive and rapid PbSCC in view of the relatively large amounts of Pb in deposits throughout the SGs. It seems that a reasonable interpretation involves the following:

1. As N_2H_4 is added to the secondary side, lead may be prevented from oxidizing to the soluble forms, as shown in Figure 7(f).
2. Lead forms an array of insoluble precipitates that reduce the activity of lead. Some such precipitates are suggested in Table 29. Further thermodynamic analysis would show how these precipitates could behave at higher temperatures. Certain precipitates are more soluble than others and would be sensitive both to pH and to the possible formation of more complex minerals. Thus, in the presence of certain precipitate-forming species, the lead is immobilized by a compound that reduces the activity of Pb. Therefore, the lead is not available to produce PbSCC.
3. Lead is more soluble in more acidic environments as shown in Figure 7(f). Increasing the $pH_{300^\circ C}$ above 5.5 to 6 would reduce the tendency to form soluble lead. However, this tendency is not consistent with the observations, which are discussed in this section, that PbSCC occurs readily in more alkaline solutions.

It should be assumed that Pb will continue to be problematic in steam generators, as identified in the introduction to Section 5.2.5.

In view of the interpretation that the activity of Pb is lowered by other species and is therefore not available to produce PbSCC, great care should be given to determining the critical species that react to lower the Pb activity. If further efforts by the industry to purify the secondary system continue, it is possible that some critical species and group of species could be lowered beyond that necessary to prevent Pb from producing PbSCC.

Lead is of interest to the reliability of steam generators for the following reasons:

1. Lead is ubiquitous as shown in the data from hideout return and analysis of deposits in Figures 59 through 69.
2. Pb produces SCC in both Alloys 600 and 690 at high pH, where Alloy 690 can sustain even more intense SCC than Alloy 600 in lead-contaminated environments. At near-neutral and low pH, Alloy 690 may be more resistant than Alloy 600. But, some low pH work indicates that it is prone to PbSCC in the pH_T 3 to 4.5 range.³⁶⁴
3. Pb produces both TGSCC and IGSCC, and the reasons for the occurrence of these different morphologies is not established.
4. Pb can produce SCC over the entire range of pH as shown in the mode diagram of Figure 82(b).
5. Relatively small concentrations of Pb in the range of 1 ppm in an aqueous solution can produce relatively rapid SCC in Alloy 600MA.

When considering both the ubiquity and the high concentrations of lead adjacent to SG tubes together with the severity of PbSCC, it is surprising that any

TABLE 26
Experience with Lead in Commercial PWR Steam Generators

Plant and Date	Experience
St. Lucie-1, 1987	St. Lucie-1 sustained a significant amount of detectable degradation in the sludge pile region and egg crate supports. Examination of pulled tubes showed mixed IGSCC and TGSCC. ^(A) Lead was detected in deposits and on crack surfaces. It was concluded that the presence of lead was an important factor in the degradation.
EDF plants with 600MA tubes, 1990-1993	Examination of deposits from many plants and correlation of deposit composition with occurrence and morphology of SCC led to the following conclusions: (1) increasing amounts of lead in deposits correlated with increasing amounts of transgranular SCC in the sludge pile region, and (2) the concentration of lead did not correlate strongly with increasing total degradation until the concentration of lead in the deposits exceeded 6,400 ppm. ^{(B),(C)}
Bruce-A, Unit-2, 1990-1991	Bruce-A, Unit-2 is a CANDU plant, but is covered here because its experience is directly applicable to PWRs since it had 600MA tubes. It sustained significant SCC of tubes at the upper bundle supports that was found to be associated with large amounts of lead in the SGs that come from shielding material left in the SG during an outage. ^(D) The cracking was mixed intergranular and transgranular, but predominantly intergranular.
Doel-4, 1992	Doel-4, SG-B sustained significant SCC in free-span regions and at TSPs as a result of lead shielding left in SG-B in about 1986. ^(E) Most cracking was intergranular. The other SGs were not affected; apparently, the blowdown demineralizers were effective at limiting the transfer of lead into the rest of the plant.
Kori-2, 1990	Kori-2 SG-B sustained TGSCC at TTS. EDX analysis showed 5.4% Pb and 0.225% Pb on the tube surface and in the sludge, respectively. ^(F)
Oconee, 1999	Detailed failure analysis using especially sensitive ESCA and ATEM methods showed the presence of high concentrations of lead under oxides and on crack faces of tubes with upper bundle IGC and IGSCC. ^(G) The cracking was intergranular. It was concluded that lead was probably a factor in the IGC and IGSCC.

(A) From Frye.³⁴⁶
 (B) From Cattant.³⁴⁷
 (C) From Rocher, et al.³⁴⁸
 (D) From King, et al.³⁴⁹
 (E) From Laire, et al.³⁵⁰
 (F) From Hwang, et al.³⁵¹
 (G) From Bruemmer and Thomas.³⁵²

TABLE 27
Effects of Pb in Pure Water^{(A),(B)}

Alloy No.	Type of U-Bend	Time to Cracking (weeks)			Fractional Pb + Hydrocarbon (8) ^(C)
		Pb Powder + Hydrocarbon (5) ^(C)	Pb Powder (6) ^(C)	PbO (7) ^(C)	
9A	Single	8	8	4	OK ^(D)
11A	Single	8	8	6	6
9A	Double, outer	8	8	6	OK
9A	Double, crevice	8	8	6	6

(A) From Copson and Dean.²¹⁴ ©1965 NACE International.
 (B) Air-saturated distilled water, pH 10 at start-up, 316°C.
 (C) Author's test number.
 (D) OK = no cracking at end of test, which lasted 1,350 h in Tests 5, 6, and 8 and 100 h in Test 7.

SG can retain its integrity. It appears that the Pb does not produce SCC, despite its high concentrations and ubiquity, because its chemical activity is lowered by forming insoluble compounds.

The dependencies of PbSCC on primary variables are as follows:

1. pH

PbSCC of Alloys 600MA and 600TT occurs over the range of alkaline, neutral, and acidic environments, while PbSCC of Alloy 690TT has been observed in both alkaline and acidic environments.

Figure 136(a), from the work of Miglin and Sarver,¹⁸⁸ shows environments used for PbSCC testing over a range of pH_{324°C} from 2 to 10 where specimens of Alloys 600 in various heat treatments and Alloy 690TT were exposed in solutions of different pH to liquid and saturated steam above the liquid. In Figure 136(b), the extent of PbSCC initiated in various test canisters increases with pH and with the calculated concentration of negatively charged oxyanions. The morphology of PbSCC and the depth of penetration are correlated with the calculated pH in Figure

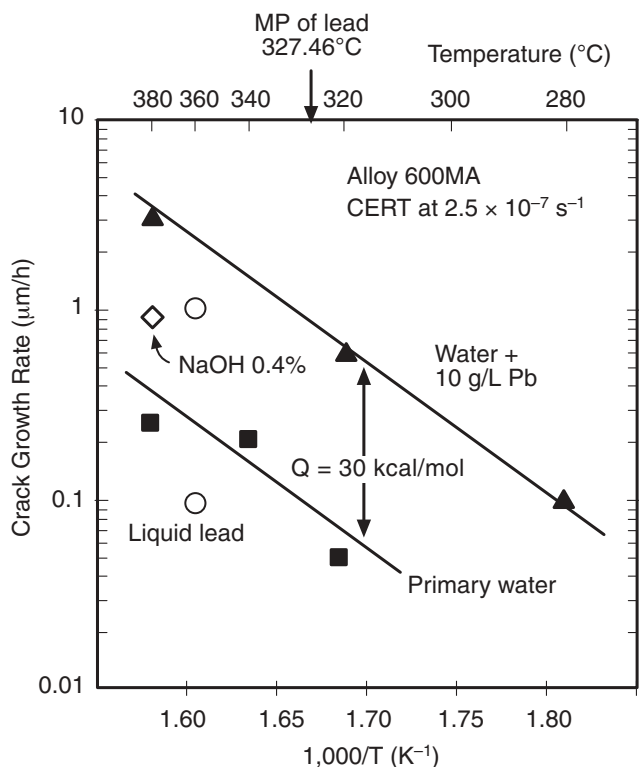


FIGURE 131. Crack growth rate vs $1,000/T$ for liquid lead, NaOH, water, and water + PbO determined by CERT at $2.5 \times 10^{-7} \text{ s}^{-1}$. From Helie, et al.³⁵⁵ Courtesy EDF.

136(c). The relative extent of PbSCC in liquid and vapor is shown in Figure 136(d).

The results from this testing of Miglin and Sarver have been analyzed in detail as shown in Figures 137(a) through (m).

Figure 137 is arranged according to increasing pH from Figures 137(a) to (m). Each lettered figure shows on the ordinate the percent of wall thickness penetrated. These data were taken from the photomicrographs in the report from Miglin and Sarver. Along the abscissa are the various alloys used in the study. These are arranged approximately according to MA of Alloy 600 at the left moving to stress relief (SR) and TT of Alloy 600 and then to TT for Alloy 690 at the right. Specific heat treatments are given at the upper left at the beginning of the figure. All designations for the figure are shown at the upper right of the figure. Each of the alloy boxes for each pH includes results from two testing times and from liquid and vapor as noted in the upper middle of the figure. All specimens were C-rings prepared from tubing as noted in the upper middle of the figure.

Features of the corrosion shown in Figure 137 are shown at the upper right. Important features of the corrosion are the following:

1. The relative amounts of TGSCC and IGSCC are shown as a ratio of TGSCC/TGSCC+IGSCC in italics. This was necessary since the

SCC sometimes contained both morphologies and the morphologies are generally specific to heat treatments, although not always. This morphology ratio is given for every specimen for which metallographic information was available. The morphology ratio for fully TGSCC is 1.0 and for fully IGSCC is 0.

2. In some cases the initiation of the SCC occurred by one morphology but shifted to another after a few grains. The initiating morphology is given as I or T for intergranular or transgranular as superscripts to the morphology ratio, e.g., 0.3^I .
3. In some cases the morphology was not taken or reported. Here, a penetration of 50% is assumed with an upward arrow. This is an arbitrary assumption but seemed consistent with the observations.
4. Sometimes the SCC initiated with IGC and these instances are noted with a "G" above the bar.

There are some clear patterns in Figure 137:

1. The intensity of SCC increases with increasing pH. However, in Figures 137(a) through (e), the environments used sulfate acidity (except for Figure 137(d)), where the PbSCC is not expected to be significant owing to the insolubility of the Anglesite (PbSO_4). The results from Figure 137(d), where lead chloride (PbCl_2) was used, are inconsistent with those from Chung, et al.,³⁶⁴ who has shown that chloride acidity promotes PbSCC of both Alloys 600 and 690 in their various heat treatments including TT.
2. There is not a significant improvement from the use of Alloy 600TT relative to Alloy 600MA.
3. Alloy 690TT seems to be significantly improved over Alloy 600 over a range of pH, especially in the acidic and neutral regions. However, other work shows that Alloy 690TT is a little different from Alloys 600MA and 600TT in lead-contaminated chloride acidity.
4. In alkaline vapor conditions, Alloy 690TT sustains aggressive TGSCC, although similar behavior is not evident in other environments for the same alloy.
5. There is a predominant tendency for the MA alloys to sustain IGSCC, consistent with Tables 30 and 31, although there are some prominent exceptions. The SR and TT alloys exhibit some tendency for TGSCC, but the behavior is mixed, although the data of Tables 30 and 31 show that the SR and TT alloys sustain predominantly TGSCC. It seems that the chemistry of environments affects the morphology as well as the heat treatment.

PbSCC in alkaline environments is epitomized by the data in Table 32, which shows that the presence of Pb accelerates SCC relative to 10% NaOH alone,

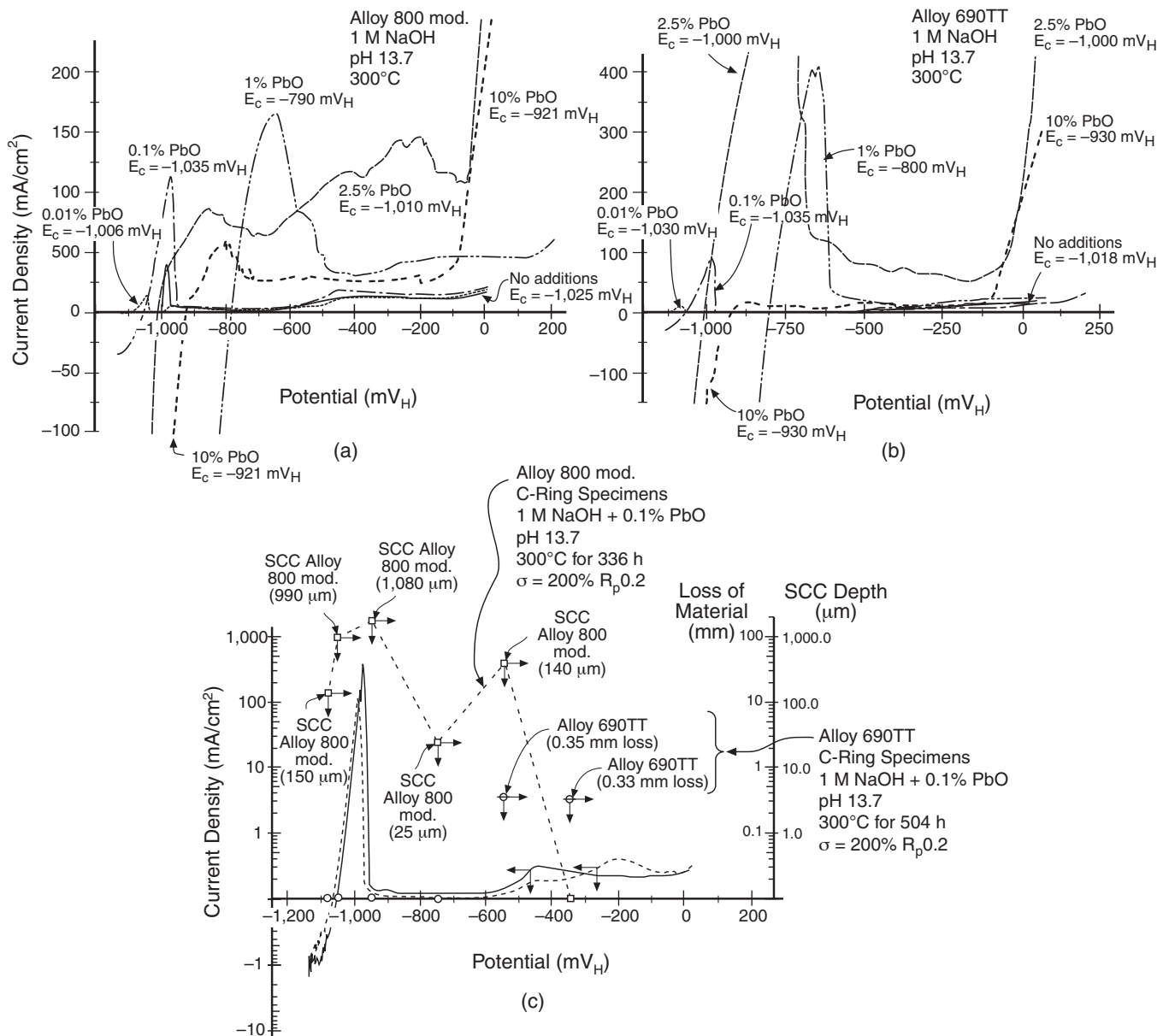


FIGURE 132. (a) Current density vs potential for Alloy 800 mod. exposed in 1 M NaOH at 300°C. Alloy 800 with range of Pb. (b) Current density vs potential for Alloy 690TT in 1 M NaOH at 300°C with various additions of PbO tested at 1 mV/s. Alloy 690TT with range of Pb. Potentials taken with reference to external Ag/AgCl electrode. Corrosion potentials, E_c , shown for each environment. (c) Current density vs potential for Alloys 800 mod. and 690TT showing SCC depth and weight loss; respectively, vs potential. From Kilian.³⁵⁶ Courtesy International Atomic Energy Agency.

especially for Alloy 690TT. Figure 138 shows that adding 1% PbO to 10% NaOH substantially accelerates penetration by IGA, relative to the SCC sustained in the NaOH alone, for both Alloys 600MA and 600TT. Some localized transgranular branching was observed.

Figure 139 shows that PbSCC occurs readily in AVT water to concentrations as low as 0.1 ppm. Figure 140 shows similar results for Alloys 600MA and 600TT for two stresses in deaerated water. In acidic solutions, Figure 141 from Sakai, et al.,³⁶⁷ shows

that PbCl₂ concentrations at least as low as 1.45×10^{-3} M/L in a chloride solution produce rapid SCC and general corrosion for both Alloys 600MA and 690TT.³⁶⁷ The rate is not changed significantly with 1.45×10^{-3} M/L. In acidic sulfate solutions, the rate of SCC is not much changed with the addition of Pb, as shown in Figure 124 from the work of Pierson and Laire.²¹⁰

The fact that PbSCC occurs over the full range of pH most likely results both because Pb is soluble, as shown in Figure 7(f), over the full range of pH, and

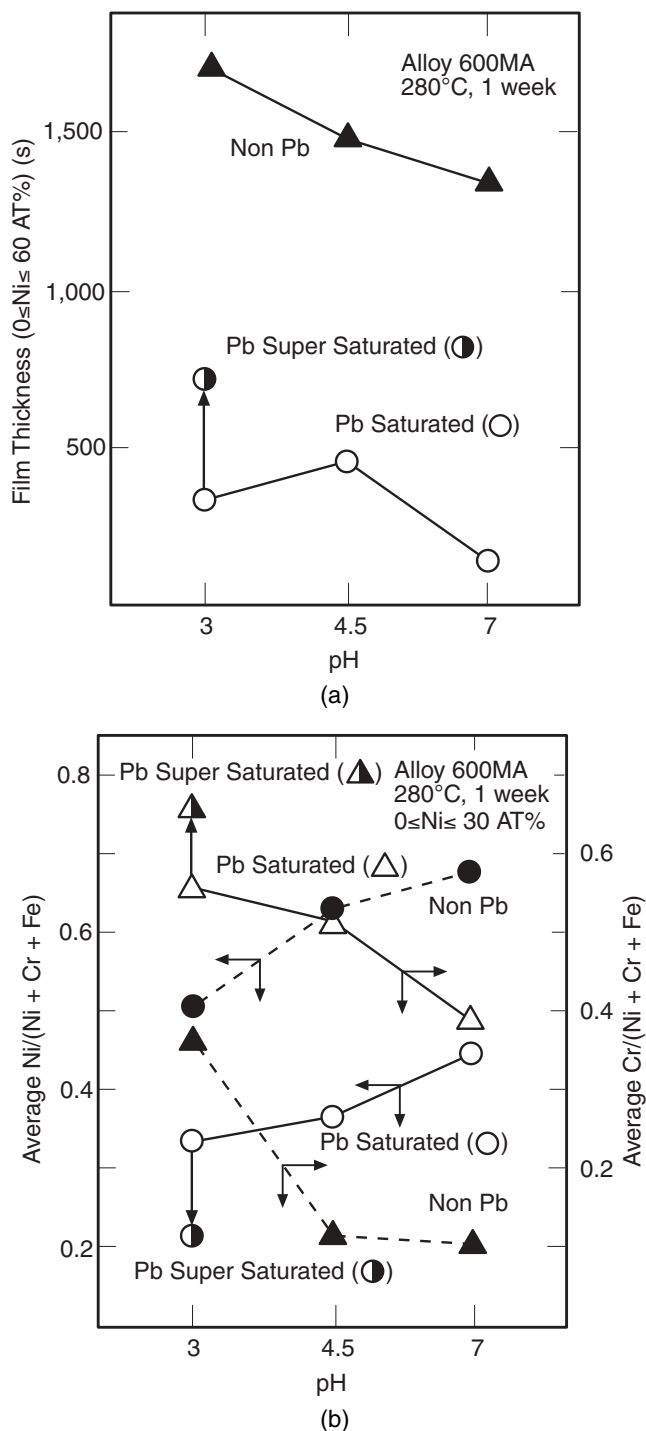


FIGURE 133. (a) Film thickness on Alloy 600MA exposed in $PbCl_2$ at various concentrations at 280°C for 1 week. pH adjusted with HCl. (b) Average relative concentrations of Ni and Cr after exposure to solutions with and without $PbCl_2$ at 280°C for 1 week. pH adjusted with HCl. From Sakai, et al.³⁵⁷ ©1990 NACE International.

Pb species are effective in reducing the protective quality of the passive film.

2. Potential

PbSCC has not been investigated significantly as a function of potential except for electrochemical

studies in Figure 132 from Kilian,³⁵⁶ who studied Alloy 690TT and 800, and by Chung, et al.,³⁶⁴ and Hwang, et al.,³⁶⁸ both in acidic solutions, and by Pierson and Laire²¹⁰ in Figure 124. The main contribution of the lead, as shown in Figures 132(a) and (b), is to increase the height and width of the active peak. It appears that the occurrence of PbSCC follows the active peak and then diminishes in the passive region where PbSCC has diminished, as shown in Figure 132(c). PbSCC also would be bounded at lower potentials by the half-cell equilibria for the oxidation of Pb to soluble species. Such a result is consistent with the patterns for AkSCC and AcSCC. Figure 132(c) shows that Alloy 800 mod. exhibits SCC over a range of potentials while Alloy 690 exhibits only GC.

While the study was not direct, Byers, et al.,³⁵⁹ interpreted one of their accelerated results as due to oxygen contamination in the cover gas. Also, the original work by Copson and Dean,²¹⁴ shown in Table 27, was conducted in pure but aerated and ammoniated water. The occurrence of PbSCC in Copson's aerated experiments as well as in the deaerated experiments of Figures 139 and 140 suggests a range of PbSCC of at least several hundred mV; such a range is generally consistent with the width of active peaks observed by Kilian, as shown in Figure 132. PbSCC is most probably bounded at lower potentials by the half-cell equilibria associated with the oxidation of Pb to soluble species, as shown in Figure 7(f).

3. Species

In alkaline solutions, only the interaction of NaOH and Pb have been investigated. As shown in Table 32 and Figure 138, Pb accelerates AkSCC. Pb in pure water and AVT environments greatly accelerates SCC in neutral water, as shown in Figures 139 and 140. In acidic solutions, it seems that Pb produces a greater increment of acceleration in chloride environments than in sulfate environments based on Figure 141, as compared with the low-pH region of Figures 136(b) and 124.

Relevant to possible inhibition, Lu, et al.,³⁷³ have investigated, using polarization measurements, the effect of silica (SiO_2) added to solutions containing Pb and have shown that the SiO_2 retards the polarization currents generally in neutral, alkaline, and acidic chemistries.

It is relevant to note that Pement, et al.,¹⁷⁴ have shown that arsenic also accelerates SCC similarly to Pb, although there is not sufficient work to establish a linkage between Pb- and As-accelerated SCC. Nonetheless, the fact that As also accelerates SCC suggests that PbSCC is a more general phenomenon than being restricted only to Pb. Perhaps, Sb species would accelerate SCC also.

It is likely that concentrations of N_2H_4 , oxygen, copper, and hydrogen will affect the occurrence of PbSCC with it being most likely accelerated by oxidiz-

ing conditions and most likely diminished by relatively reducing conditions relative to the Pb^{2+} equilibria in Figure 7(f).

4. Alloy Composition

The general effects of Cr and Fe on the PbSCC and PbGC of Ni-Cr-Fe alloys are shown in Figure 142 based on work by Sarver³⁶⁶ and Flint and Weldon⁸² in deaerated high-purity water at 316°C. In these figures, the composition of Alloy 690 is just outside regions where SCC and serious scaling occur.

Despite the trends noted in Figure 142 for the beneficial effects of chromium, the proneness of Alloy 690TT to PbSCC in caustic environments seems equivalent to that of Alloy 600MA, as shown in Figures 137 and 141 and Table 32. It seems that Alloy 600TT is somewhat improved over Alloy 600MA, as shown in Figures 134, 137, 138, and 144.

The PbSCC of Alloy 690TT is shown with effects of stress in Figures 143 and 144 in Section 5.2.5.7.

In addition to Alloys 600 and 690 sustaining PbSCC, Sarver³⁶⁶ has shown that Alloys 601 (UNS N06601), x-750 (UNS N07750), 721 (UNS N07721), and 604 (UNS N06604) sustain PbSCC.

5. Alloy Structure

Aside from the improvement in resistance to PbSCC provided by the TT treatment for Alloy 600 relative to the MA treatment, there are no data describing effects of alloy structure. In fact, Vaillant²⁶⁹ points out that effects of Pb obscure any benefits from carbides being preferentially distributed at the grain boundaries.

6. Temperature

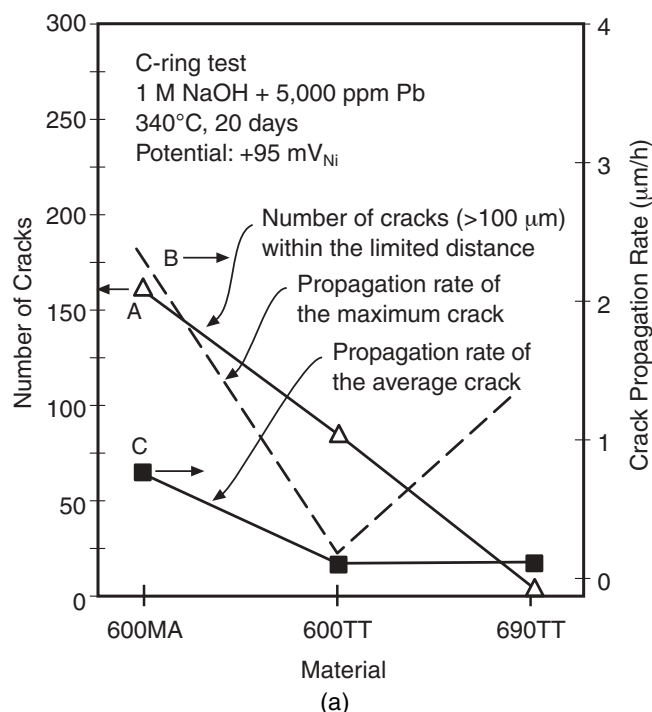
The crack growth rate has been determined by Helie, et al.,³⁵⁵ vs $1,000/T$ for primary water and the same water plus PbO , as shown in Figure 131. Lead increases the growth rate by about an order of magnitude relative to pure water without Pb, and the activation energies for crack growth in pure water and pure water with lead are the same, i.e., 30 kcal/mol. Figure 143 shows a significant increase in PbSCC for Alloy 690TT from 288°C to 324°C.

7. Stress

Small concentrations of lead lower the threshold stress for PbSCC in NaOH solutions, as shown in Figure 143. Figure 144 also shows the effect of stress in an alkaline solution; Alloys 800, 690TT, 600MA, and 600TT were exposed to a 10% NaOH + 1% PbO solution at 350°C. Here, Alloy 800 is the most prone to PbSCC and Alloy 600TT the least. Alloy 690TT is quite prone to PbSCC also but exhibits a higher threshold stress.

Figure 141 shows that both Alloys 600MA and 690TT exhibit a dependence upon stress at lower concentrations of $PbCl_2$, but such a dependence is not discernible at higher concentrations.

5.2.6 Reduced Sulfur SCC (S^{ν} SCC) — Low-valence sulfur SCC (S^{ν} SCC) is pertinent since sulfate impurities and released resins accumulate in heat-



Location \ Element w/o	O	Pb	Ni	Cr	Fe
Near crack	8.92	1.96	49.85	29.79	9.47
Crack mouth	4.21	1.39	62.53	24.02	7.85
Middle crack	4.60	1.78	60.69	24.96	7.96
Crack tip	4.41	0.12	59.65	27.61	8.21
Matrix	0.06	0.00	60.58	30.19	9.17

Composition and conditions of test: 1 M NaOH, 5,000 ppm Pb, 95 mV_{Ni}
Alloy 690TT

(b)

FIGURE 134. (a) Number of cracks and crack propagation rate for Alloys 600MA, 600TT, and 690TT exposed in 1 M NaOH + 5,000 ppm Pb at 340°C for 20 days at 95 mV_{Ni}. (b) Chemical composition of SCC surfaces of Alloy 690TT exposed to 1 M NaOH + 5,000 ppm Pb for 20 days at 95 mV_{Ni}. From Hwang, et al.³⁶¹ Courtesy of KAERI.

transfer crevices. N_2H_4 can react with these species to produce lower-valence sulfur according to the thermodynamic inclination of such reactions to occur, as shown in Figure 33. Lower-valence sulfur species accelerate degradation of alloys, including Alloys 600 and 690, in two ways, as illustrated in Figure 145. In Figures 145(a) and (c), the +6 and +4 valences, sulfate and sulfite, do not affect either hydrogen entry nor do they tend to accelerate general corrosion. However, sulfur species of lower valences, +2.5, +2, and -2 (tetrathionate, thiosulfate, and sulfide), tend to accelerate the entry of hydrogen into metals and tend to accelerate general and localized corrosion, as

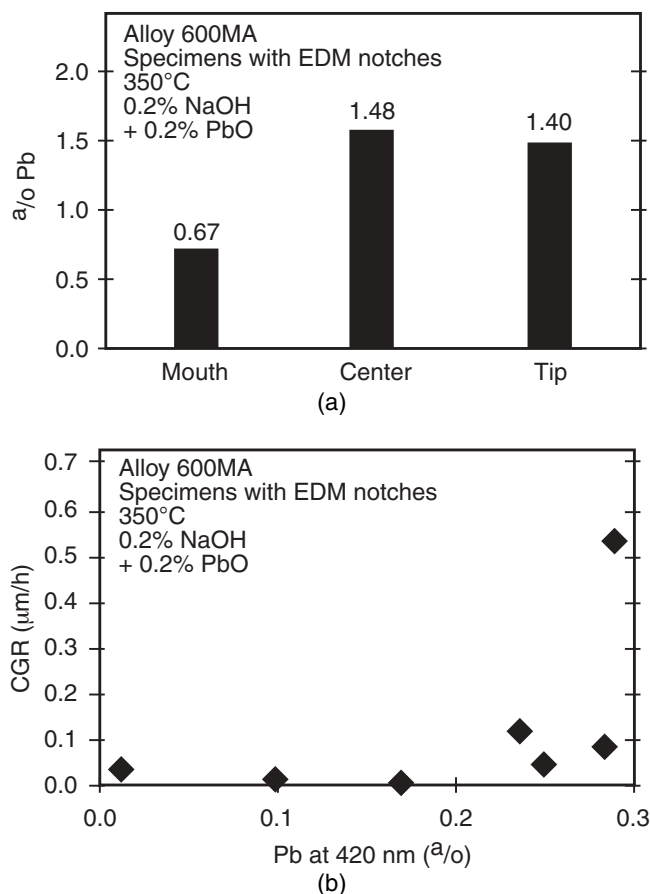


FIGURE 135. (a) Distribution of Pb across opened crack faces from specimens of Alloy 600MA tubing exposed to a 0.2% NaOH + 0.2% PbO at 350°C exposed for times between 163 h and 456 h measured by AES. Average surface concentrations before sputtering plotted. (b) Crack growth rate vs Pb measured at 420 nm into the surface deposit. From Byers, et al.³⁵⁹ ©1997 by the American Nuclear Society, La Grange Park, Illinois.

shown in Figures 145(b) and (d). Thus, with this undesirable effect and the inevitability of producing lower-valence sulfur from reactions with N_2H_4 , there should be a continuing concern for the undesirable effects of lower-valence sulfur species. Further, Alloy 690TT is prone to S^{2-} -SCC and sometimes exhibits transgranular S^{2-} -SCC. Daret, et al.,¹⁷⁶ have reported on the accelerated corrosion of Alloy 600MA due to reduced sulfur, as shown in Figure 70.

There is a long history in corrosion associated with the deleterious effects of “reduced sulfur” on the corrosion of commercial alloys. Therefore, it should not be surprising that it is of concern for Alloy 600.

Included in this discussion are effects of low-valence sulfur species, mainly $S_2O_3^{2-}$ and $S_3O_4^{2-}$, in connection with the S^{2-} -SCC of sensitized Alloy 600. This topic is relevant to the extensive damage sustained in the TMI Unit-1 OTSG steam generators in 1981 when sodium thiosulfate ($Na_2S_2O_3$) in a holding tank was

inadvertently released to the primary coolant during a shutdown period. In OTSGs, the Alloy 600 tubing is sensitized owing to the global heat treatment applied to the fabricated vessel to achieve stress relief. The damage here was extensive in the upper tubesheet area and required many tubes to be explosively expanded in the tubesheet below the damaged area.³⁷⁶

In general, lower-valence sulfur species are deleterious to metals according to Figure 145, and this subject has been studied extensively, especially in the fossil fuel and petroleum processing industries. Thus, the inevitability of N_2H_4 reducing SO_4^{2-} is of historic and well-founded concern for the performance of SG tubing.

S^{2-} -SCC is distinctly different from AcSCC and AkSCC since it does not occur in SO_4^{2-} solutions while it is aggressive in the S^{2-} form as shown in Table 33. However, the effects of lower-valence sulfur have not been studied systematically over the range of relevant pH. Also, Rochester and Eaker⁷⁵ in Table 13 have shown that sulfides occur sometimes inside cracks in OTSG upper bundle regions. Since reduced sulfur species are sometimes found inside advancing SCC, although the exterior environment contains S^{6+} , it may be necessary to note that S^{2-} -SCC is mainly associated with reduced sulfur species in the external environment outside advancing SCC. The reduction of SO_4^{2-} from the outside environment to S^{2-} inside, advancing SCC may occur by the reaction between SO_4^{2-} and metal to produce metal sulfides.

The stable species of sulfur at 300°C are shown in Figure 146. Mainly, it should be noted that the transition from the +6 states to the -2 states occurs slightly above the H_2O/H_2 half-cell equilibrium. In the acidic range below the +6/-2 transition, H_2S is the most stable species and is volatile; the bisulfide exhibits a narrow range of stability contrary to a much broader range at lower temperatures; the sulfide is stable, and generally insoluble, above pH 7. The intermediate species of SO_3^{2-} , $S_3O_4^{2-}$, and $S_2O_3^{2-}$ are unstable relative to the species shown in Figure 147; it is reasonable that they might occur as intermediates in the reduction of SO_4^{2-} and HSO_4^- by N_2H_4 , the half cell for which is shown in Figure 33.⁽⁴⁾

When nickel is present with sulfur species, the stability diagram of Figure 146 changes to that of Figure 147, where Ni-S species at 25°C are shown. While this diagram is not directly applicable at 300°C, it should be generally indicative of tendencies. Most significant is the broad range of stability of NiS over the range of pH and potential. This means that NiS is stable, as in nature, in preference to NiO. This diagram further means that sulfates are reduced by nickel to NiS. The soluble species are not evident until potentials are attained that are not within the range of PWR chemistries.

The effect of sulfur species on the stability of Alloy 600MA has been studied at 95°C by Fang and

⁽⁴⁾ Courtesy of W.T. Lindsay, April 4, 2002. Private communication.

TABLE 28

Chemical Analysis of SCC from Alloys 600MA and 690TT Exposed in 300 ppm Solution of $PbCl_2$ at pH 4.5 at 340°C for 2,500 h and 150% of the Yield Stress. Distance from Outside Surface Shown.^(A)

Alloy	Location	Distance from Surface (μm)	Composition (w/o)				
			Ni	Cr	Fe	Pb	Cl
600MA	Crack mouth	~0	73.33	16.63	8.13	1.08	0.03
	Mid crack	45	73.90	16.84	7.88	0.35	0.05
	Tip	83	74.14	16.64	8.19	0.02	0.04
	Matrix	—	73.84	17.23	7.90	0.0	0.02
690TT	Crack mouth	5	50.52	29.20	7.77	3.73	0.06
	Mid crack	18	58.90	29.55	8.08	1.77	0.03
	Tip	32	59.68	31.26	8.75	0.31	0.0
	Matrix	—	59.77	31.15	8.81	0.0	0.0

^(A) From Sakai, et al.³⁶⁰ ©1992 NACE International.

Staehele,³³⁸ and their results from polarization studies at pH6_{95°C} are shown in Figure 148. These results show that decreasing valence decreases the breakdown potential and raises the passive current densities. Two of the species, $S_3O_4^{2-}$ mainly and $S_2O_3^{2-}$ somewhat, produce accelerated rates of reduction that obscure the anodic behavior at lower potentials.

Despite the inevitable degradation of SG tubes due to lower-valence sulfur species, including Alloy 690TT, little work has been conducted both on the conditions that promote the reduction of SO_4^{2-} and on the conditions for the S^y -SCC of any SG tubing alloys over the range of pH. Only the review of Sala, et al.,¹⁸⁰ the work of Daret, et al.,¹⁷⁶ in Figure 70, the work of Balakristian,⁽⁵⁾ and the work of Sakai, et al.,³⁷⁷ provide fundamental insights. Sala reviewed past work and noted that other authors had accumulated relevant evidence for the reduction of SO_4^{2-} ; she also conducted direct experimental work showing that N_2H_4 would reduce SO_4^{2-} , especially in the presence of catalysts such as magnetite.

As shown by the data in Figures 136 and 137, Miglin and Sarver¹⁸⁸ found that crack initiation in pH 9.9 solution containing PbS is not much different from the same solution containing PbO, but that crack depths were much greater in the PbO case than the PbS case. Both species affect SCC in the vapor phase. The SCC due to PbS is transgranular. Helic³⁷⁸ obtained a similar result, including TGSCC, although he found no SCC of Alloy 690 as did Miglin. Sulfide is occasionally observed in deposits shown in Figures 59 through 66 and Tables 11 and 12 and is often seen in oxides in crevices and on crack faces as for Figure 70.

The dependencies of S^y -SCC on primary variables are as follows:

1. pH

The potential-pH diagrams of Figures 146 and 147 imply that S^y -SCC is likely to occur over the full

⁽⁵⁾ Courtesy of R.L. Tapping, AECL, Chalk River, Ontario, January 3, 2002. Private communication.

TABLE 29

Solubility, w/o, of Some Lead Salts in Water at 25°C^(A)

Salt	Solubility (w/o)
PbNO ₃	36.9
Pb(CH ₃ COO) ₂	35.6
PbCl ₂	1.08
PbF ₂	6.6×10^{-2}
PbO	6.8×10^{-3}
PbSO ₄	4.5×10^{-3}
PbCO ₃	1.1×10^{-3}
2PbCO ₃ · Pb(OH) ₂	1.6×10^{-4}
PbS	8.6×10^{-5}
Pb ₃ (PO ₄) ₂	1.4×10^{-5}

^(A) From Agrawal, et al.,³⁵³ Seidell,³⁶² and Stephen and Stephen.³⁶³

range of pH. However, insufficient data are available to test such a correlation.

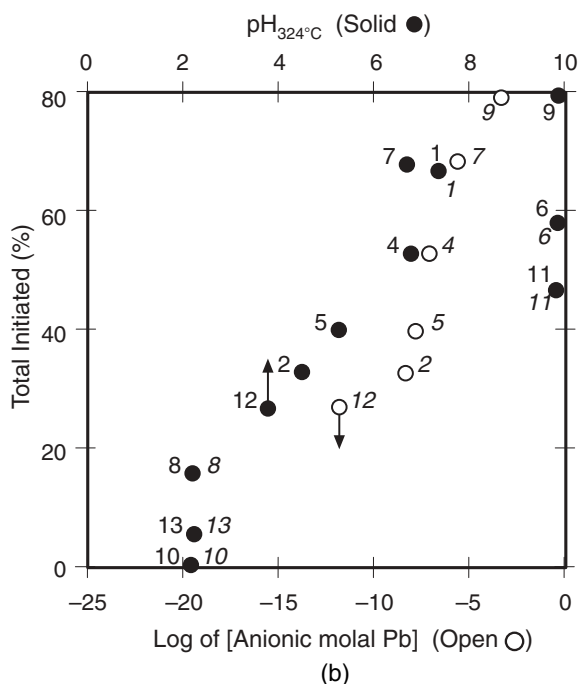
In high-pH solutions, Tables 33 and 34 show that lower-valence sulfur species accelerate S^y -SCC. In Table 33, $Na_2S_2O_3$ exhibits the same intensity of SCC as does PbO relative to only NaOH and produces S^y -SCC in Alloys 800, 690TT, and 600MA in tests at 350°C.

In Table 34, data from cathodic polarization scans of stressed specimens in a 50% NaOH solution with various additions showed that neither sodium carbonate (Na_2CO_3) nor sodium sulfate (Na_2SO_4) produced significant corrosion nor SCC, whereas the lower-valence species of sodium sulfide (Na_2S), sodium hydrosulfide ($NaHS$), and sodium thiosulfate ($Na_2S_2O_3$) produced extensive TGSCC in Alloy 690MA and extensive corrosion in Alloy 600. Since these tests were conducted as cathodic scans, it is not possible to determine the critical range of potential for the occurrence of SCC. Cathodic scans tend to prevent the oxidation of these lower-valence species. However, the results are indicative and consistent with expectations for the differences between lower and higher valences of sulfur, as illustrated in Figure 145.

Canister	Log (molal) Pb(OH) ₃	Environment
1	-6.47	AVT + 0.1 m PbO
2	-8.28	AVT + 0.1 m PbSO ₄
3	—	AVT + 0.1 m PbSiO ₃
4	-7.07	AVT + 0.1 m Pb(H ₂ BO ₃) ₂
5	-7.82	AVT + 0.1 m PbCl ₂ + 0.1 m PbO
6	—	1.0 m NaOH
7	-5.64	Morpholine + 1.0 m NaOH + 0.1 m PbO + 3.0 m H ₃ BO ₃
8	-19.6	Morpholine + 1.0 m PbSO ₄ + 0.1 m NaHSO ₄ + 0.3 m H ₃ BO ₃
9	-3.40	1.0 m NaOH + 0.1 m PbO
10	-19.6	0.1 m PbSO ₄ + 0.1 m NaHSO ₄ + 0.3 m H ₃ BO ₃
11	—	1.0 m NaOH + 0.1 m PbS
12	-11.9	0.2 m PbCl ₂
13	-19.6	0.1 m PbSO ₄ + 0.1 m NaHSO ₄

AVT: All-volatile-treated water (NH₃OH + N₂H₄ to pH 9.3). Morpholine concentration of 10 ppm. Solutions prepared with deoxygenated, high-purity water.

(a)



(b)

HMA Alloy 600 Heat 96834

Canister	pH _{324°C}	SCC/IGC Attack Mode	SCC Attack Depth (% TW)
10	2.2	None	0
13	2.2	IGC	1
8	2.2	IGC	4
12	3.8	IGC	7
2	4.5	IGSCC	9
5	5.3	TG/IGSCC	16
7	6.7	IGSCC	60
4	6.8	TG/IGSCC	50
3	7.1 ^(A)	TG/IGSCC	78
1	7.3	TG/IGSCC	50
6	9.9	IGC	4
11	9.9	IGC	10
9	9.9	TG/IGSCC	35

^(A) Estimated.

(c)

Canisters Where More Damage was Observed in Vapor Than in Liquid^(A)

Canister	pH _{324°C}	Inspection	Material Condition
4	6.8	2nd	LMA/SR
6	9.9	1st	HMA, LMA, LMA/SR, LMA/TT
7	6.7	1st	LMA
7	6.7	2nd	LMA/SR
9	9.9	2nd	HMA, 690TT
11	9.9	2nd	LMA/TT, 690TT

^(A) See Figure 137 for bases.

(d)

FIGURE 136. (a) Environments used in each canister. (b) Total percent of specimens with initiated SCC vs pH and vs concentration of anionic Pb for 13 canisters containing solutions with different pH at 324°C with C-rings taken from SG-type tubing loaded to 0.5% total strain. (c) PbSCC morphology and maximum depth of PbSCC as percent through-wall. (d) Canisters where more damage was observed in vapor than in liquid phase. From Miglin and Sarver.¹⁸⁸ Used by permission of EPRI.

The results in Tables 33 and 34 show clear effects of lower-valence sulfur and their deleterious effects on a range of alloys, including Alloy 690 in the 10% and 50% NaOH solutions. However, these results need clarification.

In the range of lower pH where experiments were conducted with AVT chemistry, the results from work

in model boilers by Daret in Figure 70 show clearly that the SCC of Alloy 600MA is due to the presence of sulfides, while Alloy 690 was not attacked in these same tests.

In the range of pH_{RT} 3, results in Figure 149(a) with sensitized Alloy 600 show that S^y-SCC occurs rapidly with increased concentrations.¹⁷⁸

Material	Condition	Results from Modified Huey Test, mg/dm ² /day
Alloy 600 LTMA ^(A)	Low temp. mill anneal, 926°C anneal	11.4
Alloy 600 HTMA ^(A)	High temp. mill anneal, 1,024°C anneal	26.1
Alloy 600 NX5185	Combustion engineering heat number	31.8
Alloy 600 NX9276	Combustion engineering heat number	24.1
Alloy 600 SR ^(A)	Low temp. mill anneal + stress relief, 621°C/10 h	27.0
Alloy 600 TT ^(A)	Low temp. mill anneal + thermal treatment, 704°C/16 h	26.6
Alloy 690 TT ^(A)	Mill anneal + thermal treatment, 1,080°C anneal + 705°C to 720°C/5 h	—

All B & W Alloy 600 Specimens 0.038 Carbon

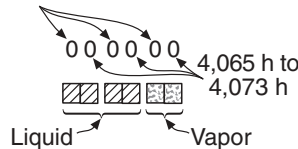
Specimens 0.075 OD x 0.043 Wall Tubing

Test 325°C

All C-rings 0.5% Strain

▨ Liquid ▩ Vapor

2,056 h to 2,063 h



- 0 = No corrosion
- X = Specimen removed; not in 4,065 to 4,075 h test
- $0.x = \frac{TGSCC}{TGSCC + IGSCC}$
- G = IGC, intergranular cracking
- P = Small pits
- P' = Large pits
- S = Slight SCC penetrations
- R = Rough surface
- W = Wastage
- I = Intergranular initiation
- T = Transgranular initiation
- ↑ = Arbitrary assumption, 50% penetration

(A) Specimens prepared by Babcock & Wilcox.

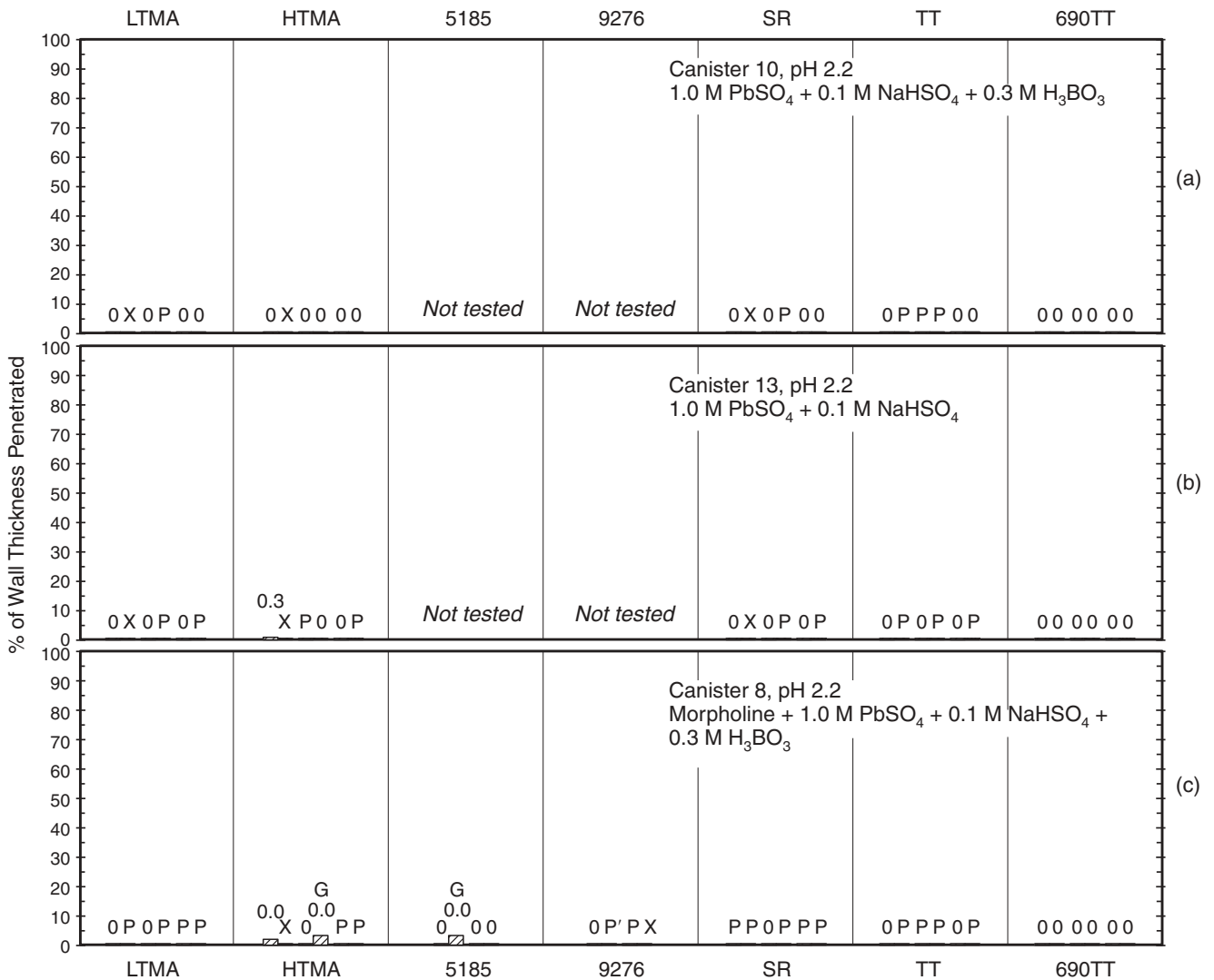


FIGURE 137. Percent of wall thickness penetrated vs alloy for different values of pH_T and different environmental chemistries. From Miglin and Sarver.¹⁸⁸ Used by permission of EPRI.

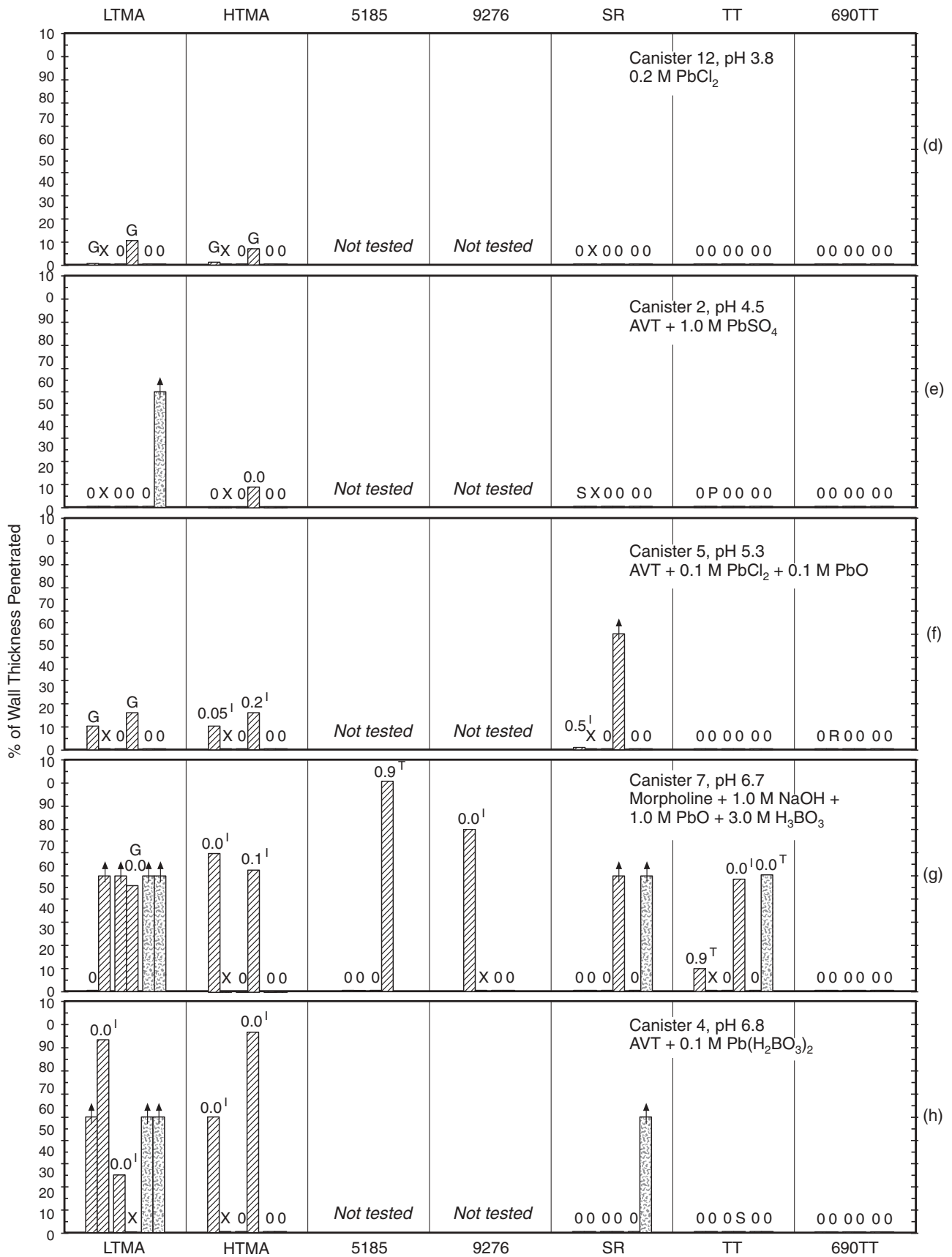


FIGURE 137 (continued). Percent of wall thickness penetrated vs alloy for different values of pH_T and different environmental chemistries. From Miglin and Sarver.¹⁸⁸ Used by permission of EPRI.

Downloaded from http://meridian.allenpress.com/corrosion/article-pdf/60/2/115/1536060/1_3287716.pdf by Edward Richey on 14 September 2022

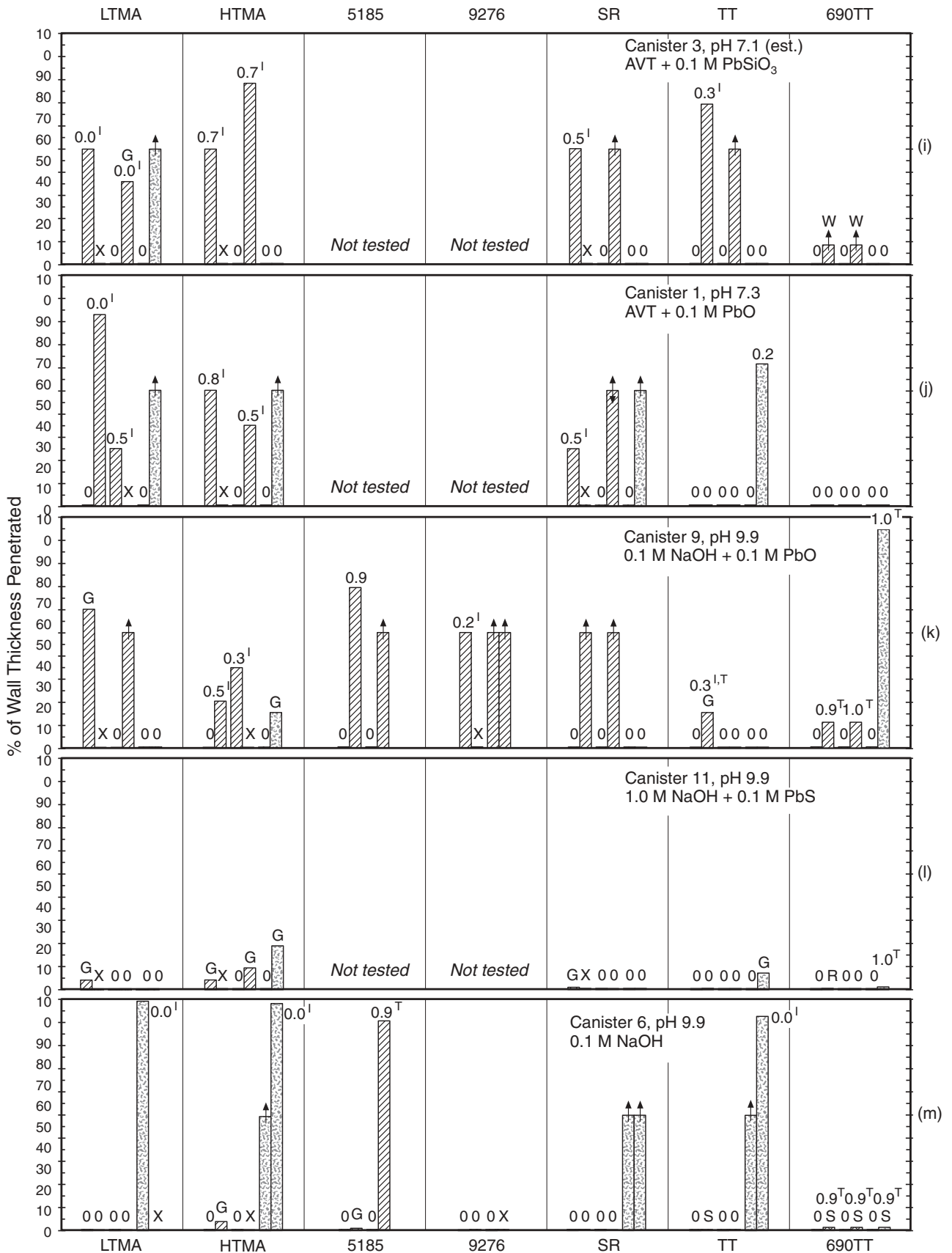


FIGURE 137 (continued). Percent of wall thickness penetrated vs alloy for different values of pH_T and different environmental chemistries. From Miglin and Sarver.¹⁸⁸ Used by permission of EPRI.

TABLE 30

Effect of Heat Treatment on the PbSCC of Alloy 600 in Pure Deaerated AVT Water Containing Lead at 332°C^(A)

Material Condition Mill Annealed	Inspection Time		Crack Path	
	350 h	1,350 h	150% YS, ^(B) 1,350 h	90% YS, 1,350 h
Purified^(C)	↑	↑	↑	↑
1,200°C/4 h	↑	↑	Predominantly IGSCC	Predominantly IGSCC
1,200°C/16 h	↑	↑	↓	↓
1,100°C/4 h	↑	↑	IGSCC	IGSCC
1,100°C/16 h	↑	↑	↑	↑
1,100°C/72 h	↑	↑	Predominantly TGSCC ^(D)	Predominantly TGSCC ^(D)
Thermally Treated				
593°C/1 h	↑	↑	IGSCC	IGSCC
593°C/10 h	No cracks with binocular microscope	All specimens cracked extensively	↑	↑
593°C/24 h	↑	↑	↓	↓
593°C/100 h	↑	↑	IGSCC	IGSCC
650°C/1 h	↑	↑	↑	↑
650°C/10 h	↑	↑	↓	↓
650°C/24 h	↑	↑	IGSCC	IGSCC
650°C/100 h	↑	↑	↑	↑
705°C/1 h	↑	↑	↓	↓
705°C/10 h	↑	↑	IGSCC	Cracking not detected
705°C/24 h	↑	↑	↑	↑
871°C/1 h	↑	↑	IGSCC	IGSCC
871°C/5 h	↑	↑	IGSCC	IGSCC

^(A) From Airey.³⁶⁵ ©1979 NACE International.

^(B) No SCC in AVT water without Pb after 7,000 h by binocular microscope. No SCC in AVT water at 4,500 h by metallography.

^(C) Purified by heat treating gas atmosphere.

^(D) Initiation seems IGSCC for several grains.

TABLE 31

SCC of Double U-Bend Specimens of Alloys 600MA and 600SN in Aerated Water with 0.67 g/L PbO at 316°C^(A)

Heat No.	Material Annealed at 1,066°C for 15 min		Material Heated at 649°C for 1 h	
	Weeks to Crack	SCC Path and Depth of Crack	Weeks to Crack	SCC Path and Depth of Crack
Lab 1	6	Deep IG	8	Deep TG
Lab 2	6	Deep IG	8	Shallow TG (2 to 5 grains deep)
Lab 3	4	Deep IG	8	Deep TG
Lab 4	2	Deep IG	8	Deep TG
Lab 5	4	Deep IG	8	Deep TG
Commercial production	8	Deep TG Deep IG	8	Deep TG

^(A) From Sarver.³⁶⁶

Since the sensitized Alloy 600 represents a nickel-rich and chromium-depleted phase at the grain boundaries, it seems that the S^y-SCC is a phenomenon that depends on lower Cr, at least in the mid-range of pH. However, the data from Figures 7 and 73 show that Cr is quite soluble in alkaline regions both with respect to pH and potential. This may account, at least partially, for the severe S^y-SCC of Alloy 690TT but much less S^y-SCC of Alloy 600MA shown in Tables 33 and 34. This effect of chromium depletion and sensitization may apply only for relatively higher oxidizing potentials. However, Daret, et

al.,¹⁷⁶ shows that S^y-SCC occurs in Alloy 600MA materials in the AVT water of model boiler tests.

2. Potential

Figures 149(c) and (d) show that the potential dependence for S^y-SCC at 22°C for sensitized Alloy 600 in thiosulfate and tetrathionate solutions is similar to that for alkaline solutions (Figure 97) and acidic solutions (Figure 123). The higher potential of the peak for tetrathionate in Figure 149(d) relative to that for thiosulfate in Figure 149(c) relates to the higher breakdown potential for the tetrathionate as shown in Figure 148. Figure 150(a) shows data that

TABLE 32
Results from Visual Examination after Tests at 350°C (Cracked Samples/Tested Samples)^(A)

Material	Time (h)	10% NaOH	10% NaOH + 0.1 M PbO	10% NaOH + 0.01 M PbO	4% NaOH + 0.02 M PbO
Alloy 800 D	500	3/3	4/4		
Alloy 800SP E	500			0/7 (2/2) ^(B)	0/7
	600			5/5	—
	750				—
	1,000				0/5 (0/2) ^(B)
Alloy 800SP C	500	15/15	15/15	0/7 (2/2) ^(B)	3/7
	600			5/5	—
	750				—
	1,000				0/2 (0/2) ^(B)
Alloy 690TT A	500	0/15	15/15	6/7 (7/7) ^(B)	0/7 (1/2) ^(B)
	750	0/13			—
	1,000	0/9			5/5
Alloy 690TT B	500	0/15	15/15	0/7	0/7
	600	—		4/5 (5/5) ^(B)	—
	750	0/13			—
	1,000	0/9			0/5
Alloy 600MA G	500	8/9	0/9 (3/3) ^(B)	0/7 (2/2) ^(B)	0/7 (2/2) ^(B)
	600	—		0/5 (2/2) ^(B)	—
	750	6/7			—
	1,000	3/3			0/5 (5/5) ^(B)

^(A) From Castano-Marin, et al.³⁶⁹ Courtesy of TMS, Warrendale, PA.

^(B) Visual examination after bending the specimens.

—: No visual examination was performed.

Blank Space: No specimens of this type were in the test.

are similar to Figure 149(c), although the latter includes a wider range of potential. The longer times of crack initiation of the data in Figure 150(a) show a greater range of SCC than is observed in Figure 149(c).

Figure 150(a) also shows that a heat treatment equivalent to Alloy 600TT produced accelerated S^v-SCC at a temperature as low as 95°C and at potentials that are oxidizing to the open-circuit potential. This indicates that Alloy 600TT tubing can be sensitized to some degree, at least for some heats.

The polarization curves shown in Figure 148 of Fang and Staehle³³⁸ are part of a larger study over the range of pH 3 to 8. They show that the same patterns persist for effects of valence and alloys, with Alloy 690 exhibiting more stability.

3. Species

S^v-SCC depends mainly on lower-valence sulfur, and the +6 valence does not accelerate S^v-SCC in the high-pH environments as shown in Table 34. Also, while the addition of carbonate generally accelerates AkSCC as shown in Figure 97, it produces no effect without reduced sulfur in static autoclave tests as shown in Table 34.

Daret, et al.,¹⁷⁶ have demonstrated clearly that N₂H₄ reduces sulfates and resins to lower-valence sulfur in normal AVT conditions at typical SG temperatures. They have shown that the amount of re-

duced sulfur does not depend on the concentration of N₂H₄ in their range of concentrations. It appears that, once the oxygen is reacted, N₂H₄ has no more effect on the electrochemical potential.

Daret, et al.,¹⁷⁶ also show that the reduced sulfur is preferentially concentrated in the steam phase. This is no doubt due to the volatility of H₂S that occurs in neutral solutions, as shown in Figure 146.

4. Alloy Composition

Table 33 shows that S^v-SCC occurs extensively for Alloys 800, 690TT, and 600MA in strong caustics. The model boiler tests of Daret¹⁷⁶ show that Alloys 600MA and 800 are susceptible in near-neutral conditions, although Alloy 690 was not affected. This pattern indicates that the reduced sulfur effect is broadly significant for alloys used for SG tubes. Such effects are also known for stainless steels and low-alloy steels from extensive work in the petroleum and fossil fuel industries.

5. Alloy Structure

Aside from the accelerating effect of sensitization shown in Figures 149 and 150, there is little information available. Figure 150 shows that increasing sensitization accelerates S^v-SCC, that mill-annealed material sustains no SCC in thiosulfates at low temperatures, and that Alloy 600TT may be susceptible to SCC in thiosulfates.

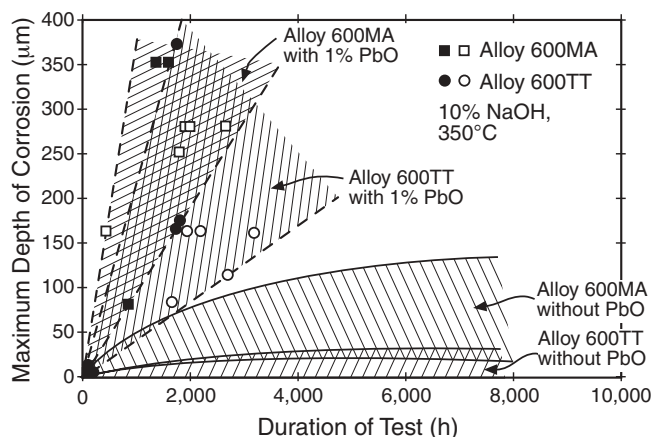


FIGURE 138. Depth of IGA and GC vs time for Alloys 600MA and 600TT exposed at 350°C in 10% NaOH with and without additions of PbO. From Vaillant, et al.³⁷⁰ Courtesy of CEFRACOR (Centre Français de L'Anticorrosion), Paris, France.

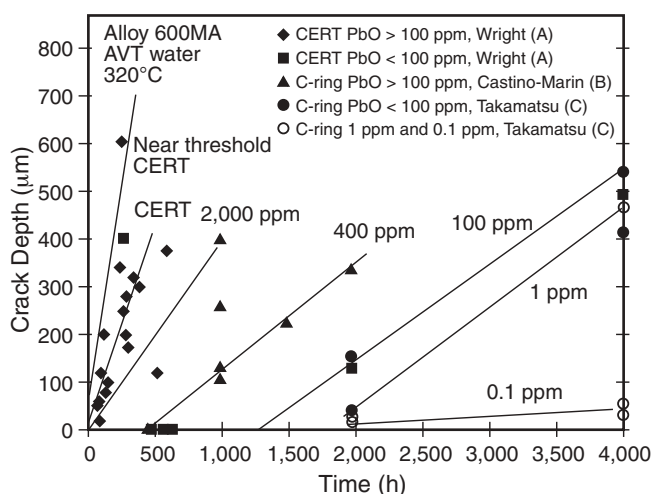


FIGURE 139. Crack depth vs time data for Alloy 600MA in AVT water at 320°C with various concentrations of PbO. From Wright and Mirzai,³⁷¹ with data from [A] Wright,³⁷² [B] Castano-Marín, et al.,³⁶⁹ and [C] Takamatsu, et al.³⁵⁸ Courtesy of TMS, Warrendale, Pennsylvania.

6. Temperature

Figure 149(b) shows that the activation energy for SCC of sensitized Alloy 600 is low and most likely related to chemical or liquid phase processes.

7. Stress

Figure 150(b) shows that the crack propagation rate of solution-annealed Alloy 600 increases rapidly with stress intensity according to what is probably Stage I behavior. This rate decreases with decreasing potential and is negligible at the deaerated corrosion potential. The higher rates are likely related to film breakdown conditions based on values of the applied potentials, although the -400 -mV data are from a region of apparently stable passivity while the $+100$ -mV data are from a region of breakdown of passivity.

5.2.7 Doped Steam SCC (DSSCC) — A steam phase occurs in heat-transfer crevices in steam generators depending on the superheat. Figures 10, 79, and 80 show schematic views of heat-transfer crevices indicating that a substantial area contains a steam phase. Figure 79 shows such a dryout region based on calculations of an asymmetrically located tube in a deposit-free drilled hole. The substantial increase in concentration of species as well as the large differences between the inside of crevices and the adjacent free-spans shown in Figures 59 through 68 and Tables 11 and 12 indicate features related to concentration and dryout. Also, the high apparent activation energies for SCC at tube supports shown in Figure 18 indicate a strong dependence on superheat. Finally, the general pattern of SCC in drilled holes as shown in Figure 16 follows the pattern of dryout.

While there is evidence for a steam phase in heat-transfer crevices, especially at higher superheat, together with the accompanying concentration of chemicals, most of the corrosion work described herein has been conducted in single-phase aqueous environments with some of the LPSCC work conducted in steam. This raises serious questions regarding the relevance of the corrosion work conducted in aqueous solutions to most of the failures that have occurred in SGs.

To identify this regime of environment and resulting SCC associated with the steam environment inside heat-transfer crevices, the term “doped steam stress corrosion cracking” (DSSCC) is suggested. Chemically, this is not so precise as AkSCC, AcSCC, and the others; however, this identity emphasizes an important issue that needs to be considered. The term, “doped steam,” is illustrated by the work of Dehmlow¹⁸⁷ shown in Figure 75 in which he conducted experiments in the steam phase in contact with an aqueous phase at lower temperature that contained small quantities of various chemicals, e.g., “dopants” as is the popular term. Since this term is widely used and understood, it is used here to identify a steam phase that contains chemicals, some of which can be aggressive.

Treating DSSCC according to the seven principal variables as done in the other submodes is not convenient since there are so few data and since these data do not fit categories readily. The larger issue here is a question of implication and proof: i.e., is DSSCC a major issue and how should it be evaluated? These issues are discussed as follows, based on various observations and investigations:

1. Dehmlow's Work¹⁸⁷

Dehmlow's experimental results are shown in Figure 75 where he studied the behavior of Alloys 600MA and 690TT as well as two weld materials at four applied stresses using a hydrogenated steam environment at 399°C and 100 ppm each of sodium

sulfate (Na_2SO_4), sodium nitrate (NaNO_3), sodium chloride (NaCl), and sodium fluoride (NaF) in the water phase. Accelerated failures occurred for Alloy 600MA at all stresses including zero applied stress (although it is likely that his specimens contained high residual stresses). Failures occurred at higher applied stresses for the weld material EN82H. Failures occurred extensively as early as 7 days; this is quite early at low stress for LPSCC at this temperature. Dehmlow's approach is reasonable in view of the idea of impurities being transported from aqueous (lower temperature) to steam phases (400°C) and possibly to a water layer in contact with the steam. Dehmlow's work may be important as a kind of "contaminated LPSCC," similar to the effect of contaminants shown in Figure 88(e) for studies of sensitized stainless steels in connection with BWR technology. Such a connection with LPSCC has yet to be explored. Certainly, the broad range of deposit chemistry shown in Figures 59 through 72 and Tables 11 and 12 would support a variety of dopants including the ones used by Dehmlow. The fact that Alloy 690 did not sustain SCC in Figure 75 is similar to the result for LPSCC where Alloy 690 also does not sustain LPSCC in low-potential pure water and may suggest a connection. It should be noted that the concentrations of species in the aqueous phase of Dehmlow's work was quite dilute relative to the inevitably saturated solutions in heated crevices.

2. Tsuruta's Work on Doped Steam³⁰³

Tsuruta, et al., examined effects of impurity species added to steam and water using tubular specimens that were cold worked by skip expansion and others that were standard tensile specimens. He found that tensile specimens stressed to 588 MPa did not sustain acceleration due to impurity additions. However, in the configuration of the skip roll transition, he found that the impurity additions of 80 ppm produced extensive SCC at 400°C and that the following effects were observed:

- F^- was the most aggressive of the single impurities.
- A synergistic effect of $\text{F}^- + \text{Cl}^-$ and $\text{F}^- + \text{SO}_4^{2-}$ produced through-wall SCC in 30 h but no synergistic effect of $\text{Cl}^- + \text{SO}_4^{2-}$ was observed.
- A combination of $\text{F}^- + \text{Cl}^- + \text{SO}_4^{2-}$ gave the greatest acceleration.
- Acidic additions did not accelerate failure whereas alkaline additions did. This is consistent with the findings shown in Figures 136 and 137.

As with the work by Dehmlow, the work of Tsuruta was not carried out with the saturated chemicals expected in heat-transfer crevices.

3. Miglin's Work on Steam and Water Phases for PbSCC¹⁸⁸

Figures 136 and 137¹⁸⁸ from Section 5.2.5 on PbSCC show the dependence of PbSCC on pH for

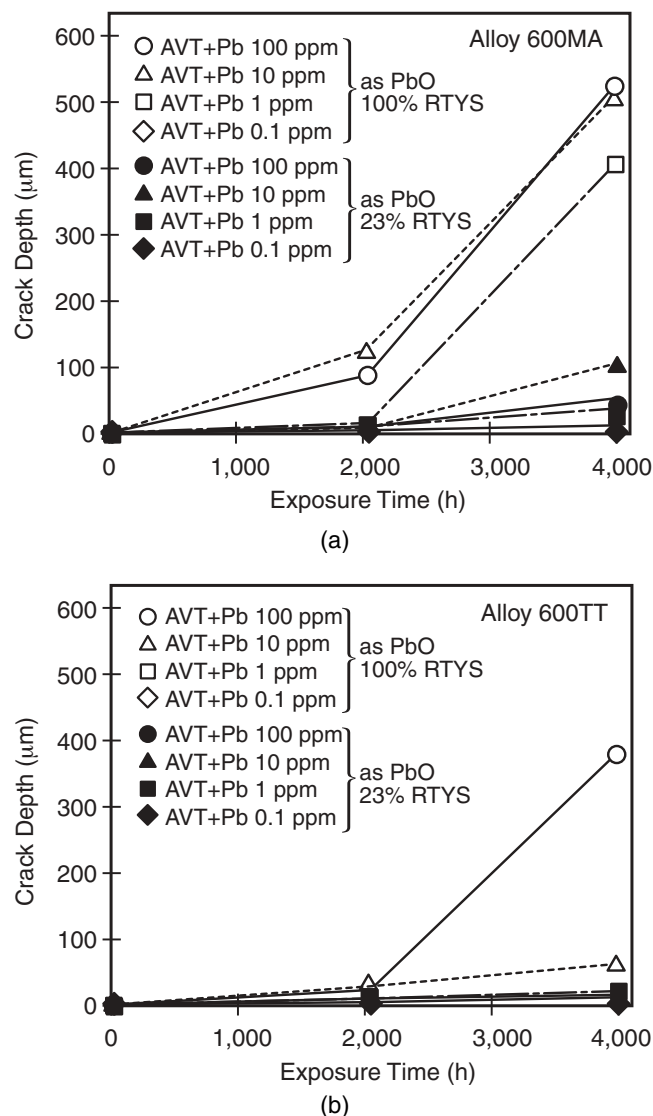


FIGURE 140. Crack depth vs time for various concentrations of Pb at two stresses and for Alloys 600MA and 600TT in deaerated AVT water containing 0.26 ppm NH_3 + 0.1 ppm N_2H_4 . From Takamatsu, et al.³⁵⁸ ©1997 by the American Nuclear Society, La Grange Park, Illinois.

SCC in water and wet steam phases. The extent of PbSCC initiation increases with increasing pH in the aqueous phase; and the extent of PbSCC in the steam follows the same pattern but starts at higher pH. While PbSCC occurs in the water phase at lower pH, it does not occur in the steam phase until the bulk pH_T increases to about 7. Miglin's work suggests that acidic environments are not sufficiently volatile or at least do not interact on the surface in equilibrium with the steam. Miglin's work also shows that the wet steam phase is substantially aggressive to Alloy 690 at the higher pH; this result differs from that of Dehmlow, with supercritical steam, although the ranges of pH and chemistries of the liquid media are different.

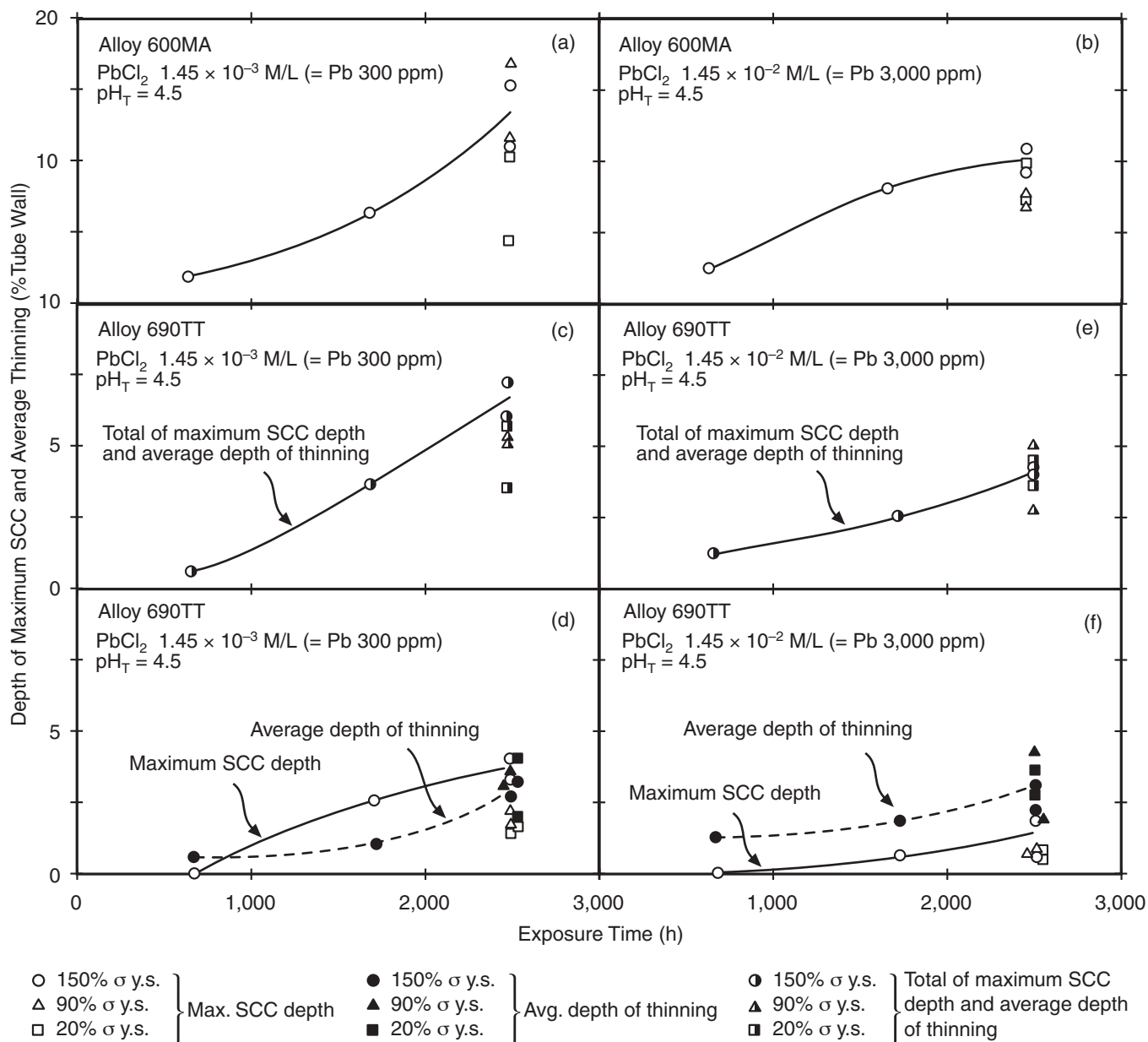


FIGURE 141. Depth vs time for PbSCC at $\text{pH}_{340^\circ\text{C}} = 4.5$ in with various applied stresses for 2,500 h exposure in water, where $O_2 < 5$ ppb and Pb added as PbCl_2 . From Sakai, et al.³⁶⁷ (a) Alloy 600MA at 1.45×10^{-3} M/L of PbCl_2 , (b) Alloy 600MA at 1.45×10^{-2} M/L of PbCl_2 , (c) Alloy 690TT at 1.45×10^{-3} M/L of PbCl_2 , Total of maximum SCC depth plus average depth of thinning. (d) Alloy 690TT at 1.45×10^{-3} M/L of PbCl_2 , Maximum SCC depth plus average depth of thinning. (e) Alloy 690TT at 1.45×10^{-2} M/L of PbCl_2 , Maximum SCC depth plus average depth of thinning. (f) Alloy 690TT at 1.45×10^{-2} M/L of PbCl_2 , Maximum SCC depth plus average depth of thinning. From Sakai, et al.³⁶⁷ ©1991 by the American Nuclear Society, La Grange Park, Illinois.

4. Economy's Work on Temperature Dependence¹⁷⁷

Figure 74 shows that the initiation time for LPSCC follows a monotonic dependence on $1,000/T$ from hydrogenated steam to water. This suggests that the mechanistic processes at least for LPSCC are the same. These results suggest that data from water and steam phases, at least for pure water, are relevant to each other. What this means for solutions containing chemical species is not clear, although it

can be noted that many of the relevant salts are sparingly soluble in steam; and, of course, sulfur could be easily transformed to H_2S under appropriate test conditions.

5. OTSG Cracking in Superheat Region^{75,185}

The superheated region of OTSG SGs is nominally dry, yet extensive SCC has occurred in this region, especially at scratches, as shown in Figure 71. Further, extensive IGC occurs randomly on surfaces, not at the scratches. Also, as noted in Figure 71 and

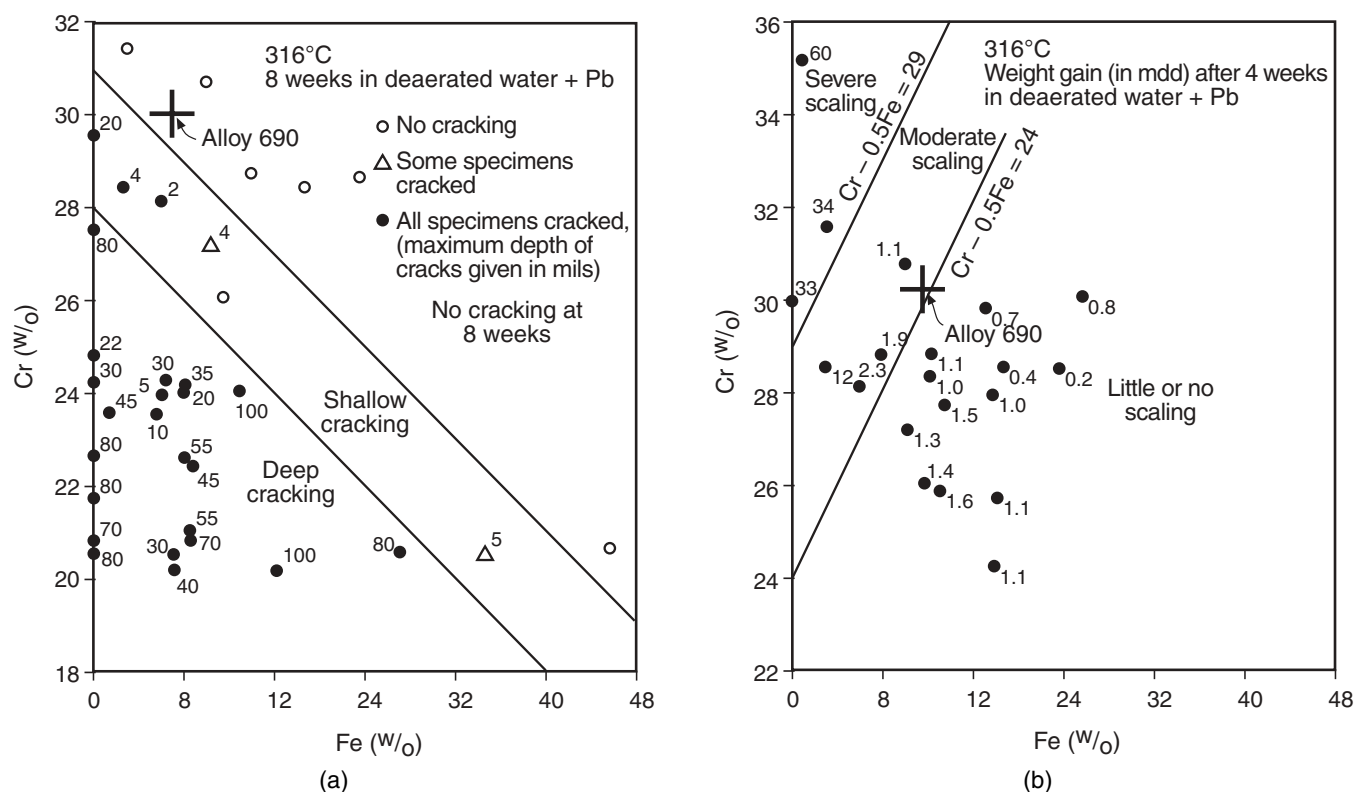


FIGURE 142. (a) Maximum depth of SCC of Ni-Cr-Fe alloys after 8 weeks in deaerated water plus Pb at 316°C. (b) Weight gain of Ni-Cr-Fe alloys after 4 weeks in deaerated water plus Pb. From Sarver, et al.³⁶⁶

Tables 13 and 14, extensive transport of species has occurred along the cracks including to the tips. This suggests that the SCC and possibly the contaminated surfaces are functioning as capillaries and are stabilizing an aqueous phase, while the outside bulk environments are dry steam. Perhaps a more direct interpretation is that SCC is occurring in the steam phase.

6. Model Boiler Testing

Daret and coworkers have conducted model boiler testing^{176,384-387} for evaluating alloys, water chemistry, and inhibitors. Daret and Cassagne³⁸⁸ compare relative advantages of isothermal and model boiler testing. They note that isothermal testing provides good data for evaluating the dependencies of SCC on important variables; however, the model boiler testing provides information more like the heat-transfer crevices. They compare, for Alloy 600, results from isothermal and model boiler tests approximately as follows: (a) An applicable crack growth rate in NaOH for Alloy 600MA in isothermal tests at 320°C might be $1.8 \mu\text{m h}^{-1}$, whereas an equivalent crack growth rate in the model boiler would be $2 \mu\text{m h}^{-1}$ to $9 \mu\text{m h}^{-1}$. (b) A threshold stress for AkSCC of Alloy 600MA might be 0.8 to 0.9 of the yield stress (200 MPa to 250 MPa) of the tubing at 320°C, whereas a threshold in the model boiler is in the range of 120 MPa. (c) With respect to comparing

Alloy 600MA with Alloy 600TT, they find that the crack growth rates are the same for both heat treatments in isothermal testing; for model boiler testing with sludge they find that the average crack growth rates are $2 \mu\text{m h}^{-1}$ to $8 \mu\text{m h}^{-1}$ for the MA product and only $0.4 \mu\text{m h}^{-1}$ for a TT tube. While these comparisons are probably not ideal, they indicate that the model boiler produces a more severe test and differentiates better among heat treatments. How this increased severity relates to steam phases is not clear; but it seems that the heat-transfer crevice is more severe and that, according to observations in the various papers of Daret and coworkers, accelerated corrosion may be focused at the liquid-steam interface. They have not explicitly evaluated the doped steam case with the exception of the reduced sulfur case referred to in no. 7 of this section.

7. Concentration of Reduced Sulfur in Vapor

Daret, et al.,¹⁷⁶ investigated the reduction of sulfur species in N_2H_4 -containing environments under SG conditions. They found that reduced sulfur species concentrated preferentially at least by an order of magnitude in the vapor phase. This result is quite likely associated with the formation of H_2S according to the prediction in Figure 146. However, similar gaseous species, which are stable in low-potential environments, including PH_3 , NH_3 , and CH_4 , might also be formed and segregate preferentially to the steam

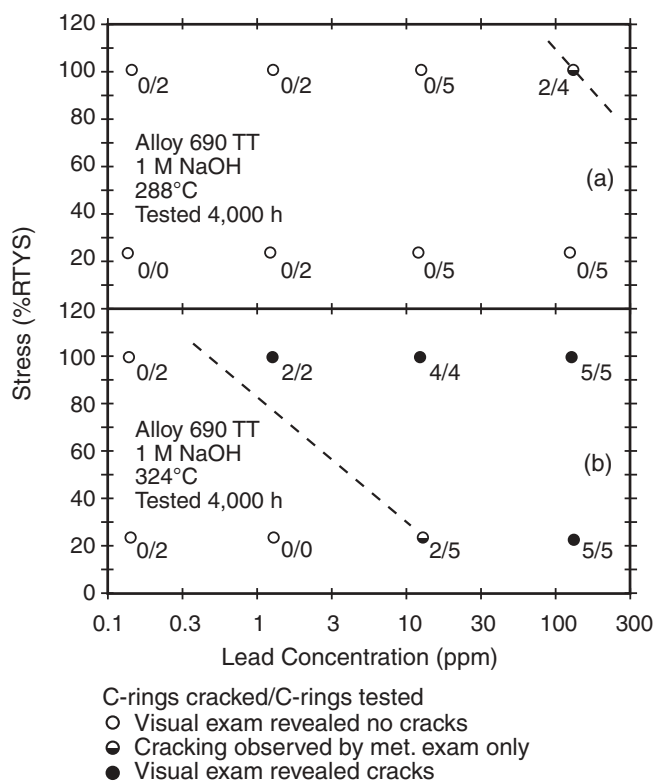


FIGURE 143. Stress vs lead concentration for the PbSCC of Alloy 690TT in 1 M NaOH at 288°C and 324°C. From Sarver. Courtesy of J.M. Sarver, Babcock and Wilcox, Alliance, Ohio, November, 2001. Private communication.

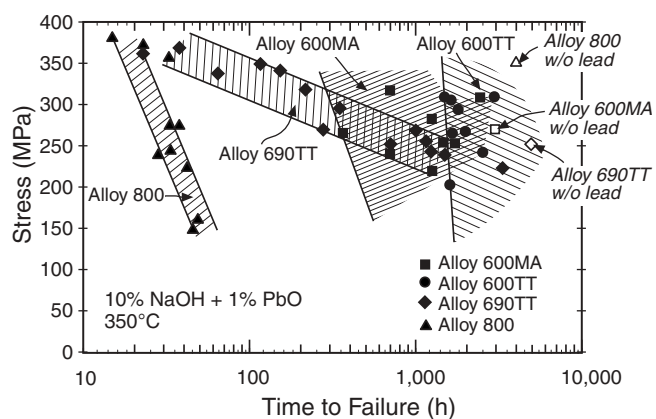


FIGURE 144. Stress vs time-to-failure of Alloys 600MA and 600TT (two tubes), 690TT (four tubes), and 800 (two tubes) in 10% NaOH + 1% PbO at 350°C. From Vaillant, et al.³⁷⁴ Courtesy of EDF and Rocher, et al.³⁷⁵ Courtesy of CEFRACOR (Centre Français de L'Anticorrosion), Paris, France.

phase. In particular, the segregation of H₂S may accelerate both GC and SCC and also accelerate the entry of hydrogen into adjacent alloys.

8. Water Layers

Lee and Staehle³⁸⁹⁻³⁹³ have investigated the thickness of water layers on various substrates to 85°C as a function of relative humidity. An example of their

results is shown in Figure 151 for nickel substrates at 7°C and 85°C. At a 100% relative humidity, the thickness of the water layer would be about 2.4 nm at 7°C and 3.2 nm at 85°C. They obtained similar data for iron and copper substrates. How these data would relate to a heat-transfer surface on a tube in a crevice is not clear. Comparing the data from Figures 151(a) and (b) suggests that the thickness of the water layer increases with temperature. Whether this trend persists and whether it is applicable in a heat-transfer crevice with its complexity of chemistry and deposits is not clear. Nonetheless, the data indicate that a water layer might be stable in the steam-saturated environment inside a heated crevice.

9. Complex Environments

Table 20 from Vaillant and Stutzmann³⁹⁴ shows SCC data for simple and complex environments involving both liquid and vapor phases. In four cases, SCC was observed in the wet (but not superheated) vapor phase, and in three cases the SCC in the vapor phase was on the same order as that in the liquid. In Table 20, the environments were complex so that identifying critical compositions in the vapor phase is not possible.

10. Capillary Condensation

It is reasonable that the porosity of a packed crevice and the formation of deposits as described in Figures 59 through 68 would provide geometries that would stabilize aqueous phases based on the Kelvin equation.³⁹⁵ Further, the SCC and IGC are typified by tight geometries and there is clear evidence for liquid phase movement along these geometries in Figure 72. Such stabilization together with the formation of a liquid layer may produce the basis for electrolytes on the tube surfaces regardless of an intermediate steam phase. The concentration of species in this electrolyte would be in equilibrium with the concentrated liquid at the water/steam interface.

11. Implications

1. There remain major questions as to whether most of the existing isothermal corrosion data taken in the liquid phase of autoclaves applied to any of the significant modes of SCC in steam generators and whether the more relevant data are those such as Dehmlow's,¹⁸⁷ Miglin and Sarver's,¹⁸⁸ and Daret and Cassagne's.³⁸⁸ This matter requires serious attention from the point of view of predicting future performance.

2. The question of prediction in the future depends strongly on the properties of line contact supports, how deposits accumulate, and how these deposits cause local chemistries, steam environments, and stress gradients. There is little work in this area and much better quantification is required from the point of view of DSSCC.

3. There has been no definitive work on the mechanistic processes associated with DSSCC, and whether such a submode is legitimately unique has

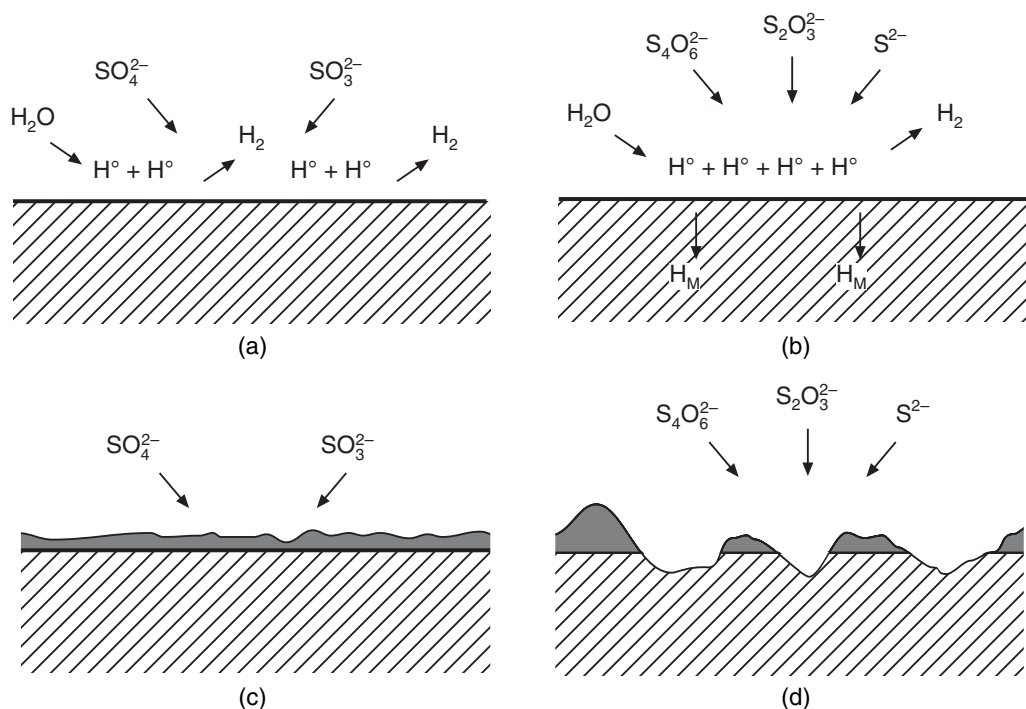


FIGURE 145. Schematic view of effects of sulfur anions on the entry of hydrogen and corrosion as applied to high-nickel alloys. (a) +6 and +4 species do not affect the entry of hydrogen. (b) +2.5, +2, and -2 species promote the entry of hydrogen owing to the poisoning effect on the combination reaction, $\text{H}^\circ + \text{H}^\circ = \text{H}_2$. (c) +6 and +4 species do not significantly affect general and localized corrosion. (d) +2.5, +2, and -2 species accelerate general and localized corrosion.

not been established. DSSCC, for example, could simply be one of the other submodes but with a thin water layer where kinetic processes are relatively more rapid or slowed.

5.2.8 Organic SCC (OgSCC) — The deposits shown in Figures 55 and 59 through 72, Tables 8, 9, and 12 indicate that organic species have been observed in deposits and hideout return. On the other hand, relatively limited work has been conducted to assess the significance of organic species. Several workers have suggested in various forums that organic species may be important in view of their well-known complexing to produce organo-metallic species and in view of the fact that other metals, notably titanium, sustain SCC in alcohol solutions depending on their chain length.³⁹⁶

There are no data to assess the dependence of OgSCC on principal variables. Since there are no data, there is little basis for speculation aside from the fact that the question should be considered.

Daret,³⁸⁵ using model boilers, has shown that acetic acid (CH_3COOH) and formic acid (CH_2O_2) produced no SCC on Alloy 600. When a mixture of acetic, glycolic ($\text{C}_2\text{H}_4\text{O}_3$), and formic acids were added to a dilute alkaline solution with 0.06 mg hg^{-1} sodium during 189 days of testing, the corrosion was inhibited. When the same mixture was added to dilute sulfuric acid (H_2SO_4) of $1 \text{ mg hg}^{-1} \text{ SO}_4^{2-}$, only shallow IG penetrations were produced over 160 days.

Pierson, et al.,³⁹⁷ investigated the effects of resins and acetic acid together with Pb in SO_4^{2-} , Fe_3O_4 , and Na_2SiO_3 . They discovered that both the resins and acetic acid accelerated SCC. Under some conditions, these effects were obscured by effects of Pb.

Vaillant and Stutzman³⁹⁴ could show no specific effect of acetic acid in simple solutions shown in Table 20, but its combination in more complex species produced aggressive SCC.

Despite the paucity of data, the possibility that OgSCC is important and cannot be neglected.

5.2.9 Low-Temperature SCC (LTSCC) — In conducting research on crack growth, Smialowska had removed a cracked specimen of highly stressed Alloy 600MA tubing from an autoclave, allowed it remain on a laboratory table, and later noticed that the SCC had continued to grow at room temperature. This finding, with further test verification, was reported by Xia, et al., in 1991.³⁹⁸ They reported both crack initiation and growth at room temperature in highly stressed specimens of Alloy 600MA for up to 6 weeks following removal of the specimens from the autoclave in which they had been exposed to a high-temperature hydrogenated environment. The maximum room temperature crack growth, starting from an undetectable crack, was about 10 mm after 6 weeks. They attributed the cracking to effects of hydrogen that had been absorbed by the metal in the high-

TABLE 33

Results from Visual Examination of Specimens Exposed^(A) to Alkaline Solutions at 350°C with Added Species (Cracked Samples/Tested Samples)^(B)

Material	10% NaOH	10% NaOH + 0.1 M CuO	10% NaOH + 0.1 M PbO	50% NaOH + 5% Na ₂ S ₂ O ₃	0.75% M Na ₂ SO ₄ + 0.25% M FeSO ₄	0.75% M Na ₂ SO ₄ + 0.25% M FeSO ₄
Alloy 800 7-73243	3/3	3/3	4/4	4/4	4/4	0/4 (3/4) ^(C)
Alloy 800SP 81373	15/15	15/15	15/15	15/15	15/15	11/15 (15/15) ^(C)
Alloy 690TT WF816T	0/15	0/15	15/15	14/14	0/15	1/15
Alloy 690TT 764408	0/15	0/15	15/15	15/15	0/15	0/15
Alloy 600MA 1450	8/9	0/9 (2/9) ^(C)	0/9 (3/9) ^(C)	2/9	6/9 (8/9) ^(C)	9/9

^(A) 500-h exposure; C-ring specimens; 2% strain.

^(B) From Briceno and Castano.³⁷⁹ Used by permission of EPRI.

^(C) Visual examination after bending the samples.

stressed area during the preceding high-temperature autoclave exposure.

The observations of crack growth at low temperature by Xia, et al.,³⁹⁸ incited a series of experiments by Mills and his coworkers.^{216,399-402} Their experiments were conducted using thicker specimens of the pre-cracked fracture mechanics type. They found that some materials exhibited drastically reduced fracture toughness (reduced by a factor of as much as 1/100) when tested in low-temperature hydrogenated water. The crack growth rate in these tests was rapid, in the range of mm/min, and was attributed to hydrogen from the water or from corrosion at the crack tip, rather than to stored hydrogen in the metal from prior high-temperature exposure. As illustrated in Figure 152, the materials found to be most susceptible, in order of decreasing susceptibility, were EN82H weld metal, EN52 weld metal, and Alloy 690. Surprisingly, Alloy 600 was found to be not susceptible to this mode of LTSCC. While the fracture resistance is reduced in low-temperature water, the degree of embrittlement is relatively small, and there is no evidence of a transition of morphology of fracture to intergranular. Alloy 690 sustains substantial intergranular LTSCC in the general range of temperatures at 93°C and below. These results are in accordance with the well-known trend of intergranular carbides to promote hydrogen embrittlement of austenitic materials at 100°C to 200°C. Alloys 600 and 690 weld metals, namely EN82H and EN52, are prone to intergranular LTSCC, and their fracture resistance in low-temperature water is reduced by 1 to 2 orders of magnitude.

These data in Figure 152 were obtained at slow strain rates with compact tension (CT) specimens ex-

posed to hydrogenated water. Their general patterns suggest that hydrogen is somehow responsible for the large decreases in elastic-plastic fracture toughness (J_{Ic}). This possibility is supported by the accelerating effect of hydrogen additions in Figure 152(b). In addition, the degree of embrittlement and intergranular morphology associated with LTSCC in water were reproduced by testing hydrogen pre-charged specimens in air. However, the patterns in Figure 152 indicate that Alloy 690TT is particularly prone to LTSCC, especially as compared to Alloy 600MA, which is contrary to the general response of this alloy for many of the submodes and especially to LPSCC, which is argued by some to be based on a hydrogen-related process.²⁸³⁻²⁸⁴ The patterns of these results in Figure 152 are also similar to the extensive testing using CERT for specimens with smooth surfaces in that slow strain rates produce more intense SCC than higher rates.

In summary, with regard to LTSCC, there appear to be two modes: (1) a slow crack growth mode that affects thin wall, highly stressed Alloy 600MA specimens that have absorbed large concentrations of hydrogen in highly stressed areas during high-temperature exposure to hydrogenated water, and (2) a rapid crack growth mode that affects Alloy 690 but not Alloy 600 and appears to be caused by hydrogen from the low-temperature hydrogenated water environment and/or corrosion at the crack tip, and is little affected by stored hydrogen from previous exposures. The rapid growth rate mode of LTSCC occurs only at rather high applied stress intensities, and thus is more of a concern in thick wall materials than in thin wall steam generator tubes in which high stress intensities usually do not occur.

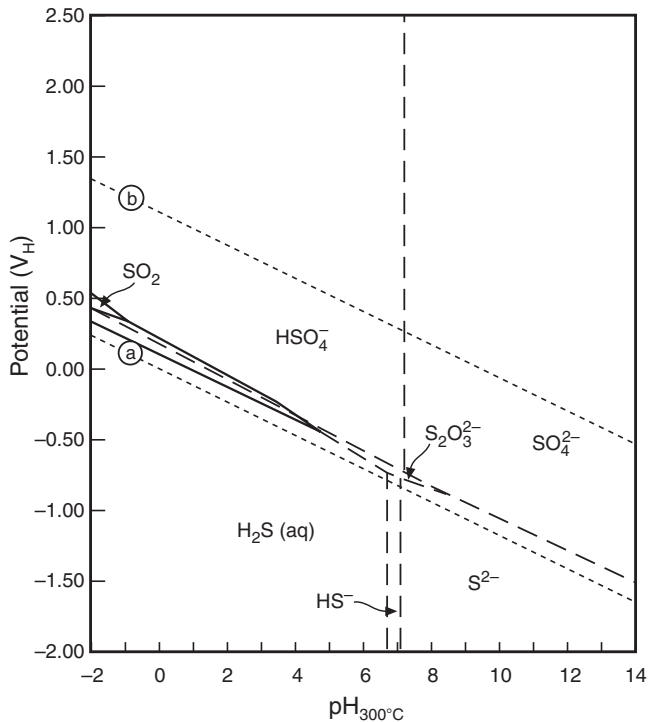


FIGURE 146. Potential vs pH diagram for the stability of sulfur species in aqueous environments at 300°C. From Chen, et al.¹⁰⁸

5.3 Development of Alloy 690

Since Alloy 690TT is now the dominant material for SG tubing, it is appropriate to review the foundation upon which it was developed. The need for an improvement began to emerge in the late 1960s when the work of Coriou received support from others and when AkSCC began to occur in the lower temperature early plants as noted in Figure 92. The early work that was the basis for qualifying Alloy 690 was the following:

1. Chloride testing: Copson published in 1957 and 1959²²⁷⁻²²⁸ data for the SCC of Ni-Cr-Fe alloys as a function of nickel concentration exposed to boiling MgCl₂. These data showed that above about 45% Ni, no SCC occurred, as shown in Figure 89.
2. Lead testing: Flint and Weldon in 1972⁸² conducted a series of experiments in lead environments to determine the optimum conditions for various combinations of Ni-Cr-Fe. Their results are shown in a later publication and the results are shown in Figure 143. These data show that the Alloy 690 composition is optimum for minimizing both SCC and scaling.
3. Aerated double U-bend and sensitized: Flint and Weldon⁸² and Copson, et al.,²³⁹ in 1972 reported the results of tests of double U-bends where alloys of various compositions were sensitized. These data are given in Table 24.

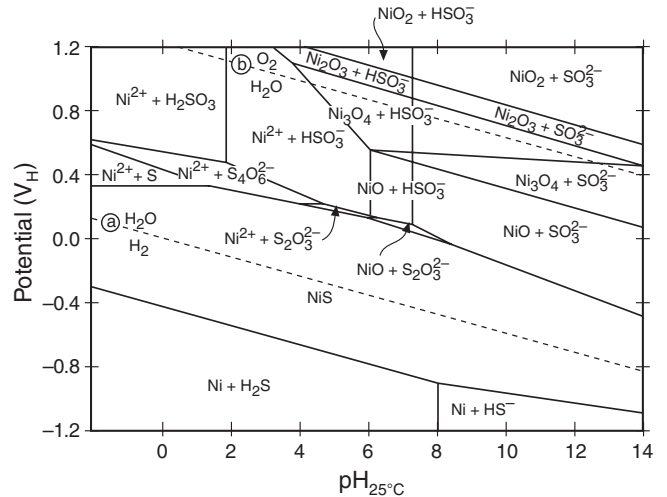


FIGURE 147. Potential vs pH diagram for the stability of Ni-S-H₂O species in aqueous environments at 25°C. From Bandy, et al.¹⁷⁸ ©1983 NACE International.

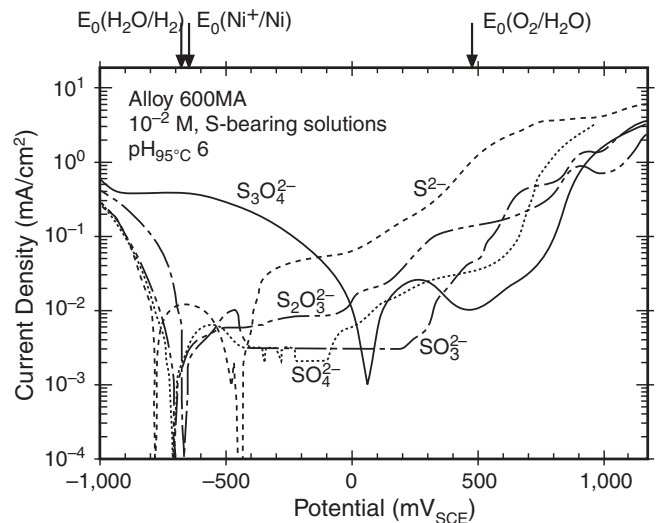


FIGURE 148. Current density vs potential for Alloy 600MA in sulfur bearing solutions at 10⁻² M at pH_{95°C} = 6 with sulfur valences from +6 to -2. From Fang and Staehle.³³⁸ ©1999 NACE International.

4. Aerated 50% and 90% NaOH: Flint and Weldon⁸² in 1972 and Copson, et al.,²³⁹ in 1972 published results, shown in Table 18, for alloys with various iron and chromium concentrations exposed to 50% and 90% aerated NaOH. They showed that the Alloy 690 compositions did not sustain SCC at 28% Cr and above in 50% NaOH but did at 90% NaOH.
5. Deaerated 50% NaOH and metallurgical effects: McIlree and Michels⁸³ in 1974 published work shown in Figure 91 concerning the effects of metallurgical processing on stainless steel, Alloy 800, Alloy 690, Alloy 600, and

TABLE 34

Results of Cathodic Polarization Scans in 50% NaOH with 5% Additions at 316°C^(A)

5% Addition	Alloy 600		Alloy 690	
	Worst Case	Observations	Worst Case	Observations
Na ₂ CO ₃	No difference ^(B)	General attack	No difference ^(B)	Slight g.b. intrusions
Na ₂ S	TT ^(C) ring	Heavy general attack	MA ^(D) C-ring	TGSCC ^(E)
NaHS	No difference	Heavy general attack	MA C-ring	TGSCC
Na ₂ S ₂ O ₃	No difference	Heavy general attack	MA C-ring	TGSCC
Na ₂ SO ₄	No difference	Slight general attack	MA C-ring	Slight g.b. intrusions

^(A) Courtesy of P. King, Babcock and Wilcox, Alliance, OH, September 2001. Private communication.

^(B) No difference indicates no substantial difference between ring or C-ring specimens for mill-annealed and thermally treated condition.

^(C) TT: Mill annealed plus 704°C/16 h.

^(D) MA: Heat treatment not defined.

^(E) TGSCC: Transgranular stress corrosion cracks.

Alloy 201. These data showed that Alloy 690 in the sensitized conditions was inferior to Alloy 600 in the same condition.

These data are mainly those upon which Alloy 690 was qualified. These data are notable for their lack of testing in the LPSCC modes since it had been so well confirmed by 1974. However, such work was undertaken by others as the industry moved to qualify the alloy for applications in SGs, the first of which was to occur in 1985. Ultimately, it was shown that Alloy 690TT does not sustain LPSCC, at least in hydrogenated pure and primary water.

Contemporary data for the performance of Alloy 690 are included with the discussions of the submodes in Section 5.2.

5.4 Significance

5.4.1 Experience —

The Alloys and Their Submodes

1. Since its initial application, Alloy 600 has been shown to sustain SCC in at least the following submodes: AkSCC (including ASSCC), LPSCC, AcSCC (including CuSCC, ClSCC), HPSCC, PbSCC, S^v-SCC, and DSSCC. These are all applicable to the secondary side including possibly LPSCC. Further, there seem to be more complex environments, including alumino-silicates and possibly others, that may produce SCC or may aggravate the other submodes. In addition, IGC has been observed with many of these SCC submodes as an ancillary or adjunct morphology of corrosion occurring in approximately the same chemistry as the SCC. All of these submodes have been reproduced in the laboratory and most are believed to have occurred in service at some time, although ascribing some occurrences to specific environments is not always possible.

2. Alloy 690TT has sustained no corrosion-induced failures in the field since its first application in 1989. However, in laboratory testing, the following submodes have been observed: PbSCC, AkSCC, AcSCC, S^v-SCC, HPSCC, and LTSCC. Alloy 690TT has exhibited no LPSCC under any circumstances of

laboratory testing except for one case of a low-temperature heat treatment. However, in laboratory testing, the SCC of Alloy 690 can be as rapid or more rapid than that for Alloy 600MA. Nevertheless, despite these possible submodes of SCC, it seems that the high purity of secondary coolants and the line contact tube supports in new SGs have minimized the possibility of SCC occurring for Alloy 690TT, at least for relatively short times. Service experience shows that Alloy 690TT has not sustained any SCC after 14 years in the oldest SG.

3. Alloy 600TT sustains SCC in the same submodes as Alloy 600MA, including LPSCC, but the rates are less or mitigated. On the average, Alloy 600TT seems to provide an advantage of a factor of two to four in time to failure over Alloy 600MA in the more aggressive liquid phase environments and about 4 to 5 in operating steam generators.

4. In the laboratory, Alloy 800 sustains the same submodes of SCC as Alloy 600MA except for the LPSCC submode that was the essential basis for the early switch from Alloy 600MA to Alloy 800 by one vendor. The lack of significant failures in Alloy 800 in operating steam generators is attributed to its resistance to LPSCC and to similar near-neutral pH corrosion modes, coupled with generally good water chemistry and the use of line contact stainless steel tube supports.

5. Once initiated, all of the submodes of SCC can be characterized by Weibull statistics. Utilizing this method has permitted predicting the future occurrence of corrosion, and has been useful for helping to identify when steam generator replacement is likely to be required.

6. The TG morphology has been observed for AcSCC, S^v-SCC, PbSCC, and LPSCC at lower pH and lower temperatures. When such morphologies are observed, it is not clear that they should be ascribed, as they have in the past, uniquely to PbSCC. Further, PbSCC also occurs intergranularly, so that this morphology does not necessarily mean the absence of lead.

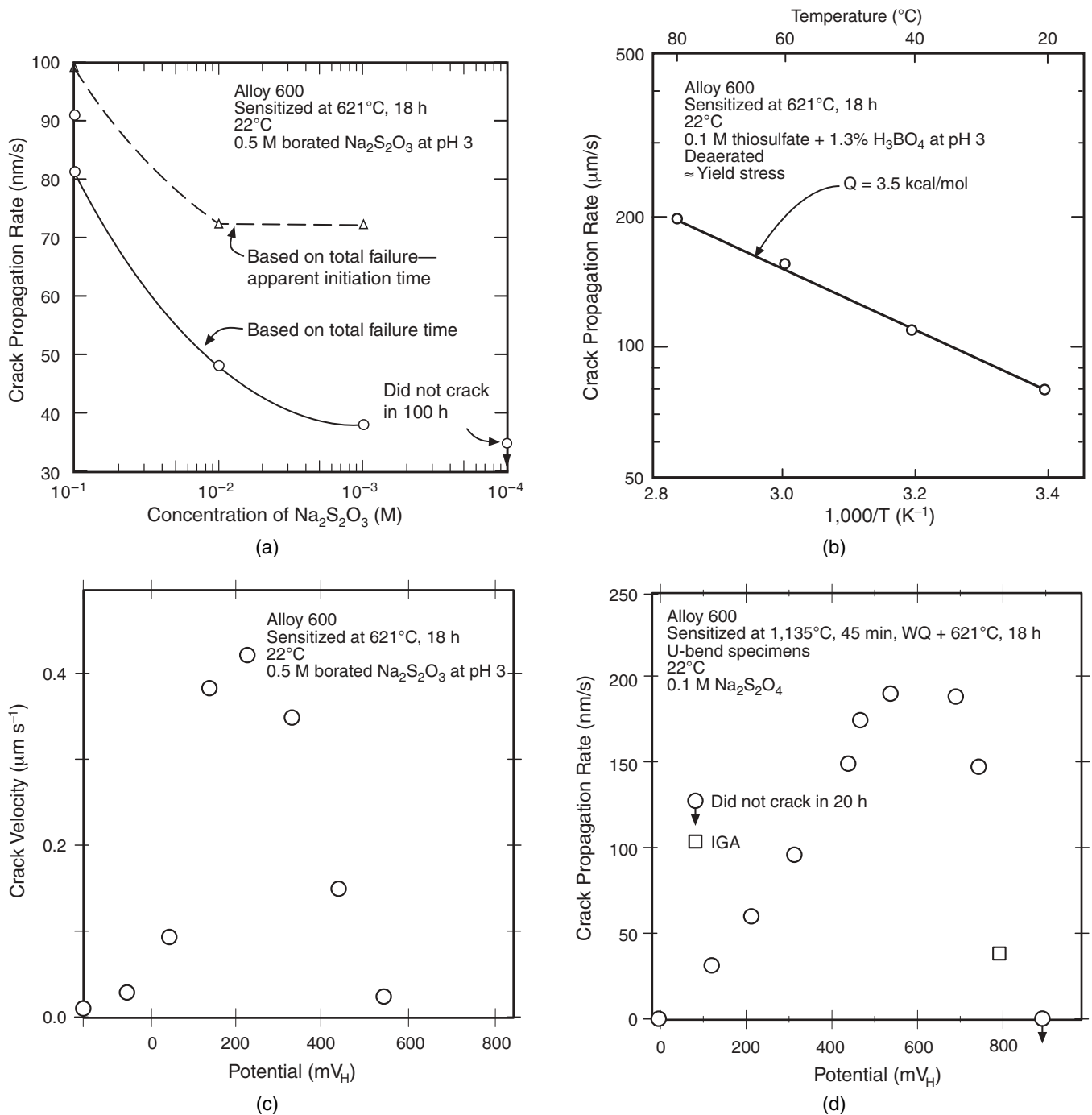


FIGURE 149. (a) Crack propagation rate vs concentration of $\text{Na}_2\text{S}_2\text{O}_3$ for sensitized Alloy 600 exposed at 22°C at $\text{pH}_{22^\circ\text{C}} = 3$. From Bandy, et al.¹⁷⁸ (b) Crack propagation rate vs $1,000/T$ for sensitized Alloy 600. From Bandy, et al.¹⁷⁸ ©1983 NACE International. (c) Crack velocity vs potential for sensitized Alloy 600 exposed at 22°C in 0.5 M borated $\text{Na}_2\text{S}_2\text{O}_3$ at pH 3. From Newman, et al.³⁸⁰ ©1983 NACE International. (d) Crack propagation rate vs potential for sensitized Alloy 600 exposed in 0.1 M $\text{Na}_2\text{S}_2\text{O}_4$ at 22°C . From Bandy and van Rooyen.³⁸¹ ©1984 NACE International.

7. The seven principal variables as they characterize submodes of AkSCC, LPSCC, HPSCC, and PbSCC are sufficiently quantified that correlation relationships can be developed. The submodes of S^{y} -SCC, DSSCC, and probably AcSCC are not well enough quantified to allow such correlations to be developed.

Alloy Structure

1. The most significant feature of alloy structure for Alloy 600 that promotes SCC via several of the submodes, at least for LPSCC, is the distribution of carbides mainly in the matrix and away from the grain boundaries.

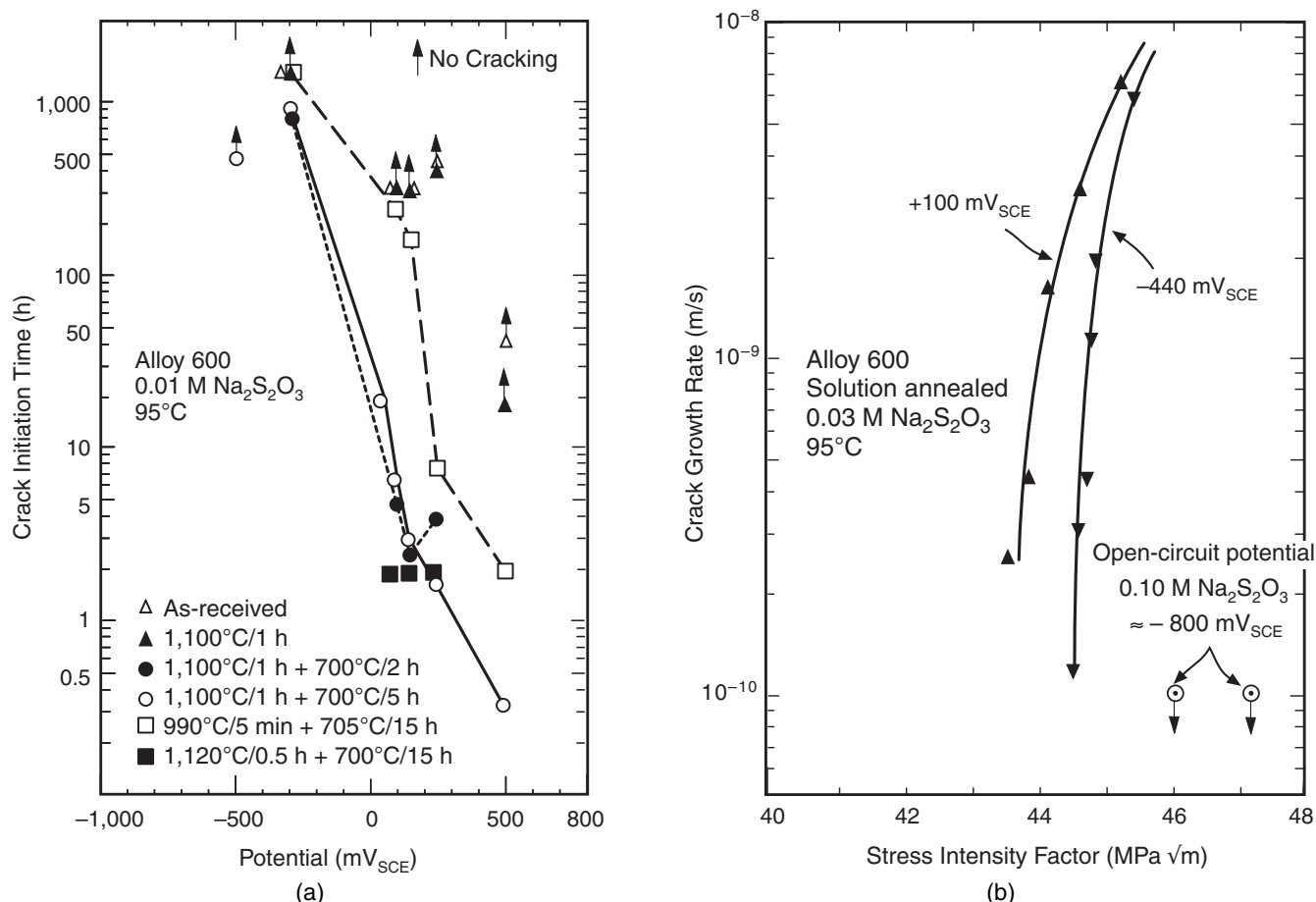


FIGURE 150. (a) Crack initiation time vs potential for Alloy 600 in both annealed and annealed plus sensitized heat treatments exposed to 0.01 M Na₂S₂O₃ at 95°C. From Tsai, et al.³⁸² ©1993 Elsevier Science. (b) Crack growth rate vs stress intensity for Alloy 600 solution annealed and exposed to Na₂S₂O₃ at various potentials and 95°C. From Tsai, et al.³⁸³ ©1989 NACE International.

2. Sensitizing heat treatments and thermal treatments minimize but do not eliminate the proneness of Alloy 600 to SCC. However, sensitizing heat treatments promote SCC in low-valence sulfur species at low temperature.

3. Low-temperature mill annealing (LTMA) accelerates LPSCC relative to high-temperature mill annealing (HTMA).

Environments

1. The early environments that produced SCC in heat-transfer crevices of early steam generators were highly alkaline and resulted from inadequate water chemistry, especially the use of phosphates, but also inadequate control of purity. The AkSCC/AkIGC produced by these environments was aggressive. However, these alkaline environments became infrequent in later years owing to the improved water chemistry.

2. The next important environment was an aggressive solution that resulted from the reactions of phosphates in heat-transfer crevices. These environments produced aggressive local general corrosion.

3. Next, the important environments, as they corroded carbon steel support plates and tubesheets, were oxidizing with aggressive species such as chlorides. The resulting corrosion and expansion of corrosion products produced denting and pitting on the secondary side, probably due to local acidic environments, and the denting caused LPSCC on the primary side.

4. As water chemistry improved, the average environments in heat-transfer crevices that sustain SCC have been characterized as being in the mid-range of pH, although environments at the surfaces of tubes may be more alkaline. To these environments, N₂H₄ was added to lower the potential in heat-transfer crevices; and alkalizers were added, such as ammonia and later other more complex amines. The local environments in heat-transfer crevices continued to produce SCC and IGC, although the submodes involved are unclear. It appears likely that the submodes producing this SCC are some combination of AcSCC, LPSCC, S^y-SCC, PbSCC, and DSSCC:

- a. While the AcSCC is significantly aggressive in the acidic range—in fact, this submode extends from low pH to pH_T of about 9, and possibly higher—and includes contributions of sulfate and chloride, AcSCC acts over a range of potentials.
 - b. PbSCC produces SCC at low concentrations of Pb and the morphology of the SCC is both TG and IG. It is difficult to distinguish these effects from those of AcSCC. PbSCC requires only ppm concentrations of Pb in the liquid or steam to produce SCC. There are generally high concentrations (~1,000 ppm) of Pb in SG deposits. It appears that the occurrence of PbSCC depends on whether the activity of the Pb in the liquid or steam has been reduced by forming insoluble compounds with other chemicals.
 - c. S^{Y} -SCC results from the availability of sulfur in lower valences. Such lower valences result from the reduction of SO_4^{2-} by N_2H_4 with catalytic effects of magnetite and other species or crystal structures. S^{Y} -SCC can produce SCC that is both TG and IG.
 - d. LPSCC may occur on the secondary side despite the generally low stresses on secondary-side tube surfaces in crevice areas. First, the presence of N_2H_4 lowers potentials into the range where LPSCC can occur. Second, the presence of chemical species may accelerate LPSCC or reduce the threshold stress. This possibility has never been considered except in high-temperature (400°C) steam, where chemical species in the 100-ppm range cause large increases in SCC susceptibility. In addition, there is support for these effects from the work in contaminated BWR environments.
 - e. DSSCC is important since many heat-transfer crevices contain steam, and the reactions that occur in steam or the steam/water interface can be quite aggressive. Further, there is little experimental work that is directly relevant to this case since most past work in the laboratory has been conducted in liquid phases. In addition, much of this work has not considered the importance of removing hydrogen nor the addition of N_2H_4 . It is possible that most of the observed SCC in crevices is due to this submode for which there is little supporting laboratory information. Further, most of the present research on DSSCC has been conducted using dilute aqueous phases rather than the concentrated or saturated ones that are typical of heated crevices.
5. There have been occasional occurrences of serious cracking in wetted free-span areas at scratches. These events seem to be related to the locally high residual stresses and cold work caused

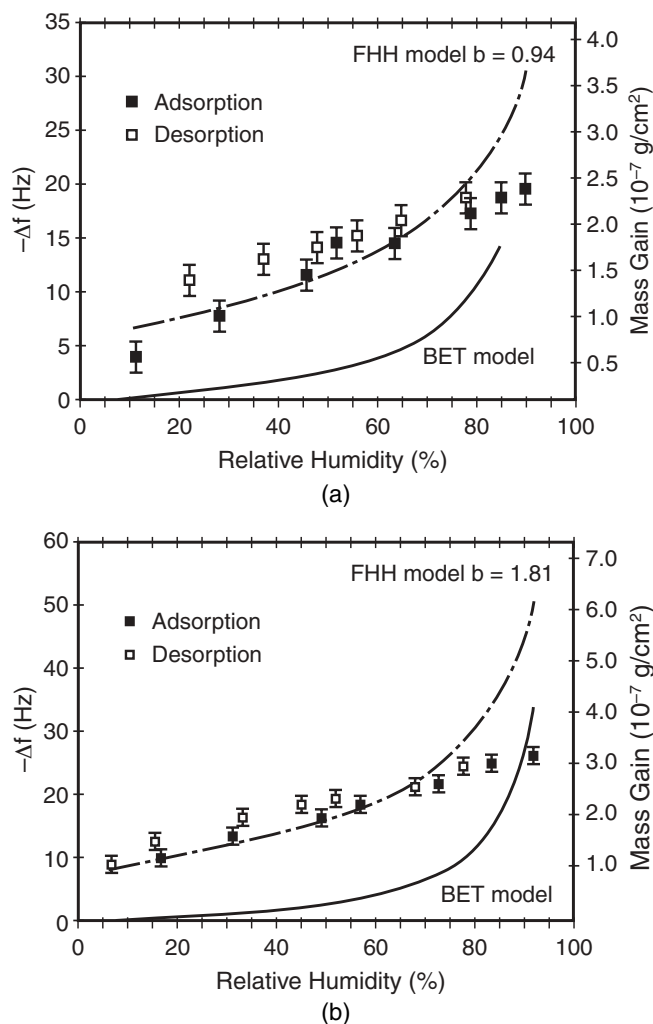


FIGURE 151. Frequency change in a quartz microbalance experiment and mass gain of water vs relative humidity for a nickel substrate at: (a) 7°C and (b) 85°C. From Lee and Staehle.³⁸⁹ Courtesy of Wiley-VCH.

by the scratches. There is some evidence that the resulting SCC is LPSCC, but this is not clear. In superheated environments, such as in the upper bundle of OTSGs, free-span cracking also has occurred, most frequently at scratches. The mode of this SCC is not clear although there is some evidence for PbSCC in some cases.

6. In general, the anodic submodes such as AkSCC, AcSCC, PbSCC, and S^{Y} -SCC exhibit about the same dependencies upon potential; the SCC is essentially negligible at the deaerated open circuit, but increases with increasing potential and then diminishes as a generally bell-shaped dependence upon potential. Sensitized Alloy 600 exhibits a similar shape. This pattern probably accounts for the apparent benefit of N_2H_4 treatments. However, this possible lowering of potential may activate LPSCC, and practically no data are available for this submode in contaminated environments.

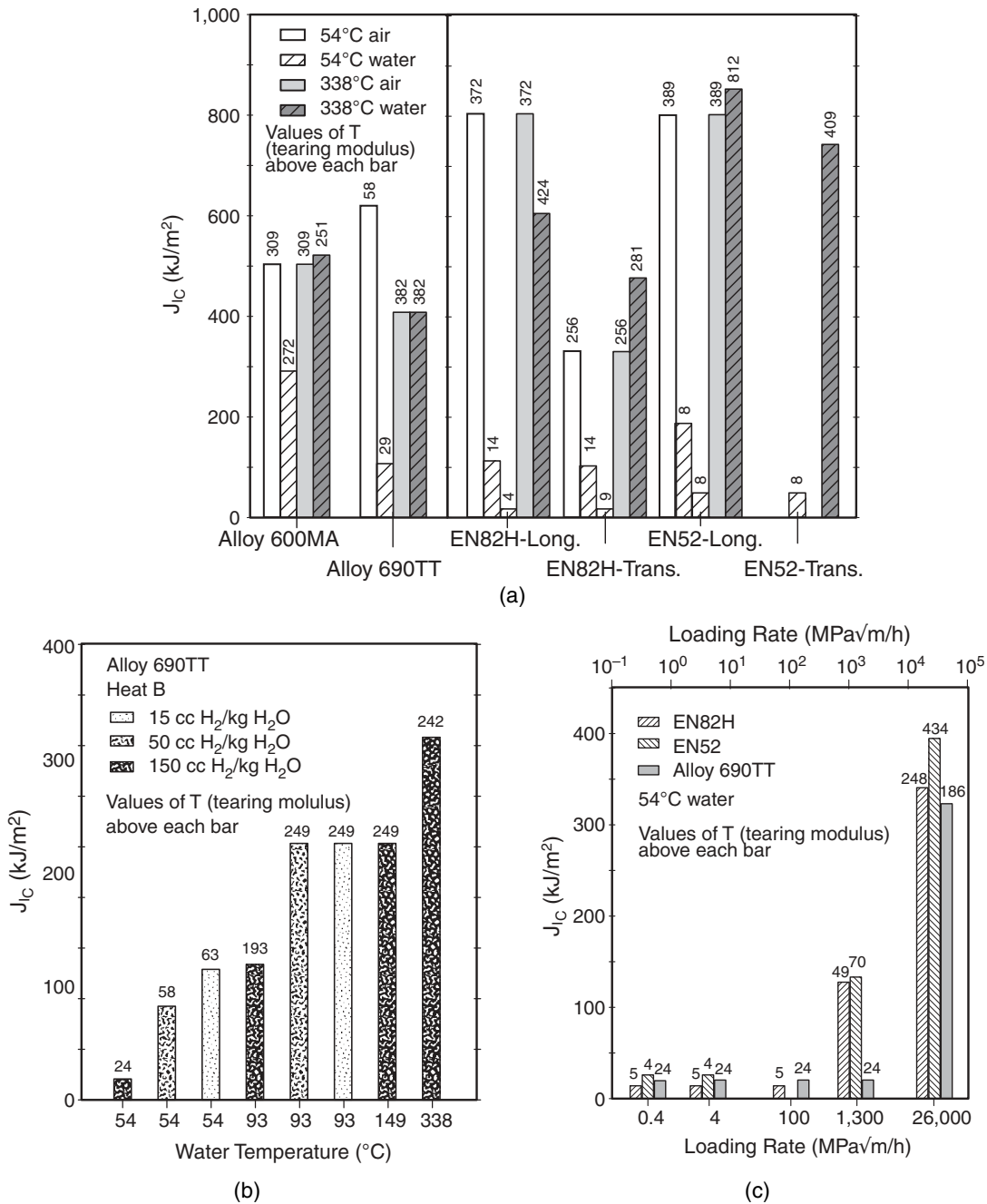


FIGURE 152. J_{IC} results for Alloy 600MA, Alloy 690TT, EN82H, and EN52. EN82H and EN52 welding materials tested in longitudinal and transverse orientations. Tearing moduli given above each bar. Tests conducted at pH 10.1 to 10.3 with oxygen less than 100 ppb and conductivity in range from 18 $\mu\text{S}/\text{cm}$ to 90 $\mu\text{S}/\text{cm}$. From Brown and Mills.²¹⁶ ©1996 NACE International. (b) J_{IC} results for Alloy 690TT tested at different temperatures and concentrations of hydrogen. From Mills and Brown.⁴⁰¹ Courtesy of TMS, Warrendale, Pennsylvania. (c) J_{IC} results for different loading rates in 54°C water. From Mills, et al.⁴⁰² Used by permission of EPRI.

7. The chemistry in heat-transfer crevices is complex and, while general trends are somewhat apparent, in detail it is not clear that such environments are readily quantified. This uncertainty prevents predicting the details of local environments and is compounded by the uncertainty introduced by effects of steam and steam/water interfaces.

5.4.2 Potential Problems with Alloy 690TT — The industry should give increased attention to the possible development of corrosion problems with Alloy 690TT and should do the necessary research to quantify and address these problems before they become severe. This work should address systematically each of the problems described in this section.

There are a number of reasons for considering the possibility that serious corrosion problems could eventually develop with Alloy 690TT in operating steam generators:

1. Steam blanketed areas and concentrated impurities are likely to develop at heat-transfer crevices at line contact tube supports and may lead eventually to corrosion problems. While these conditions may be less severe in line contact than in drilled hole tube support geometries, it is reasonable to conclude that line contact crevices can produce locally severe conditions. Also, lack of cylindrical support permits tube bursts to occur, making the allowable size of cracks at supports smaller for line contact supports than for drilled hole supports.
2. In addition to concerns about the accumulation of deposits at tube supports, the TTS crevices have not changed from previous designs, still involve high stresses, and are likely locations for corrosion problems to develop. In addition, some denting has been observed at these locations, and the dynamic straining associated with denting is well known to promote SCC.
3. While Alloy 690 has exhibited good performance thus far in plant applications, it is inherently a more reactive alloy than Alloy 600 as a result of its higher chromium concentration. This high reactivity makes it likely that there are conditions under which Alloy 690TT could sustain rapid corrosion in steam generators.
4. Some of the submodes of SCC that eventually produced extensive SCC of Alloy 600 did not occur until after many years of service and occurred even with nominally good water chemistry. This experience implies that the good experience to date with Alloy 690TT does not assure that it will not eventually sustain serious corrosion problems.
5. Alloy 690, while it has exhibited excellent performance in operating SGs, has been shown in the laboratory to sustain AcSCC, PbSCC, S^v-SCC, and AkSCC. All of the submodes studied in the laboratory for Alloy 600MA were eventually observed in operating plants. This experience indicates that the submodes identified with Alloy 690TT in the laboratory could also eventually occur in operating steam generators.
6. Conditions for DSSCC are not defined for Alloy 690TT, although experiments in lead environments in wet steam show that this submode, especially in more alkaline environments, is more virulent for Alloy 690TT than Alloy 600MA.
7. PbSCC is presently minimized by the lowering of Pb activity by the formation of insoluble lead precipitates. If concentrations of species that produce such precipitates, most likely SiO₂, SO₄, PO₄, alumina (Al₂O₃), and others, are lowered, the virulent effects of lead may become more important. These effects of lead are important because lead is so aggressive even at ppm concentrations, and since lead has been shown to be aggressive toward Alloy 690TT at high and low pH.
8. S^v-SCC is favored by the availability of sulfur, e.g., SO₄²⁻ and resin fines, and the use of N₂H₄. The conditions for the formation of low-valence sulfur species are not well defined nor is the resulting SCC. However, from existing information, it is clear that this submode is inherently virulent and that it is aggressive toward Alloy 690TT at high pH. S^v-SCC is likely to be more virulent at lower pH or in steam because the sulfur tends to form HS⁻ in these situations.
9. While existing data show that Alloy 690TT is not prone to LPSCC, few experiments in contaminated environments, such as those that can develop on the secondary side, have been conducted. Further, the use of high concentrations of N₂H₄ places the surfaces in the range of potentials where LPSCC can occur.
10. Tests indicate that LTSCC is more likely for Alloy 690 than for Alloy 600, at least for thick materials. How this submode would activate in a practical sense is not clear, although it would most likely be in shutdown conditions. LTSCC may be particularly important in the case that initial defects are produced by pitting or early SCC occurring at operating temperatures.
11. There is not sufficient information from laboratory testing to estimate the occurrence of first failures in a statistical sense, although rough, lower-bound, pessimistic estimates can be developed.
12. There is virtually no fundamental understanding for the principal variables that affect the various submodes. Such work is highly desirable for predicting long-term performance.

6.0 CONCLUSIONS

This article was prepared to develop a quantitative basis, using existing information, for predicting stress corrosion cracking on the secondary side of PWR steam generators having tubes of Alloy 600MA and similar alloys. This article is a second step in developing this predictive capability following the first step, which is described in a previous report (NUREG/CR-6737, ANL-01/20, RWS 151) concern-

ing a statistical framework. This quantitative basis for prediction utilizes data from existing laboratory and service performance of Alloys 600MA, 600TT, and 690TT.

The subjects considered in this article are: introduction to SCC problems on the secondary side (Section 1.0); SG design as it affects mechanical configurations that are critical to corrosion (Section 2.0); bulk water chemistry as it relates to controlling local chemistry in heat-transfer crevices (Section 3.0); local chemistry in heat-transfer crevices (Section 4.0); and submodes of SCC together with the metalurgy of tubing materials (Section 5.0).

At the end of each section is a summary of what has been learned since the beginning of commercial PWR technology, mainly as it is useful to the present work of predicting SCC. Also, at the end of each section is an assessment of potential future problems that relate to corrosion.

The approach to modeling the occurrence of SCC in the overall project consists of the following:

1. A statistical framework that emphasizes the occurrence of early failures. This work has been completed and is the subject of the report, NUREG/CR-6737, ANL-01/20, RWS 151.
2. A physically based description of the submodes of SCC as they occur in specific environments such as alkaline, low potentials, acidic, lead, and reduced sulfur. These submodes are analyzed and evaluated in terms of their dependencies on the seven primary variables that affect corrosion: pH, potential, species, alloy composition, alloy structure, temperature, and stress. These analyses are derived from existing data and appropriate mathematical models. Starting from the present analyses of data, additional work is required to build the mathematical models of the submodes. This work will be the subject of a separate report.
3. A description of the local environments in heat-transfer crevices, the chemistries of which are relevant to evaluating the seven primary variables that control the intensities of submodes.
4. Quantifying a link between bulk chemistry measured by operating plants and local chemistry in heat-transfer crevices.
5. A total model for predicting early shallow cracks that includes the submodes in a statistical framework that responds to environmental chemistries over time.

In this article, the present understandings of the dependencies of each submode of SCC for Alloy 600MA, as well as for Alloy 600TT and Alloy 690TT, on the primary variables of pH, potential, species, alloy composition, alloy structure, temperature, and stress, are described and evaluated. In many cases,

there are broad agreements on the various dependencies; in other cases, such as the reduced sulfur submode, which is critical to the reliable performance of Alloys 600TT and 690TT as well as Alloy 600MA, there is little useful quantitative information.

There are four major submodes: AkSCC, LPSCC, AcSCC, and HPSCC. These are shown in Figure 82(a). In this article, the term "major" means that these submodes relate generally to features of the potential-pH relationships as shown in the potential-pH diagrams. There are also minor submodes, as shown in Figure 82(b), such as PbSCC and S^{V-} SCC that depend less on the prevailing thermodynamics for bounding conditions and more on kinetic processes. "Minor" is not meant non-importance but rather the lack of obvious connection with potential-pH diagrams. In fact, both the PbSCC and S^{V-} SCC are among the most virulent submodes for Alloy 600MA and are potentially important for Alloys 600TT and 690TT.

The following are summarized: (1) quantitative aspects of submodes; (2) local environments of heat-transfer crevices in which SCC occurs; (3) tubing alloys; (4) future problems and priorities.

Quantitative Aspects of Submodes

The following submodes of SCC as they apply to the secondary side, and mainly to Alloy 600MA, are assessed and analyzed in this article:

1. *Alkaline SCC (AkSCC)*, Section 5.2.1 — AkSCC is the main submode that affected the early steam generators, especially when the water chemistry was not well controlled and there was little appreciation for the importance of heat-transfer crevices. The domain of AkSCC occupies a region just above the H_2O/H_2 half-cell equilibrium until about, at the most, 300 mV above with the dependence on potential having a bell shape; it extends from concentrated NaOH to about pH_T 9 according to a generally monotonic decrease.

AkSCC in this article includes the effects of other species such as alumino-silicates as they seem to be part of this submode. However, this connection has yet to be verified.

Existing information permits good quantitative descriptions of the dependence of AkSCC upon pH, potential, some species (such as silica), alloy composition, alloy structure, temperature, and stress. It is possible to develop an expression for these dependencies from existing information with reasonable confidence. This submode and LPSCC are best supported by quantitative dependences from experimental work.

This submode is of less practical interest now since the present water chemistries are relatively pure, and the environments formed inside heat-transfer crevices are generally understood, based on measurements from plants, to be neutral to moderately acidic or alkaline.

2. *Low-Potential SCC (LPSCC), Section 5.2.2* — Low-potential SCC was formerly called PWSCC, but this term is slowly being abandoned since it implies that SCC can occur only on the primary side or only in pure water. Neither of these is true. The term, “low potential” is based on the domain of potential and pH in which this submode occurs; such an approach avoids emphasizing the component and, instead, emphasizes the chemical domain as do, e.g., AkSCC and AcSCC.

It has been thought that LPSCC would not be applicable to the secondary side owing to its lower temperatures and the lack of intentionally added hydrogen. However, neither of these aspects rule out LPSCC on the secondary side. LPSCC has been observed at temperatures as low as 280°C and possibly to 250°C usually with high stresses and cold work at these lower temperatures. Further, the broad usage of high concentrations of N_2H_4 causes the potential on the secondary side to decrease into the LPSCC domain. Finally, existing work has not considered the effects of impurities. It must be concluded that LPSCC, especially in the mid-range of pH, should be seriously considered as a possible submode of SCC for Alloys 600MA and 600TT on the secondary side.

LPSCC has been quantitatively characterized with respect to potential, alloy composition, alloy structure, temperature, and stress. However, little information has been developed either for its dependence upon pH or upon the high concentrations of contaminating species that can develop in heat-transfer crevices on the secondary side. In this regard, LPSCC has been nominally evaluated in the doped steam experiments where low concentrations of species are added to an aqueous environment in equilibrium with saturated or supercritical steam. This environment produces rapid SCC in Alloy 600MA, but Alloy 690TT has been immune in such environments. However, these experiments have used only dilute concentrations of species and have not approached the concentrations or array of species that are observed in heat-transfer crevices. The question of whether Alloy 690TT will sustain LPSCC in heat-transfer crevices is still open.

3. *Acidic SCC (AcSCC), Section 5.2.3* — AcSCC occupies a domain slightly above the H_2O/H_2 half-cell equilibrium and extends for possibly 300 mV in the positive direction. Its dependence upon potential is not so well characterized as AkSCC, so this dependence upon potential is estimated. The lowest pH at which AcSCC has been measured is in the range of pH_T 2. The intensity decreases more or less monotonically to about pH_T 9, thus including the mid-range of pH.

AcSCC is important since it includes the mid-range of pH and since the broad application of the molar ratio index in plants causes the pH in crevices to stay neutral to slightly acidic.

The AcSCC submode includes the chloride SCC (ClSCC) and copper SCC (CuSCC) submodes. While it once appeared that the latter two might be separate from AcSCC, since the early work on AcSCC had been conducted in sulfate systems, it now appears that both ClSCC and CuSCC are integral parts of an acidic submode. Such an acidic submode occurs also in low-alloy steels and in stainless steels.

AcSCC is less well characterized than AkSCC and LPSCC, but enough is known that it can be functionally described. The shape of the intensity vs potential dependency appears to be similar to AkSCC, and there is enough evidence to support this assumption that it can be described credibly. The dependence upon pH is well described by numerous investigators and their results agree well. The importance of the various species and the magnitudes of their effects are not so clear. The central chemistry studied for AcSCC is based on sulfates. Chlorides alone produce AcSCC, but their interaction with sulfates has not been studied. At pH_T of 2 to 2.3, chlorides in H_3BO_3 produce AcSCC at temperatures as low as 100°C. Similar SCC at about 100°C is observed in NaOH.

When the potential is raised by lowering hydrogen concentration and adding CuO, AcSCC occurs in Alloy 690TT at 320°C. Further, recent work on more complex solutions shows that combinations of several species including acetic acid produce AcSCC. There is some information to show that Alloy 600MA sustains slightly more AcSCC than Alloy 600TT and that Alloy 690TT is significantly more resistant. Otherwise, there is little information on effects of alloy composition and structure. Some information on effects of temperature show a relatively low activation energy in the range of 15 kcal/mol. Available information on effects of stress suggest that the threshold for AcSCC is similar to that of AkSCC being about half of the yield stress or lower.

The intensity of both AcSCC and AkSCC seems to decrease as the pH approaches the solubility minimum for NiO. This pattern occurs also in low-alloy steels.

4. *High-Potential SCC (HPSCC), Section 5.2.4* — HPSCC is not relevant generally to SGs and has been studied mainly in connection with BWR environments since the relatively high oxygen in the normal BWR chemistry produces potentials that are 600 mV to 700 mV above the H_2O/H_2 half-cell equilibrium. Available data show that MA heat treatments for Alloy 600 do not sustain HPSCC until at least 200 mV, and more generally about 400 mV, above the H_2O/H_2 half-cell equilibrium.

HPSCC is relevant to SGs only in the case that oxygen or other oxidizing impurities such as copper oxides enter the system, especially at startup.

The pH over which HPSCC occurs is not well described since most of the work has been in support of

BWR environments at about pH_T 5.5. A small amount of work shows that HPSCC is confirmed to pH as high as pH_T 9. The minimum potential for the onset of HPSCC in Alloy 600MA has been described by several investigations, and the results are consistent. However, these minima are too high to be of interest to SGs. Minima for sensitized Alloy 600 extend to lower potentials than for the MA treatment and possibly to the potentials in the range of SGs.

The effects of species on HPSCC, such as those in SG heated crevices, have not been studied generally, although there is some work on sulfates. The effects of alloy composition are not well characterized for the high-nickel alloys but are better characterized for the stainless steels; effects of alloy structures of the sensitized types are similar to those for stainless steels. The dependence upon temperature for sensitized alloys is well characterized, but it does not exhibit the conventional $1/T$ behavior; instead, at temperatures below about 290°C , sensitized stainless steel and Alloy 600 show both positive and negative dependencies on $1/T$. There is little information on the temperature dependence for Alloy 600MA materials for HPSCC.

5. *Lead SCC (PbSCC), Section 5.2.5* — PbSCC is of interest since it can produce aggressive SCC in Alloys 690TT and 600TT as well as in Alloy 600MA. Such PbSCC can occur in the range of a few ppm lead in solution while, on the other hand, there are extensive concentrations of Pb in deposits in SGs. Also, PbSCC occurs over the full range of pH of interest to free surfaces and in both alkaline and acidic crevices. While only a relatively small number of specifically attributable cases of PbSCC in operating plants have occurred, there is a serious question as to whether there have been more cases that were not recognized.

The fact that Pb produces rapid SCC, including with Alloy 690 at high pH, with concentrations in the ppm range of lead is not a phenomenon for which there are analogous examples from other environments that provide insights to a detailed mechanism. However, better understood is the reason that the large concentrations of lead in deposits do not produce extensive PbSCC despite the low threshold of concentration required to produce PbSCC. This results from the formation of insoluble compounds with many species including silica, phosphate, sulfate, carbonates, and others; the formation of such compounds significantly reduces the activity of Pb, apparently to below that required to produce PbSCC.

Because immunity from PbSCC depends on the formation of insoluble compounds, efforts to remove impurities from secondary water should give careful consideration to which species are important for minimizing the activity of Pb. Otherwise, the wrong

impurity species might be removed or decreased with the result of accelerating PbSCC.

In the past, the identification of SCC as PbSCC has been based on the occurrence of a transgranular morphology. However, this submode also occurs by IGSCC. Further, other submodes exhibit TGSSC, including AcSCC, $\text{S}^{\nu}\text{-SCC}$, and LPSCC. Thus, the morphology of SCC found in failures is not a reliable guide to the causative chemical species.

The dependence of PbSCC on pH is reasonably well described as it occurs in Alloy 600 over the full range, from at least pH_T 3 to pH_T 12. The occurrence of PbSCC over this range of pH is probably related to the high solubility of lead. The dependence of PbSCC on potential is not well defined except that experiments in both aerated and deaerated as well as in neutral to mildly alkaline environments show similar intensities of PbSCC. It seems that the minimum potential for PbSCC is defined by the equilibria involving $\text{PbO}^{\times}(\text{aq})/\text{Pb}$; the maximum potential for PbSCC seems to be in the range of a fully aerated solution.

Effects of other species on PbSCC have not been extensively characterized, although chloride-based environments seem to produce more intense PbSCC probably related to the high solubility of PbCl_2 . Possible inhibitors via the formation of insoluble compounds have not been characterized except for some work on SiO_2 . There is little information from systematic characterizations of effects of alloy composition and alloy structure on Pb; however, PbSCC occurs in many alloys including Monel[†], stainless steels, high-strength alloys, and others. Some information on the temperature dependence shows that the activation energy is low, suggesting that a chemical process is rate controlling. Work on stress shows that the threshold for PbSCC is low and in the range of the stress dependence of AkSCC.

6. *Reduced Sulfur SCC ($\text{S}^{\nu}\text{-SCC}$), Section 5.2.6* — $\text{S}^{\nu}\text{-SCC}$ is important for many of the same reasons as PbSCC. First, normally occurring sulfate species, as well as sometimes resin particles, although having low concentrations in the bulk, are concentrated in heat-transfer crevices. The presence of relatively high concentrations of N_2H_4 reduces the higher valence sulfur to lower valences, as low as -2 , based on both field and laboratory measurements. Also, when nickel reacts with sulfate, nickel sulfide is produced. While there is only sparse information on the range of $\text{S}^{\nu}\text{-SCC}$, it has been produced in model boilers operating on AVT as well as in isothermal laboratory studies in alkaline solutions. Also, $\text{S}^{\nu}\text{-SCC}$ produces rapid SCC in Alloy 690 based on studies only in highly alkaline solutions. Finally, despite the paucity of information on $\text{S}^{\nu}\text{-SCC}$, it should be assumed that it occurs over the full range of pH in view of the patterns of solubility of lower-valence sulfur.

The dependence of $\text{S}^{\nu}\text{-SCC}$ upon potential is not clear. Also, it is confused by the fact that high poten-

[†] Trade name.

tials would oxidize lower-valence species to higher valences. For sensitized materials, the dependence on potential is well defined, at least at low temperatures. How this applies to MA materials is not clear.

The main effect of the alloys, based on existing information, involves the difference between sensitized and MA structures; the former are prone to S^{ν} -SCC at low temperatures. There is some evidence that the TT heat treatment accelerates S^{ν} -SCC, but this occurs at potentials that are out of the SG domain. The effect of temperature has been studied only for sensitized Alloy 600; and the activation energy is low, being in the range of liquid processes. Some work on the effects of stress on crack growth rate of sensitized materials has been conducted. However, there is little information on the effect of stress on MA material. It would be reasonable to assume that the stress dependence is much like AkSCC.

The state of sulfur that produces S^{ν} -SCC even in the reduced state is not clear. Sulfur in the -2 state can exist as H_2S , HS^- , and S^{2-} (Öetal sulfide). While the first two provide mobility, they occur in the range below about pH_T 7, whereas NiS occurs at higher pH. How this insoluble form produces large effects of S^{ν} -SCC in strong alkaline solutions is not clear. Such an effect may result from the fact that sulfide films tend not to be protective.

7. Doped Steam SCC (DSSCC), Section 5.2.7 — DSSCC describes the submode involving SCC that occurs or is accelerated in steam environments where chemical additions to the liquid phase greatly accelerate the SCC in the saturated or superheated steam. This submode is relevant to SGs for several reasons. First, inside heated crevices there is generally a steam phase, depending on the extent of packing and the configuration of the surroundings, as a result of the high superheat. Second, some of the experimental work has shown that the doped steam regime is aggressive. Third, virtually all the laboratory work upon which existing dependencies are based has been conducted in fully aqueous environments despite the obvious importance of the steam phase. Fourth, existing studies of DSSCC have been conducted at low concentrations of added (doped) species in the adjacent liquid phase rather than the concentrated solutions that exist in heated crevices. There is little information on dependencies of DSSCC on the primary variables.

8. Organic SCC (OgSCC), Section 5.2.8 — OgSCC is identified because a variety of organic species has been observed in deposits and blowdown; further, such species are known to form soluble complexes with Fe-Cr-Ni alloys. Some work has found, generally, that organic species, acetate and formate, do not by themselves produce or accelerate SCC. Other work shows that SCC can be accelerated by acetates. Thus, there is little general information and almost no perspective on this subject; but, such work is im-

portant, nonetheless, in view of the ubiquity of organic species that have been observed in SG deposits. Further, in other systems, e.g., titanium alloys, alcohols produce aggressive SCC that is somehow related to soluble complexes that are formed between titanium and alcohols.

9. Low-Temperature SCC (LTSCC), Section 5.2.9 — There are two modes of LTSCC. The first mode was first detected in 1989 when an Alloy 600MA specimen tested for LPSCC was removed from an autoclave, and the crack was observed to continue to grow on the laboratory bench regardless of the specimen being in laboratory air at room temperature. This mode of LTSCC appears to involve slow crack propagation, in the range of mm/month, and to result from hydrogen adsorbed during high-temperature autoclave exposure. LTSCC in these conditions have been studied only for Alloy 600MA.

The second type of LTSCC involves rapid crack propagation, in the range of mm/s, at temperatures below $100^{\circ}C$ in hydrogen-containing water. In this mode, the affected materials exhibit low-fracture toughness when preexisting cracks are present. The rapid crack propagation is attributed to the effects of hydrogen, with most of the hydrogen coming from the hydrogenated water environment or from crack tip corrosion, as opposed to coming from previously adsorbed hydrogen in the metal. This second mode is most intense in Alloy 690 and several nickel alloy weld metals, but not Alloy 600.

There are four important features of LTSCC. First, Alloy 600MA is susceptible to the first type of LTSCC but not the second, and Alloy 690 is susceptible to the second type but not the first. Second, materials exposed to hydrogenated environments, i.e., lower potentials, are more prone to damage. Third, this phenomenon is limited to relatively low temperatures in the range of $100^{\circ}C$ or lower, except for Alloy X-750, where it can occur up to about $150^{\circ}C$. Fourth, the effects of the second mode of LTSCC are more pronounced at lower strain rates.

LTSCC should be considered carefully especially in shutdowns and startups. Further, using high N_2H_4 during shutdowns should be assumed to exacerbate the propensity toward LTSCC.

Local Environments in Which SCC Occurs

A quantitative description of local environments in heat-transfer crevices provides inputs to the dependencies of the submodes on the primary variables, i.e., if the primary variable is pH, then a quantitative description of pH in the local environment is required. In this article, the current quantitative understanding of local environments in heat-transfer crevices is assessed.

1. Chemistry inside Heat-Transfer Crevices — The chemistry inside heat-transfer crevices controls the occurrence of SCC. This local environment results

from a concentrated aqueous solution that arises from the accumulation of low-volatility dissolved compounds from the bulk water. Some solids inside the crevice may result from suspended products in the water; but most of the solids that are found inside crevices result from precipitation from concentrated aqueous solutions that have reached solubility limits. While the chemistries of bulk environments are well controlled, the chemistries inside heat-transfer crevices are neither controlled nor predictable, owing to the highly variable nature of their development. N_2H_4 has been shown to accumulate in crevices, although its instability and volatility minimize its concentration.

Certain features of the chemistry in heat-transfer crevices seem to be reasonably well defined:

- a. The pH_T inside heat-transfer crevices normally tends to be in the range of neutral, but with uncertainties, based on hideout return data and chemistries of the deposits. The pH may be somewhat alkaline or acidic in some cases, especially during startup transients and chemistry upsets.
- b. Certain species concentrate in heat-transfer crevices preferentially relative to the adjacent free-span, and several investigations find the same results: Mg, SiO_2 , Ca, Cr_2O_3 , carbon, molybdenum trioxide (MoO_3), PbO, SnO_2 , MnO, and Al_2O_3 all concentrate in heat-transfer crevices a factor of two or more greater than on the adjacent free-spans.
- c. Concentrations of species in crevice solutions may be on the order of 10^6 or more greater than in the bulk environment, with the peak concentration being established by thermodynamically defined limits.
- d. Cations, e.g., Na^+ and K^+ , concentrate about a factor of 10 more than anions, e.g., Cl^- and F^- , although sulfate concentrates about the same as cations. Higher volatility species, such as H_3BO_3 , concentrate significantly less than these species.
- e. The rate at which low-volatility species accumulate in crevices depends on the product of their bulk concentration and time.

2. *Physical Conditions* — Heat-transfer crevices become well-packed early in the life of steam generators mainly with iron oxide but also with other species. This packing often leads to a local steam phase inside the crevices, depending on its geometry. Owing to the small dimensions, the gradients of temperature, liquid, chemistry, and electrochemical potential produce significant variability in the detail of local chemistries in the crevice.

3. Transformations —

a. Sulfur

When sulfur enters heat-transfer crevices, it seems to enter either as SO_4^{2-} or possibly reduced

sulfur from resin particles. Sulfur tends to occur as +6 or +4 valences and may come from SO_4^{2-} in the water or from the decomposition of resin particles. From a corrosion point of view, these species are not much more aggressive than other acid forming ionic species. However, the presence of N_2H_4 may reduce these species to lower valences to produce sulfides, thiosulfates, and tetrathionates, all of which accelerate SCC and other localized corrosion. Further, such species have been observed inside SCC and inside heat-transfer crevices in operating plants and model boilers; and SCC has been shown to result directly from the presence of these species.

b. Lead

Lead enters heat-transfer crevices from a variety of sources. While small concentrations of lead readily produce SCC in laboratory tests, the lack of extensive PbSCC in plants seems to result from the formation of insoluble Pb compounds, which lower the activity of Pb below that required to produce PbSCC. The identity of these compounds and their properties is not known.

c. Organics

The presence of superheat, steam, and dynamic conditions inside heat-transfer crevices may facilitate carbon from various sources forming various organic species such as acetic acid, formic acid, propionate, pyruvate, valerianate, oxalate, and glycolates. Such species also may be available in the water and may be concentrated in crevices. The importance of these to corrosion singly or in combinations has not been extensively considered.

4. *Alumino-Silicates* — Studies of deposits in heat-transfer crevices taken from operating steam generators have shown that alumino-silicate-type compounds are sometimes observed where SCC and IGC occur. Efforts to explain the mechanistic link between this environment and the occurrence of corrosion have not produced a comprehensive rationalization. It seems that silica is more often an inhibitor. However, a study of the interaction among SiO_2 , sodium monoxide (Na_2O), and water has shown that certain combinations produce rapid SCC of both Alloy 600 and 690; and certain combinations are inhibitive. The reason for such a range of reactions seems related to the polymeric nature of silica.

5. *Line Contact Crevices* — The new SG designs, as well as some older ones, utilize line contact designs such as egg crate and broached holes with flat lands. In spite of the hope that deposits should not form in line contact configurations, in contrast to drilled holes, in fact, deposits have been observed. However, there have been no experimental studies of the concentration of species inside these species nor the possible occurrence of steam in such crevices.

6. *Top of Tubesheet Crevices* — The geometry of crevices at the top of tubesheets has not changed significantly from the use of Alloy 600MA to Alloy

690TT, except for the elimination of the deep tubesheet crevices used in some early steam generators. The top of tubesheet geometry, with shallow crevices that are covered by accumulated sludge, is implicit in a vertical steam generator, and has led to significant corrosion at some plants. Corrosion at this location has been mitigated by better water chemistry and by chemical cleaning. However, the possibility of corrosion here cannot be neglected in view of past experience.

Tubing Alloys

1. Alloy 600MA is by now well characterized with respect to its metallurgy and much of its corrosion behavior. However, aside from its proneness to numerous mode-location cases of corrosion, three important patterns have emerged:

- a. There is a high heat-to-heat variability. This is based on rigorous studies of heats in single steam generators. Further, there appears to be no consistent dependence of this variability on factors such as chemistry, strength, or microstructure. The dependence of different corrosion modes on these factors is inconsistent.
- b. Surface preparations strongly affect the onset of SCC depending on the nature and extent of mechanical damage of thin surface layers.
- c. The presence of locally high stresses due to scratches, dings, and dents can incite SCC, which seems like LPSCC, on the secondary side at free-spans. Once the SCC starts in the disturbed region, it propagates into the nondisturbed region.

2. Alloy 600TT produces improvements by about a factor of two to four in tests but does not produce immunity to any of the submodes of corrosion. Service experience shows that little corrosion of Alloy 600TT has been observed except where the material has been highly stressed or cold worked, such as by roll expansion or denting.

3. No corrosion-induced failures have occurred in service for Alloy 690TT. However, laboratory studies have shown that Alloy 690TT sustains SCC readily in some environments: caustic plus lead, caustic plus reduced sulfur, slightly oxidizing mildly acidic, highly alkaline, and highly alkaline plus silicate. The absence of service failures is probably as much due to improved control of water chemistry as to the alloy. It should be noted that the SCC in the upper bundles of OTSGs did not occur until after about 15 to 20 years, and now that mode is progressing rapidly. Also, LPSCC was slow to start except for the early influence of denting where the LPSCC was exacerbated by slow straining.

Future Problems and Priorities

The main objective of this article is to formulate a reliable model for the SCC on the secondary side of

steam generators with respect to quantifying the dependencies of submodes on the primary variables. In the process of this analysis, certain potential problems that may affect the reliability of steam generators have become evident as follows:

1. Laboratory tests indicate that PbSCC is an aggressive submode for Alloy 690TT, Alloy 600TT, and Alloy 600MA. It is doubtful that lead can be avoided in plants. However, the absence of extensive PbSCC in plants seems to result from the formation of insoluble lead compounds, thereby lowering the activity of Pb combined with other species such as SiO_2 , SO_4^{2-} , PO_4^{3-} , and possibly more complex compounds, or from adsorption reactions such as on magnetite. In view of the industry trend toward increasingly pure secondary environments, it is possible that the species that render Pb innocuous could be removed and thereby release Pb capable of producing PbSCC.

2. Reduced sulfur that results from the reduction of high-valence sulfur species by N_2H_4 can produce extensive S^{V} -SCC of Alloys 690TT, 600TT, and 600MA. The S^{V} -SCC has been studied less than PbSCC; more work is needed here to define the conditions for the reduction of +6 valences and the effects of pH and potential, as well as other primary variables, on the occurrence of S^{V} -SCC.

3. The line contact crevices used in modern SGs still accumulate deposits and in some cases extensively. There is little information on the concentration of species in such crevices.

4. Environments inside heat-transfer crevices are complex and are not readily specified. These complexities involve: the presence of steam, boiling point elevation with increasing concentrations of soluble species, precipitation of solid phases from supersaturated solutions, change in the available volume for convection due to precipitation, and kinetic processes related to input and output processes.

5. While it is now clear that the environments inside many heat-transfer crevices are partly steam, virtually all past work has been conducted in liquid environments. It is not clear how much of the latter work is applicable to corrosion in the steam phase. Further, DSSCC has been demonstrated to occur, and sometimes more intensely, including for Alloy 690TT in one study. Doped steam studies have considered mainly relatively low concentrations of species in the liquid phase and have not considered properties in the steam phase relating to more concentrated solutions in the liquid as occur in heat-transfer crevices.

6. There is little information on the reasons for the wide ranges of SCC that result from heat-to-heat variability.

7. More complex local environments including multiple species such as NaOH, SiO_2 , and organic acids may be aggressive, but there is little systematic information here. Further, organic acids have been

studied only to the extent of acetic acid, formic acid, and glycolic acid while additional organic species have been identified in SG deposits. In addition, only limited consideration has been given to how interactions of organic species with other inorganic species affects occurrences of SCC.

8. The deposit-covered crevice at the top of the tubesheet continues in modern designs since this geometry is inherent in vertical steam generators. A small amount of denting has been observed at this location, and much of the SCC in the past has occurred here. However, little attention has been given to this geometry with respect to measuring the magnitude of concentrating species, the existence of a steam phase, and the likelihood of continuing long-term slow denting.

9. It has been conventional to consider Alloy 690TT as immune to LPSCC. However, this conclusion is based on studies in pure water or primary water and limited testing in doped steam environments. This nominal immunity is not based on tests in environments that are typical of heat-transfer crevices, having high concentrations of dissolved solids and two-phase steam/water conditions.

10. AcSCC is important because it extends from quite acidic environments to pH of about 9. Further, in some experiments this environment has produced AcSCC of Alloy 690 in mildly oxidizing conditions.

ACKNOWLEDGMENTS

The work in this paper was supported by the United States Nuclear Regulatory Commission (USNRC) through Argonne National Laboratory (ANL), contract no. OF-00664, "Development of Models for Initiation of SCC on the Secondary Side of Steam Generators." We especially appreciate the support of J. Muscara of the USNRC and W. Shack of ANL.

We are indebted to the following for their discussions of the ideas, many contributions of information, and advice on the work in this article: M. Akashi of IHI, P. Andresen of General Electric, P.V. Balakrishnan of AECL, A. Baum of Bechtel Bettis Inc., P. Berge formerly of EDF, L. Bjornkvist of Vattenfall, S. Bruemmer of PNL, F. Cattant of EDF, P. Combrade of Framatome, J. Congleton of the University of Newcastle upon Tyne, G. Cragnolino of SWRI, J. Daret of CEA, D. Diercks of ANL, R. Eaker of Duke Power, Z. Fang of Medtronic Corporation, D. Feron of CEA, T. Gendron of AECL, G. Gdowski of LLNL, J. Gordon of Framatome, B. Gold of Westinghouse (retired), M. Hall of Bechtel Bettis Inc., B. Hermer of Bechtel Bettis Inc., H. Hirano of CRIEPI, S.S. Hwang of KAERI, I.S. Hwang of Seoul National University, B. Keefer of Bechtel Bettis Inc., L. Keeton of Bechtel Bettis Inc., R. Kilian of

Framatome, P. King of Babcock and Wilcox, U.C. Kim of KAERI, J.S. Kim of KAERI, I.H. Kuk of KAERI, T. Kusakabe of Mitsubishi, N. Lewis of KAPL Inc., B. Lindsay formerly of Westinghouse, C. Laire of LABORELEC, J. Lumsden of Rockwell, D. Macdonald of Pennsylvania State University, A. McIlree of EPRI, B. Miglin of Shell, P. Millett formerly of EPRI and now with iSagacity, B. Mills of Bechtel Bettis Inc., M. Mirzai of OPG Nuclear, A. Molander of Studsvik, M. Morgenstein of Geosciences Management Institute, J. Muscara of the USNRC, H. Nagano formerly of Sumitomo, F. Nordmann of EDF, S. Odar of Framatome, Y.-S. Park of Yonsei University, R. Parkins of the University of Newcastle upon Tyne, H. Pickering of Pennsylvania State University, A. Pourbaix of CEBELCOR, D. Rochester of Duke Power, T. Sakai of Nuclear Fuel Industries, B. Rosborg formerly of Studsvik, B. Sala of Framatome, G. Santarini of CEA, J. Sarver of Babcock and Wilcox, N. Sato formerly of Hokkaido University, B. Schneider of Babcock and Wilcox, P. Scott of Framatome, B. Shack of ANL, M. Seo of Hokkaido University, D. Shettel of Geosciences Management Institute, S. Smialowska of The Ohio State University, T. Shoji of Tohoku University, N. Sridhar of SWRI, B. Stellwag of Siemens, S. Suzuki of TEPCO, H. Takamatsu of KEPCO, B. Tapping of AECL, C. Thompson of KAPL Inc., T. Tsuruta of Mitsubishi, F. Vaillant of EDF, L. Thomas of PNL, G. Was of the University of Michigan, M. Wright of AECL, and T. Yonezawa of Mitsubishi.

In addition, we appreciate very much those who reviewed all or parts of this work, in particular: C.B. Bahn of Seoul National University, F.V. Balakrishnan of AECL, A. Baum of Bechtel Bettis Inc., F. Cattant of EDF, J. Congleton of University of Newcastle-upon-Tyne, J. Daret of CEA, R. Eaker of Duke Energy, R. Gold of Westinghouse (retired), J. Gordon of Framatome, K. Holter of Bechtel Bettis Inc., R. Janik of Bechtel Bettis Inc., R. Hermer of Bechtel Bettis Inc., B. Lindsay formerly of Westinghouse (retired), J. Lumsden of Rockwell, G. Lynch of Bechtel Bettis Inc., F. Miller of Bechtel Bettis Inc., B. Mills of Bechtel Bettis Inc., T. Myser of Bechtel Bettis Inc., H. Nagano formerly of Sumitomo Metals (retired), H. Pickering of Pennsylvania State University, V. Prescop of Bechtel Bettis Inc., A. Pourbaix of CEBELCOR, G. Santarini of CEA, N. Sato of Hokkaido University (emeritus), P. Scott of Framatome, B. Shack of ANL, B. Tapping of AECL, C. Thompson of KAPL Inc., T. Tsuruta of Mitsubishi, and F. Vaillant of EDF.

In addition, R. Staehle is greatly indebted to his energetic and professional staff who participated in the preparation of this article: M.E. Ilg, B. Lea, J. Daugherty, E.K. Rediger, T. Springfield, J. Ilg, N. Clasen, and G. Staehle.